Design of Selective Peptide Inhibitors of Anti-Apoptotic Bfl-1 Using Experimental Screening, Structure-Based Design, and Data-Driven Modeling

by
Justin Michael Jenson

B.S. Chemistry and Biomedical Engineering
University of Utah, 2012

SUBMITTED TO THE DEPARTMENT OF BIOLOGY IN PARTIAL FULFILLMENT OF THE REQUIREMENTS FOR THE DEGREE OF

DOCTOR OF PHILOSOPHY IN BIOLOGY AT THE MASSACHUSETTS INSTITUTE OF TECHNOLOGY

JUNE 2018

Signature redacted

Signature of Author: _____
Department of Biology
May 25, 2018

Signature redacted

Certified by: _____
Amy E. Keating
Professor of Biology and Bioengineering
Thesis Supervisor

Signature redacted

Accepted by: _____
Stephen P. Bell
Professor of Biology
Co-Chair, Biology Graduate Committee

Design of Selective Peptide Inhibitors of Anti-Apoptotic Bfl-1 Using Experimental Screening, Structure-Based Design, and Data-Driven Modeling

by

Justin Michael Jenson

Submitted to the Department of Biology on May 25, 2018
in Partial Fulfillment of the Requirements
for the Degree of Doctor of Philosophy in Biology

ABSTRACT

Protein-protein interactions are central to all biological processes. Designer reagents that selectively bind to proteins and inhibit their interactions can be used to probe protein interaction networks, discover druggable targets, and generate potential therapeutic leads. Current technology makes it possible to engineer proteins and peptides with desirable interaction profiles using carefully selected sets of experiments that are customized for each design objective. There is great interest in improving the protein design pipeline to create protein binders more efficiently and against a wider array of targets.

In this thesis, I describe the design and development of selective peptide inhibitors of anti-apoptotic Bcl-2 family proteins, with an emphasis on targeting Bfl-1. Anti-apoptotic Bcl-2 family proteins bind to short, pro-apoptotic BH3 motifs to support cellular survival. Overexpression of Bfl-1 has been shown to promote cancer cell survival and the development of chemoresistance. Prior work suggests that *selective* inhibition of Bfl-1 can induce cell death in Bfl-1 overexpressing cancer cells without compromising healthy cells that also rely on anti-apoptotic Bcl-2 proteins for survival. Thus, Bfl-1-selective BH3 mimetic peptides are potentially valuable for diagnosing Bfl-1 dependence and can serve as leads for therapeutic development.

In this thesis, I describe three distinct approaches to designing potent and selective Bfl-1 inhibitors. First, I describe the design and screening of libraries of variants of BH3 peptides. I show that peptides from this screen bind in a previously unobserved BH3 binding mode and have large margins of specificity for Bfl-1 when tested *in vitro* and in cultured cells. Second, I describe a computational model of the specificity landscape of three anti-apoptotic Bcl-2 proteins including Bfl-1. This model was derived from high-throughput affinity measurement of thousands of peptides from BH3 libraries. I show that this model is useful for designing peptides with desirable interaction profiles within a family of related proteins. Third, I describe the use of a scoring potential built on the amino acid frequencies from well-defined structural motifs complied from the Protein Data Bank to design novel BH3 peptides targeting Bfl-1.

Thesis Supervisor: Amy E. Keating
Title: Professor of Biology and Bioengineering

Acknowledgements

I would like to thank my graduate advisor, Amy Keating, for all the scientific and professional training she has provided me. I admire her careful and thorough approach to science. In particular, I am grateful for her willingness to help me cultivate the skills I need to be a successful scientist including scientific communication and critical thinking. I am very grateful for the many hours she dedicated to editing my writing, providing feedback for my practice talks, and working with me to peer review papers. She has done a tremendous job at setting my scientific career off to a good start.

I would like to thank to Bob Sauer and Mike Laub for serving on my thesis committee and providing helpful guidance throughout the past 5 years. I appreciate their help to see the bigger picture and to re-focus projects. I would like to thank James Van Deventer for serving on my defense committee.

Thanks to my undergraduate advisor, Susan Bock, for providing a solid foundation in experimental biochemistry. I am grateful for her lessons in good laboratory practice and how to troubleshoot experiments.

Thank you to Keating lab members past and present. In particular, I am grateful for the many collaborators I worked with during my time in the lab. First of all, I am grateful for the chance I've had to work with Vincent Xue. He was always willing to do whatever it takes to get the job done and I have learned a lot about computational biology by working with him. I am grateful for Raheleh Rezaei-Araghi's generosity and eagerness to work collaboratively. I am grateful to Vincent Frappier for his positive attitude and infectious excitement for protein design. Thanks also to Glenna Foight for the many insightful discussions about Bcl-2 proteins and Dustin Whitney for thoughtful discussions about biochemistry.

I am grateful for personnel at the MIT Koch flow cytometry core, MIT Biomicro Center, MIT Koch Biopolymers, and Biophysical Instrumentation Facility. I would like to extend a special thanks to Bob Grant from the MIT crystallography core facility for his mentorship in protein crystallography.

Thank you to the Biograd class of 2012 for the camaraderie and support throughout my time here.

I would like to thank my family. Thanks to my mom and dad for teaching me the value of education and hard work. I grew up watching them both work hard to finish advanced college degrees and their examples left a lasting impression on me. Thanks to my wife Brittney for her selfless support and abundant patience. Thanks to my boys Kit and Dash for giving me perspective and lots of motivation to get my work done efficiently.

Table of Contents

List of figures

List of tables

Chapter 1

Introduction

Protein-protein interactions (PPIs) are central to nearly every biological process including signaling, molecular recognition, immunity, transcription, translation, the cell cycle, cell division, and myriad other essential processes. The human genome encodes for ~30,000 unique proteins, and current estimates suggest that the human interactome consists of at least 400,000 PPIs[1]. Given the massive potential for interaction of a protein with many different partners, PPI selectivity is essential to protein function. Whether through the loss of interaction or formation of new complexes, abnormal PPIs can promote and drive diseases including neurodegenerative diseases and cancer.

In nature, PPIs are continually created, lost, and modulated through a combination of genomic plasticity and evolutionary selection. Gene duplications, base-pair substitutions, indels, and genomic recombinations create new proteins and diversify their amino acid sequences all while evolutionary forces shape protein interactomes. Similar processes of genetic diversification and evolutionary selection are occurring at different timescales throughout all domains of life, enabling nature to create a large number of protein sequence variants and simultaneously test them for function. It has been estimated that as many as 10^{50} protein sequences have been tested for function during the earth's 4 billion year history[2].

Given the biologically important roles of PPIs, there is tremendous practical and scientific value in interaction engineering and design. Targeting PPIs can be useful for the development of diagnostics, biosensors, research reagents, and therapeutics. Additionally, the quantitative descriptions of molecular interactions developed for protein design can be applied to studies of evolution, protein function, and molecular mechanisms of disease. However, whereas nature uses evolution to create and test

large numbers of sequences over a vast amount of time, to design proteins in the lab, affinity and specificity must be explicitly accounted for either experimentally, computationally, or by using both approaches.

Protein design is technically challenging for a number of reasons. First, sequence space is massive (20^n where n represents protein length in number of amino acids). Although there may be many possible sequences that can achieve a desired design profile, there is no guarantee that any such sequence is only a few mutations away from a known sequence, which is the space most frequently searched in design projects. Second, PPIs are structurally diverse and complex. PPIs can be formed by folded domains that fit together like pieces from a puzzle, by proteins that lack significant structure before binding, or by proteins that form 'fuzzy' complexes with high degrees of structural heterogeneity[3,4]. Further, many PPIs exhibit structural plasticity, which complicates design even when an experimentally determined structure is available. Finally, mutations can exhibit epistasis or, in other words, the effect of a mutation can differ depending on the sequence context in which that mutation occurs[5,6]. Mutational epistasis complicates protein design by creating rugged fitness landscapes.

This thesis addresses the topic of peptide design for tight and selective binding to a target protein, as well as methods and approaches for systematically navigating mutational space. To provide context for this work, it is important to recognize that there are many strategies that can be used to make a protein with desired properties. I will summarize the most common approaches to protein design, which are directed evolution (DE) and structure-based design (SBD), before discussing some emerging protein-design approaches.

Directed evolution

A common approach to design proteins with desirable PPI profiles is to use DE wherein the search through mutational space is guided by experiment[7]. Similarly to natural selection, DE relies on nucleotide sequence randomization in combination with screens or selections of protein function. By iterating through this process, mutations accumulate until a protein sequence that meets the design objectives is discovered, as illustrated in Figure 1.1 A, B.

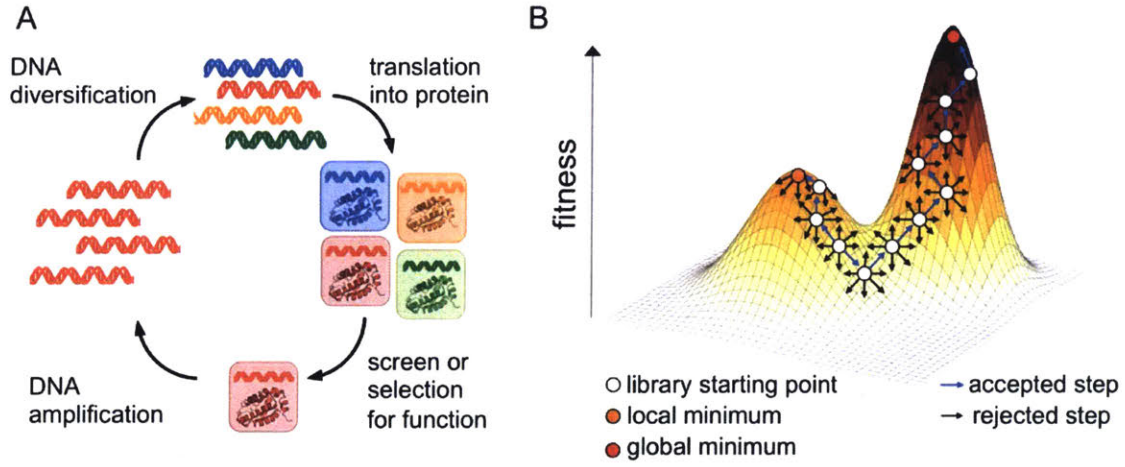

Figure 1.1. An overview of the key steps and limitations of directed evolution. A) Genetic diversity is generated and the effect of mutations is determined empirically with screens or selections. Mutations accumulate through repetition of the cycle. B) Through several rounds of directed evolution, sequence space (as illustrated here as a three-dimensional fitness landscape) can be navigated. In this illustration, identifying the maximum fitness requires crossing a "fitness valley". The ruggedness of the fitness landscape results from epistatic interactions between sets of mutations.

As in natural selection, genetic diversity is central to DE. Random mutagenesis is used to introduce mutations into a protein-coding gene whose phenotype can later be experimentally evaluated with genetic screens or selections. One of the advantages of this approach is that proteins can be designed without any detailed knowledge of their structure. This is a valuable feature, considering that the structures of many PPIs are unknown. Although mutations to a target gene can be generated *in vivo*[8], *in vitro*

methods allow more control over mutational sampling. For example, low-fidelity polymerases can be used in error-prone PCR to generate point mutations[9]. Mutational biases of nucleotide substitutions can be countered experimentally, for example by altering dNTP concentrations[10]. However, there isn't a direct correspondence between nucleotide mutations and protein mutations, so amino acid substitutions introduced in this way are biased by the genetic code. Point mutations can also be introduced at the codon level through assembly with synthetic DNA primers that contain mixed bases by assembly PCR[11,12] or DNA ligation[13,14]. Sequence diversity can also be created through mimicking homologous recombination *in vitro* with approaches like DNA shuffling[15,16] or assembly PCR[17].

Mutational space is too large to comprehensively search with existing experimental approaches for all but the shortest peptide sequences. The limit of how much mutational space can be explored in DE depends on experimental throughput and library transformation efficiency. A powerful and flexible platform for screening PPIs is yeast cell-surface display[18,19]. In this approach, protein libraries are expressed on the yeast cell surface through genetic fusion with the yeast mating adhesion receptor Aga2. Binding to fluorescently labeled target protein can be measured and screened with fluorescence-activated cell sorting (FACS). Assays that measure binding to cell surface-expressed molecules have the advantage of providing researchers with control over the stringency of the screen, which can be tuned by altering target protein concentration. This experimental design also facilitates negative screening or counterscreening against off-target binding. Yeast libraries can be as large as ~10^9 transformants, but FACS sorting speed limits the number of cells that can be screened to ~10^7. Cell-surface

display platforms have been developed for other organisms including bacteria[20] and mammalian cells[21]. Other screening approaches include modest-throughput plate-based screens and screens in artificial cell-like compartments such as water-oil emulsions for FACS-based[22] or microfluidic screening[23]. Because genetic selections don't require each library member to be inspected for phenotype, they can be used to search larger library spaces. Affinity-based selections can be used to query larger libraries using phage display (~10^{10} variants)[24], ribosome display (~10^{12} - 10^{13} variants)[25], and mRNA display (~10^{12} - 10^{13} variants)[26].

DE is routinely used to engineer proteins with enhanced binding and specificity profiles. DE approaches have proven particularly valuable in designing antibodies with enhanced affinities for their targets. For example, Boder *et al.* used DE to design a fluorescein-binding antibody that bound with a 48 fM K_D, more than 1,000-fold tighter than its parent antibody[27]. Similar approaches have been used to develop affinity matured antibodies against cholera toxin (1,300-fold improvement)[28], Her2/Neu (10-fold improvement)[29], TNF-α (30-fold improvement)[30], and many other targets as summarized in reviews by Boder *et al.*[31] and Cherf *et al.*[32] Antibody engineering using DE techniques has contributed to the development of many of engineered antibodies that have been approved for clinical use or entered clinical trials[33]. DE is also commonly used to engineer affinity agents on non-antibody scaffolds, including DARPins[34,35], knottins[36], fibronectin type III domains[37], T-cell receptors[38], interleukin-II variants[39], and myriad other proteins.

DE can be a powerful approach to protein design, but it has some limitations. For example, it can be challenging to discover sequences far from the starting template with

DE because deleterious mutations are much more frequent than beneficial mutations[40]. For example, Bershtein *et al.* demonstrated that only ~$1/10^3$ random mutations were beneficial for TEM-1 β-lactamase function, but ≥1/3 mutations were deleterious[41]. Thus, researchers typically keep the mutational load in each round of DE low to avoid masking beneficial mutations with deleterious mutations. Epistasis presents another challenge to discovering diverse functional sequence spaces, because some mutations are only beneficial after non-beneficial or deleterious mutations have accumulated, as illustrated by the fitness valley in Figure 1.1 B.

Structure-based design

PPIs can be designed computationally with the use of structure-based scoring potentials. There are three general categories of scoring potentials commonly used in computational design: physics-based potentials, knowledge-based potentials, and hybrid potentials that include both elements.

In theory, given a structure, it should be possible to explore vast amounts of mutational space by calculating the energetic effects of mutations *in silico*. Physics-based scoring potentials, including AMBER[42] and CHARMM[43], have been developed to score the potential energy of proteins using principles of molecular mechanics. Physics-based scoring potentials are mathematical models of molecular forces (van der Waals attraction and repulsion, Columbic interactions, bond energies, *etc.*) whose energetic contributions have been weighted based on chemical and physical theory or experimental measurement[44]. These scoring functions are optimized to predict the lowest-energy protein conformations by calculating the potential energy of different conformations for a single sequence, as is commonly done in molecular dynamics

simulations. Scoring with physics-based potentials is computationally expensive, which puts practical constraints on how much mutational space can be explored. These methods aren't used alone for design, at least not without introducing many approximations.

Alternatively, the effect of a mutation can be inferred from statistical (sometimes called knowledge-based) potentials derived from structures in the Protein Data Bank (PDB). These potentials are derived from frequencies of structural features like rotamer positions and the geometries of interacting residue pairs. Statistical potentials assume that structural features are Boltzmann distributed, such that the lowest energy structural features will be the most frequently observed. Since their inception in the 1970's[45], statistical potentials have been used with some success in structure prediction[46,47], structural quality assessment[48,49], PPI prediction[50], and affinity prediction[51,52]. In comparison with physics-based potentials, knowledge-based potentials are fast to evaluate and do not require structural minimization for scoring. But the accuracy of these scoring functions limits their application in design. For example, Su *et al.* reported a modest correlation (R= 0.76) between a knowledge-based scoring potential and the previously published affinities of 86 protein-protein complexes, but the standard deviation between the predictions and measured affinities was reported to be 2.24 kcal/mol ($\pm 16x\ K_D$)[51], limiting its potential use as a design tool . In attempts to improve the accuracy of these methods for design, there has been considerable work done to find new ways to define and score structural features. One promising way of describing proteins was recently developed by Mackenzie *et al*[53], who demonstrated that protein structures can be decomposed into a defined set of tertiary motifs (TERMs) that have

similar secondary, tertiary, and quaternary structure[53]. Further, TERMs have associated sequence preferences, and Zheng *et al.* showed that a statistical potential derived from the sequence statistics of TERMs predicts changes in protein stability upon mutation at least as well as state-of-the-art physics-based potentials[54]. A function that relates a sequence to its fitness on a structure can be used for design, and design using TERM energies (dTERMen) has been implemented in the Grigoryan lab and tested on a small number of problems. The dTERMen scoring procedure is outlined in Figure 1.2. Chapter 4 of this thesis demonstrates the potential of dTERMen to accurately design PPIs with highly diversified sequences.

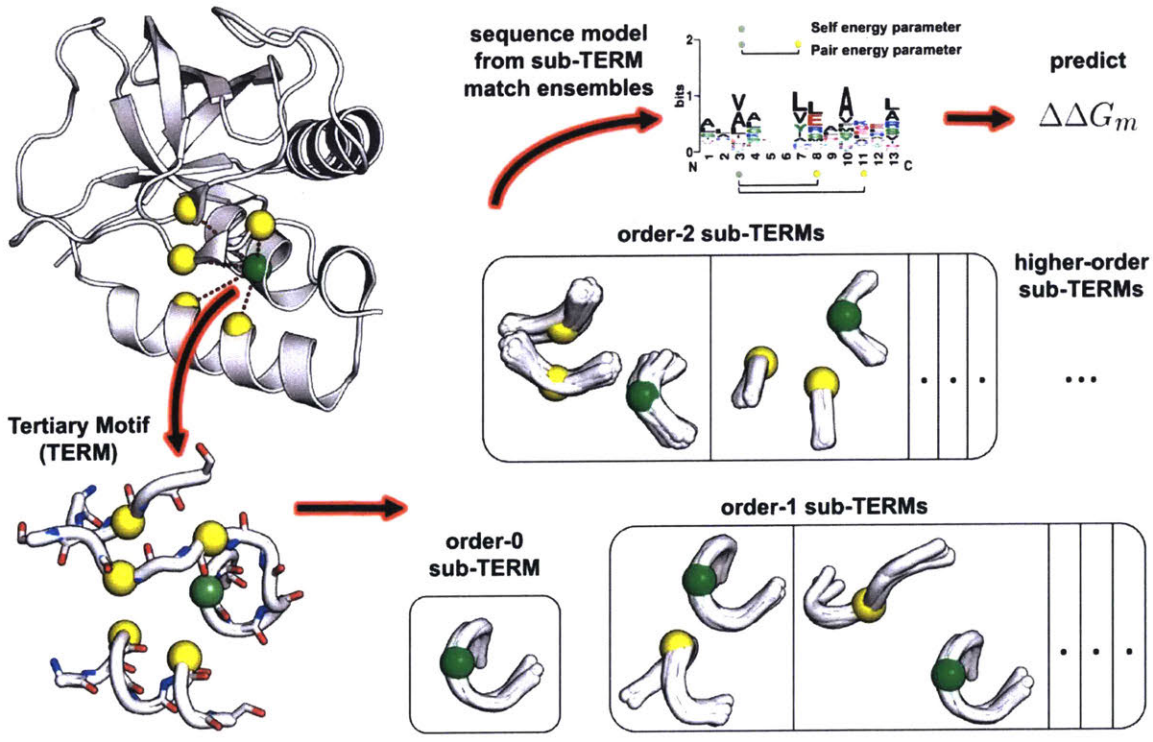

Figure 1.2. An overview of dTERMen scoring function. Mutational energies are calculated by describing the local structural environment and matching the geometry of the design template with a database of tertiary motifs (TERMs) or sub-TERMs compiled from the PDB. Positional and pair amino-acid frequencies of matching structural ensembles are used to predict the ΔΔG of mutation. Figure is from Zheng *et al*[54].

Many of the most commonly used scoring functions for protein design combine physics-based and knowledge-based scoring functions to speed scoring of large mutational spaces. For example, the Rosetta scoring function was initially developed as a statistical potential[55], but many additional physics-based energy terms have been added to account for hydrogen bonding, van der Waals interactions, solvation, *etc.*[56–58]. Another commonly used platform for protein design is FoldX, which is a scoring function based primarily on physical terms parameterized by empirical data, but includes some statistical terms from the PDB to account for backbone and side chain entropies[59]. The accuracy of the hybrid scoring functions depends on which energetic terms are used and how each term is weighted relative to each other. Scoring functions can be highly customizable, leading to significant variability between research groups and particular design tasks[44]. Hybrid potentials can be used to search large mutational spaces [60,61], though the modest accuracy of these models typically necessitates experimental screening to identify successful designs, as discussed below.

Combining experimental screening with computational design

DE and SBD are highly complementary methods that when combined can produce superior results[62,63]. For example, SBD can be used to design novel proteins that can then be further optimized with DE. This approach has been widely used in enzyme design and to design protein binders. Fleishman *et al.* used Rosetta to design proteins to bind a conserved epitope of hemagglutinin (influenza) from the 1918 H1N1 pandemic virus starting from a structure of hemagglutinin bound to an antibody fragment. They then affinity maturated the designs using DE to engineer proteins that

bind to hemagglutinin with low nanomolar affinity[61]. Similar approaches are routinely used by the Baker lab and others to design novel protein binders.

SBD can be used to guide mutational selection for focused DE libraries. As discussed in the preceding sections, experimental screens and selections are limited in the number of unique sequences that can be explored and the mutational load that can be encoded in those sequences. SBD can be used to identify which residue positions are directly involved in PPIs and predict which mutations at those positions have the most potential to improve function. Further, SBD can be used to identify and exclude potentially disruptive mutations that have the potential to "poison" any fraction of the library that encodes them. This makes it possible to construct libraries that encode larger sets of mutations that explore farther away from the design template sequence[40]. In this way, SDB can be used to design focused, combinatorial libraries that can be assembled using well-established randomization strategies[64]. This approach has been shown to be more efficient than DE by random mutagenesis. For example, focused libraries of GFP mutants designed with SBD were found to encode a broader range of fluorescent activities than mutagenic PCR-generated libraries[65]. Structure-based library design has become a routine approach to improving protein affinity, specificity[66–68], and regulation[69]. One advantage of focused, combinatorial libraries is their potential to explore epistatic landscapes, as sets of mutations have increased potential to escape local minima. An example of a focused combinatorial library that led to the discovery of a peptide with a set of episatic mutations that would be difficult to discover with DE is presented in chapter 2 of this thesis.

Data-driven design

Techniques for measuring binding affinities in high-throughput have begun to provide new opportunities for alternative and complementary approaches to protein design. Here I discuss a few of the technologies that enable high-throughput PPI affinity measurement, before discussing how these data can be used for protein design.

Peptide SPOT arrays and microarrays provide qualitative binding measurements for peptides immobilized on a solid surface either by spotting, as done for ELISAs, or by *in situ* synthesis[70,71]. In this way, hundreds or thousands of peptides to be assayed for binding in parallel. These approaches are best suited for probing mutations in short peptides. Although it is possible to synthesize peptides 50 amino acids or longer on peptide arrays[72], 6-18 amino acids is optimal[70]. Synthesis quality and yield varies from sequence to sequence, contributing to measurement uncertainty in these datasets.

A semi-quantitative measurement of affinity can be extracted from DE experiments by deep-sequencing mutant libraries before and after one or several rounds of screening or selection[73–75]. For example McLaughlin *et al.* used enrichment of a bacterial two-hybrid library containing all possible single point mutants of a PDZ domain to measure the affect of mutation over a broad range of affinities (~0.1-200 μM) as evidenced by a linear relationship between enrichment values and independently measured K_Ds (correlation coefficient not reported)[73]. In more recent work, Younger *et al.* used a *Saccharomyces cerevisiae* mating efficiency screen to measure K_Ds from <500 pM to >300 μM[74]. They reported a linear relationship between K_D and mating efficiency (R^2=0.878). Approaches like these that capture trends in binding affinities are increasingly being used as a general means to understand how function relates to

sequence, but are not currently widely adopted for protein design. Resolution of these methods might be limited in part by their reliance on separation into binary groups of either binders or non-binders. Further, biases from growth in preparation for deep-sequencing might further reduce resolution.

Screening methods that separate samples into multiple phenotypic classes have been developed to increase measurement resolution[76–79]. Reich *et al.* developed a method called SORTCERY to sort individual yeast cells from a library by their apparent degree of binding[76,80]. In this method, yeast cells are sorted and deep-sequenced to rank-order thousands of mutant peptides by affinity. SORTCERY has the advantage of not requiring a growth step between sorting and deep sequencing. Chapter 3 of this thesis presents a strategy to extract absolute affinities from SORTCERY data. Adams *et al.* used multi-state sampling in combination with titration to create binding curves from which the affinities of thousands of yeast-displayed proteins can be measured in parallel[78]. One significant advantage of this approach is that it provides researchers control over the range of affinities that are measured. A minor drawback is that this protocol requires growth steps in preparation for deep sequencing, which can contribute to measurement noise.

Another potentially rich source of experimental data that could be exploited for design is databases of measurements compiled from the literature, such as Ab-Bind[81] and SKEMPI[82]. However, measurements made for the same protein interaction can vary significantly between labs, methods, and experimental conditions, making it infeasible to make reliable comparisons across studies. Databases assembled from the

literature can also suffer from lack of mutational diversity. In particular, a disproportionately large fraction of alanine mutants are observed in these datasets.

Large mutational datasets are valuable for benchmarking the performance of computational models and improving protein design[83,84]. For example, Rocklin *et al.* used a high-throughput screen of protease sensitivity for a yeast-displayed library of mini-proteins to measure protein stability in high-throughput. By comparing the experimental measurements of stability with predictions made by Rosetta, the authors were able to reweight Rosetta energy terms and improve their design success rate[85]. Similar data-driven reweighting of Rosetta terms was shown to improve PPI design[86].

Mutational datasets can be used to build models of PPI for protein design. For example, Wiedemann *et al.* measured hundreds of single point mutants for binding to PDZ domains using SPOT arrays[87]. They then modeled the effect of mutation and designed three novel peptide ligands, all of which bound modestly tighter (< 5-fold) than the sequences from which they were designed. The model used for design assumed that each residue contributes independently to binding, which isn't always the case for PDZ domains[88].

Models that capture relationships between sequence and binding can be used to guide the design of focused libraries. This approach is particularly valuable for designing focused libraries in the absence of experimental structures. For example, Dutta *et al.* used mutational data from SPOT arrays to develop position specific scoring matrices (PSSMs) that were used to guide the selection of mutations to include in a peptide library to achieve specificity against the anti-apoptotic protein Bcl-w, for which there was no experimental structure available at the time[89]. Experimental data has also

been used for library design in enzyme engineering in the form of "scouting" experiments in which experimental data is used to provide clues as to which residues are most important for function, to guide the design of focused libraries. For example, this approach was used to change the substrate specificity of glutaryl acylase (for which no structure was available at the time) toward adipyl compounds using random mutagenesis to create a small (10,000 colony) pilot library[90]. Screening revealed three mutations that affected substrate specificity. Those three positions were randomized in subsequent libraries with saturation mutagenesis to further improve catalytic efficiency three-fold. Data-driven library design is being used to create focused libraries with reduced size that decrease the amount of screening required to engineer proteins with improved properties[91].

Machine learning on mutational datasets has been used to capture the relationship between protein sequence and complex protein properties including solubility[92,93], cellular localization[94,95], crystallization propensity[96], and protein function[97]. Additionally, there is evidence that given enough data, machine learning can be used to model epistatic effects for use in PPI design. For example, Potapov *et al.* used a large quantitative set of >4,500 coiled-coiled interactions to develop a model whose predictive performance approached experimental error when intramolecular terms were inlcuded[98]. One barrier to using machine learning in protein design is that these models tend to generalize poorly and are best suited for predicting sequences that are close to those used to train the model. Chapter 3 of this thesis provides evidence that machine learning can, at least in some cases, be used to design sequences distant from those used for model training.

Summary of protein design approaches

In this Introduction, I discussed experimental and computational approaches that have been used to design PPIs. Perhaps the most widely adopted PPI design strategy is DE, which is limited in the amount of sequence space it can explore. When a protein structure is available, SBD is a common approach to explore vast amounts of sequence space, but is rarely used on its own to design novels proteins due to accuracy limitations. SBD and DE are highly synergistic approaches that can be and increasingly are used in combination to great effect. In the absence of structure, however, it is difficult to model and explore vast amounts of sequence space. Although data-driven design is still in its infancy, the ever-growing amount of experimental data is beginning to transform PPI design. It is likely that data-driven design will greatly enhance our design capabilities, especially in combination with well established DE and SBD approaches.

Anti-apoptotic Bcl-2 protein family as a model system for protein design

The Bcl-2 protein family regulates the intrinsic pathway of apoptosis through PPIs. Anti-apoptotic Bcl-2 proteins including Bcl-2, Bcl-x_L, Mcl-1, Bcl-w, and Bfl-1 promote cellular survival by binding to BH3 motifs. BH3 motif peptides are unfolded in isolation but adopt a helical conformation upon binding, as shown in Figure 1.3. Anti-apoptotic protein interactions with BH3 motifs prevent the pro-apoptotic proteins BAX and BAK from homo-oligomerizing into pores in the mitochondrial outer membrane, a "point of no return" in apoptotic signaling[99,100].

Anti-apoptotic Bcl-2 proteins are valuable therapeutic and diagnostic targets. Overexpression of anti-apoptotic Bcl-2 proteins is known to contribute to oncogenesis

and confer resistance to chemotherapeutic agents[99]. Diagnostic determination of anti-apoptotic protein dependencies from patient samples can be used to guide clinical treatment options,[101] and therapeutic inhibition of over-expressed anti-apoptotic proteins can sensitize malignant cells to treatment[102].

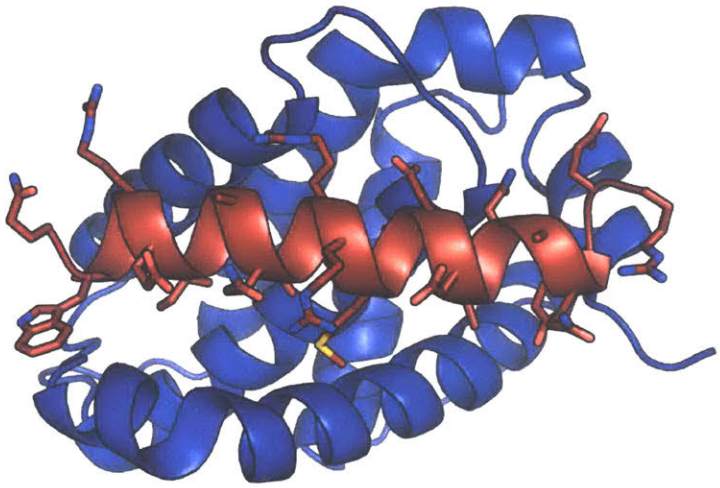

Figure 1.3. The anti-apoptotic protein Bfl-1 (blue) bound to the natural BH3 motif of Puma (red, 5UUL[103]) is shown.

There has been significant progress in targeting Bcl-2 family proteins therapeutically with BH3-mimetic small molecules. For example, the small molecule ABT-263 was found to promote apoptosis in lymphocytic leukemia cells overexpressing Bcl-2[104]. Unfortunately, cross-reactivity of ABT-263 with Bcl-x_L caused dose-limiting thrombocytopenia, ultimately leading to failure in clinical trials[105,106]. By including selectivity as a design criteria in subsequent work, a small molecule (ABT-199) that bound to Bcl-2 but not Bcl-x_L was developed and approved by the FDA for clinical use[104,107]. These results highlight the importance of sub-family selectivity when targeting

members of this protein family therapeutically. Small molecules selectively targeting Mcl-1 have since been developed[108].

As an alternative strategy, BH3 mimetic peptides are being developed to target anti-apoptotic Bcl-2 family proteins. Peptides that selectively inhibit members of this protein family are valued as therapeutic leads and as diagnostic reagents that can probe anti-apoptotic protein dependencies to guide clinical treatments[101]. Protein design has enabled the development of many selective reagents that are being used to study Bcl-2 biology and develop diagnostic assays. For example, computationally designed, focused yeast-display libraries have been used to design Bcl-x_L[89] and Mcl-1[109] selective peptides.

Selective peptides or small molecules have proven difficult to develop for Bfl-1. Dutta *et al.* used a data-driven approach to design a combinatorial library and discovered a peptide with >30 fold selectivity for Bfl-1. However, this peptide failed to inhibit Bfl-1 in cellular studies[110]. Berger *et al.* designed helical proteins with BH3 domains using Rosetta that selectively inhibit Bfl-1[111], but these proteins are comparatively large (>13 kDa), making cellular delivery a challenge. There have also been attempts at designing small molecules targeting Bfl-1[112–115], though these small molecules have only modest specificity for Bfl-1 relative to other Bcl-2 family members and bind with low affinity (high nanomolar to low micromolar).

Research approach

In my thesis work, I designed potent and selective peptide inhibitors for the anti-apoptotic protein Bfl-1. My thesis project began by designing a set of libraries to selectively target anti-apoptotic Bcl-2 proteins. In chapter 2, I describe how these yeast-

displayed libraries were designed and screened for Bfl-1 selectivity. The designed peptides were characterized biochemically using solution binding assays, mutagenesis, and X-ray crystallography. Our collaborators tested the designed peptides in cells and confirmed selective Bfl-1 inhibition of apoptotic signaling. In chapter 3, I describe my work with Vincent Xue to measure the apparent affinities of thousands of peptides from these libraries for binding to Bfl-1, Mcl-1, and Bcl-x_L in high-throughput. This work required the development of a method to extract binding affinities from datasets of binding profiles. These data were used to build a data-driven model of the specificity landscape for these proteins. Further, we used this model to successfully design highly selective peptides many mutations away from any sequence used to train the model. Finally, in chapter 4, I describe collaborative work using dTERMen to design novel sequences using structures of Mcl-1 and Bfl-1 complexes as input.

References-

1. Chen TS, Petrey D, Garzon JI, Honig B. Predicting peptide-mediated interactions on a genome-wide scale. *PLoS Comput Biol.* 2015;11(5):e1004248. doi:10.1371/journal.pcbi.1004248.
2. Mandecki W. The game of chess and searches in protein sequence space. *Trends Biotechnol.* 1998;16(5):200-202. doi:10.1016/S0167-7799(98)01188-3.
3. Borgia A, Borgia MB, Bugge K, et al. Extreme disorder in an ultrahigh-affinity protein complex. *Nature.* 2018;555(7694):61-66. doi:10.1038/nature25762.
4. Tompa P, Fuxreiter M. Fuzzy complexes: polymorphism and structural disorder in protein–protein interactions. *Trends Biochem Sci.* 2008;33(1):2-8. doi:10.1016/j.tibs.2007.10.003.
5. Miton CM, Tokuriki N. How mutational epistasis impairs predictability in protein evolution and design. *Protein Sci.* 2016;25(7):1260-1272. doi:10.1002/pro.2876.
6. Podgornaia AI, Laub MT. Protein evolution. Pervasive degeneracy and epistasis in a protein-protein interface. *Science.* 2015;347(6222):673-677. doi:10.1126/science.1257360.
7. Packer MS, Liu DR. Methods for the directed evolution of proteins. *Nat Rev Genet.* 2015;16(7):379-394. doi:10.1038/nrg3927.
8. Ravikumar A, Arrieta A, Liu CC. An orthogonal DNA replication system in yeast. *Nat Chem Biol.* 2014;10(3):175-177. doi:10.1038/nchembio.1439.
9. Cadwell RC, Joyce GF. Randomization of genes by PCR mutagenesis. *PCR Methods Appl.* 1992;2(1):28-33. http://www.ncbi.nlm.nih.gov/pubmed/1490172. Accessed April 5, 2018.
10. Vanhercke T, Ampe C, Tirry L, Denolf P. Reducing mutational bias in random protein libraries. *Anal Biochem.* 2005;339(1):9-14. doi:10.1016/j.ab.2004.11.032.
11. Gibson DG. Enzymatic Assembly of Overlapping DNA Fragments. In: *Methods in Enzymology.* Vol 498. ; 2011:349-361. doi:10.1016/B978-0-12-385120-8.00015-2.
12. Quan J, Tian J. Circular Polymerase Extension Cloning of Complex Gene Libraries and Pathways. Ho PL, ed. *PLoS One.* 2009;4(7):e6441. doi:10.1371/journal.pone.0006441.
13. Ashraf M, Frigotto L, Smith ME, et al. ProxiMAX randomization: a new technology for non-degenerate saturation mutagenesis of contiguous codons. *Biochem Soc Trans.* 2013;41(5):1189-1194. doi:10.1042/BST20130123.
14. Wells JA, Vasser M, Powers DB. Cassette mutagenesis: an efficient method for generation of multiple mutations at defined sites. *Gene.* 1985;34(2-3):315-323. http://www.ncbi.nlm.nih.gov/pubmed/3891521. Accessed April 5, 2018.
15. Stemmer WPC. Rapid evolution of a protein in vitro by DNA shuffling. *Nature.* 1994;370(6488):389-391. doi:10.1038/370389a0.
16. Ness JE, Kim S, Gottman A, et al. Synthetic shuffling expands functional protein diversity by allowing amino acids to recombine independently. *Nat Biotechnol.* 2002;20(12):1251-1255. doi:10.1038/nbt754.
17. Zha D, Eipper A, Reetz MT. Assembly of designed oligonucleotides as an efficient method for gene recombination: a new tool in directed evolution. *Chembiochem.* 2003;4(1):34-39. doi:10.1002/cbic.200390011.
18. Boder ET, Wittrup KD. Yeast surface display for directed evolution of protein expression, affinity, and stability. *Methods Enzymol.* 2000;328:430-444. http://www.ncbi.nlm.nih.gov/pubmed/11075358. Accessed April 5, 2018.
19. Boder ET, Wittrup KD. Yeast surface display for screening combinatorial polypeptide libraries. *Nat Biotechnol.* 1997;15(6):553-557. doi:10.1038/nbt0697-553.
20. Daugherty PS, Chen G, Olsen MJ, Iverson BL, Georgiou G. Antibody affinity maturation using bacterial surface display. *Protein Eng.* 1998;11(9):825-832. http://www.ncbi.nlm.nih.gov/pubmed/9796833. Accessed April 5, 2018.

21. Wolkowicz R, Jager GC, Nolan GP. A random peptide library fused to CCR5 for selection of mimetopes expressed on the mammalian cell surface via retroviral vectors. *J Biol Chem.* 2005;280(15):15195-15201. doi:10.1074/jbc.M500254200.

22. Bernath K, Hai M, Mastrobattista E, Griffiths AD, Magdassi S, Tawfik DS. In vitro compartmentalization by double emulsions: sorting and gene enrichment by fluorescence activated cell sorting. *Anal Biochem.* 2004;325(1):151-157. http://www.ncbi.nlm.nih.gov/pubmed/14715296. Accessed April 5, 2018.

23. Agresti JJ, Antipov E, Abate AR, et al. Ultrahigh-throughput screening in drop-based microfluidics for directed evolution. *Proc Natl Acad Sci U S A.* 2010;107(9):4004-4009. doi:10.1073/pnas.0910781107.

24. McCafferty J, Griffiths AD, Winter G, Chiswell DJ. Phage antibodies: filamentous phage displaying antibody variable domains. *Nature.* 1990;348(6301):552-554. doi:10.1038/348552a0.

25. Hanes J, Plückthun A. In vitro selection and evolution of functional proteins by using ribosome display. *Proc Natl Acad Sci U S A.* 1997;94(10):4937-4942. http://www.ncbi.nlm.nih.gov/pubmed/9144168. Accessed April 5, 2018.

26. Wilson DS, Keefe AD, Szostak JW. The use of mRNA display to select high-affinity protein-binding peptides. *Proc Natl Acad Sci.* 2001;98(7):3750-3755. doi:10.1073/pnas.061028198.

27. Boder ET, Midelfort KS, Wittrup KD. Directed evolution of antibody fragments with monovalent femtomolar antigen-binding affinity. *Proc Natl Acad Sci.* 2000;97(20):10701-10705. doi:10.1073/pnas.170297297.

28. Tasumi S, Velikovsky CA, Xu G, et al. High-affinity lamprey VLRA and VLRB monoclonal antibodies. *Proc Natl Acad Sci U S A.* 2009;106(31):12891-12896. doi:10.1073/pnas.0904443106.

29. Wozniak-Knopp G, Bartl S, Bauer A, et al. Introducing antigen-binding sites in structural loops of immunoglobulin constant domains: Fc fragments with engineered HER2/neu-binding sites and antibody properties. *Protein Eng Des Sel.* 2010;23(4):289-297. doi:10.1093/protein/gzq005.

30. Rajpal A, Beyaz N, Haber L, et al. A general method for greatly improving the affinity of antibodies by using combinatorial libraries. *Proc Natl Acad Sci.* 2005;102(24):8466-8471. doi:10.1073/pnas.0503543102.

31. Boder ET, Raeeszadeh-Sarmazdeh M, Price JV. Engineering antibodies by yeast display. *Arch Biochem Biophys.* 2012;526(2):99-106. doi:10.1016/j.abb.2012.03.009.

32. Cherf GM, Cochran JR. Applications of Yeast Surface Display for Protein Engineering. *Methods Mol Biol.* 2015;1319:155-175. doi:10.1007/978-1-4939-2748-7_8.

33. Saeed AFUH, Wang R, Ling S, Wang S. Antibody Engineering for Pursuing a Healthier Future. *Front Microbiol.* 2017;8:495. doi:10.3389/fmicb.2017.00495.

34. Steiner D, Forrer P, Plückthun∗ A. Efficient Selection of DARPins with Sub-nanomolar Affinities using SRP Phage Display. 2008. doi:10.1016/j.jmb.2008.07.085.

35. Seeger MA, Zbinden R, Flütsch A, et al. Design, construction, and characterization of a second-generation DARP in library with reduced hydrophobicity. *Protein Sci.* 2013;22(9):1239-1257. doi:10.1002/pro.2312.

36. Silverman AP, Levin AM, Lahti JL, Cochran JR. Engineered cystine-knot peptides that bind alpha(v)beta(3) integrin with antibody-like affinities. *J Mol Biol.* 2009;385(4):1064-1075. doi:10.1016/j.jmb.2008.11.004.

37. Koide A, Bailey CW, Huang X, Koide S. The fibronectin type III domain as a scaffold for novel binding proteins. *J Mol Biol.* 1998;284(4):1141-1151. doi:10.1006/JMBI.1998.2238.

38. Holler PD, Holman PO, Shusta E V, O'Herrin S, Wittrup KD, Kranz DM. In vitro evolution of a T cell receptor with high affinity for peptide/MHC. *Proc Natl Acad Sci U S A.* 2000;97(10):5387-5392. doi:10.1073/pnas.080078297.

39. Balaji M. Rao ‡, Ian Driver ‡, Douglas A. Lauffenburger § and, K. Dane Wittrup* §. High-Affinity

CD25-Binding IL-2 Mutants Potently Stimulate Persistent T Cell Growth†. 2005. doi:10.1021/BI050436X.

40. Goldsmith M, Tawfik DS. Enzyme engineering by targeted libraries. *Methods Enzymol.* 2013;523:257-283. doi:10.1016/B978-0-12-394292-0.00012-6.

41. Bershtein S, Tawfik DS. Ohno's model revisited: measuring the frequency of potentially adaptive mutations under various mutational drifts. *Mol Biol Evol.* 2008;25(11):2311-2318. doi:10.1093/molbev/msn174.

42. Case DA, Cheatham TE, Darden T, et al. The Amber biomolecular simulation programs. *J Comput Chem.* 2005;26(16):1668-1688. doi:10.1002/jcc.20290.

43. Brooks BR, Brooks CL, Mackerell AD, et al. CHARMM: the biomolecular simulation program. *J Comput Chem.* 2009;30(10):1545-1614. doi:10.1002/jcc.21287.

44. Boas FE, Harbury PB. Potential energy functions for protein design. *Curr Opin Struct Biol.* 2007;17(2):199-204. doi:10.1016/J.SBI.2007.03.006.

45. Tanaka S, Scheraga HA. Medium- and long-range interaction parameters between amino acids for predicting three-dimensional structures of proteins. *Macromolecules.* 1976;9(6):945-950. http://www.ncbi.nlm.nih.gov/pubmed/1004017. Accessed April 6, 2018.

46. Park J, Saitou K. ROTAS: a rotamer-dependent, atomic statistical potential for assessment and prediction of protein structures. *BMC Bioinformatics.* 2014;15(1):307. doi:10.1186/1471-2105-15-307.

47. Shen M, Sali A. Statistical potential for assessment and prediction of protein structures. *Protein Sci.* 2006;15(11):2507-2524. doi:10.1110/ps.062416606.

48. Sippl MJ. Recognition of errors in three-dimensional structures of proteins. *Proteins Struct Funct Genet.* 1993;17(4):355-362. doi:10.1002/prot.340170404.

49. Eramian D, Shen M, Devos D, Melo F, Sali A, Marti-Renom MA. A composite score for predicting errors in protein structure models. *Protein Sci.* 2006;15(7):1653-1666. doi:10.1110/ps.062095806.

50. Gohlke H, Hendlich M, Klebe G. Knowledge-based scoring function to predict protein-ligand interactions. *J Mol Biol.* 2000;295(2):337-356. doi:10.1006/jmbi.1999.3371.

51. Su Y, Zhou A, Xia X, Li W, Sun Z. Quantitative prediction of protein-protein binding affinity with a potential of mean force considering volume correction. *Protein Sci.* 2009;18(12):2550-2558. doi:10.1002/pro.257.

52. DeBartolo J, Dutta S, Reich L, Keating AE. Predictive Bcl-2 Family Binding Models Rooted in Experiment or Structure. *J Mol Biol.* 2012;422(1):124-144. doi:10.1016/j.jmb.2012.05.022.

53. Mackenzie CO, Zhou J, Grigoryan G. Tertiary alphabet for the observable protein structural universe. *Proc Natl Acad Sci U S A.* 2016;113(47):E7438-E7447. doi:10.1073/pnas.1607178113.

54. Zheng F, Grigoryan G. Sequence statistics of tertiary structural motifs reflect protein stability. Srinivasan N, ed. *PLoS One.* 2017;12(5):e0178272. doi:10.1371/journal.pone.0178272.

55. Simons KT, Kooperberg C, Huang E, Baker D. Assembly of protein tertiary structures from fragments with similar local sequences using simulated annealing and Bayesian scoring functions. *J Mol Biol.* 1997;268(1):209-225. doi:10.1006/jmbi.1997.0959.

56. Simons KT, Ruczinski I, Kooperberg C, Fox BA, Bystroff C, Baker D. Improved recognition of native-like protein structures using a combination of sequence-dependent and sequence-independent features of proteins. *Proteins.* 1999;34(1):82-95. http://www.ncbi.nlm.nih.gov/pubmed/10336385. Accessed April 6, 2018.

57. Kuhlman B, Baker D. Native protein sequences are close to optimal for their structures. *Proc Natl Acad Sci U S A.* 2000;97(19):10383-10388. http://www.ncbi.nlm.nih.gov/pubmed/10984534. Accessed April 6, 2018.

58. Alford RF, Leaver-Fay A, Jeliazkov JR, et al. The Rosetta All-Atom Energy Function for Macromolecular Modeling and Design. *J Chem Theory Comput.* 2017;13(6):3031-3048.

doi:10.1021/acs.jctc.7b00125.

59. Schymkowitz J, Borg J, Stricher F, Nys R, Rousseau F, Serrano L. The FoldX web server: an online force field. *Nucleic Acids Res.* 2005;33(Web Server):W382-W388. doi:10.1093/nar/gki387.

60. Chevalier A, Silva D-A, Rocklin GJ, et al. Massively parallel de novo protein design for targeted therapeutics. *Nature.* 2017;550(7674):74-79. doi:10.1038/nature23912.

61. Fleishman SJ, Whitehead TA, Ekiert DC, et al. Computational Design of Proteins Targeting the Conserved Stem Region of Influenza Hemagglutinin. *Science (80-).* 2011;332(6031):816-821. doi:10.1126/science.1202617.

62. Rosenfeld L, Heyne M, Shifman JM, Papo N. Protein Engineering by Combined Computational and In Vitro Evolution Approaches. *Trends Biochem Sci.* 2016;41(5):421-433. doi:10.1016/j.tibs.2016.03.002.

63. Chen TS, Keating AE. Designing specific protein-protein interactions using computation, experimental library screening, or integrated methods. *Protein Sci.* 2012;21(7):949-963. doi:10.1002/pro.2096.

64. Wang W, Saven JG. Designing gene libraries from protein profiles for combinatorial protein experiments. *Nucleic Acids Res.* 2002;30(21):e120. http://www.ncbi.nlm.nih.gov/pubmed/12409479. Accessed April 5, 2018.

65. Treynor TP, Vizcarra CL, Nedelcu D, Mayo SL. Computationally designed libraries of fluorescent proteins evaluated by preservation and diversity of function. *Proc Natl Acad Sci U S A.* 2007;104(1):48-53. doi:10.1073/pnas.0609647103.

66. Smith SN, Wang Y, Baylon JL, et al. Changing the peptide specificity of a human T-cell receptor by directed evolution. *Nat Commun.* 2014;5:5223. doi:10.1038/ncomms6223.

67. Foight GW, Keating AE. Locating Herpesvirus Bcl-2 Homologs in the Specificity Landscape of Anti-Apoptotic Bcl-2 Proteins. *J Mol Biol.* 2015;427(15):2468-2490. doi:10.1016/j.jmb.2015.05.015.

68. Chen TS, Palacios H, Keating AE. Structure-Based Redesign of the Binding Specificity of Anti-Apoptotic Bcl-xL. *J Mol Biol.* 2013;425(1):171-185. doi:10.1016/j.jmb.2012.11.009.

69. Guntas G, Hallett RA, Zimmerman SP, et al. Engineering an improved light-induced dimer (iLID) for controlling the localization and activity of signaling proteins. *Proc Natl Acad Sci U S A.* 2015;112(1):112-117. doi:10.1073/pnas.1417910112.

70. Hilpert K, Winkler DFH, Hancock REW. Peptide arrays on cellulose support: SPOT synthesis, a time and cost efficient method for synthesis of large numbers of peptides in a parallel and addressable fashion. *Nat Protoc.* 2007;2(6):1333-1349. doi:10.1038/nprot.2007.160.

71. Beyer M, Nesterov A, Block I, et al. Combinatorial Synthesis of Peptide Arrays onto a Microchip. *Science (80-).* 2007;318(5858):1888-1888. doi:10.1126/science.1149751.

72. Toepert F, Knaute T, Guffler S, et al. Combining SPOT Synthesis and Native Peptide Ligation to Create Large Arrays of WW Protein Domains. *Angew Chemie Int Ed.* 2003;42(10):1136-1140. doi:10.1002/anie.200390298.

73. McLaughlin RN, Poelwijk FJ, Raman A, Gosal WS, Ranganathan R. The spatial architecture of protein function and adaptation. *Nature.* 2012;491(7422):138-142. doi:10.1038/nature11500.

74. Younger D, Berger S, Baker D, Klavins E. High-throughput characterization of protein-protein interactions by reprogramming yeast mating. *Proc Natl Acad Sci U S A.* 2017;114(46):12166-12171. doi:10.1073/pnas.1705867114.

75. Fowler DM, Araya CL, Fleishman SJ, et al. High-resolution mapping of protein sequence-function relationships. *Nat Methods.* 2010;7(9):741-746. doi:10.1038/nmeth.1492.

76. Reich LL, Dutta S, Keating AE. SORTCERY-A High-Throughput Method to Affinity Rank Peptide Ligands. *J Mol Biol.* 2015;427(11):2135-2150. doi:10.1016/j.jmb.2014.09.025.

77. Kinney JB, Murugan A, Callan CG, Cox EC. Using deep sequencing to characterize the biophysical mechanism of a transcriptional regulatory sequence. *Proc Natl Acad Sci.*

2010;107(20):9158-9163. doi:10.1073/pnas.1004290107.

78. Adams RM, Mora T, Walczak AM, Kinney JB. Measuring the sequence-affinity landscape of antibodies with massively parallel titration curves. *Elife*. 2016;5. doi:10.7554/eLife.23156.

79. Sharon E, Kalma Y, Sharp A, et al. Inferring gene regulatory logic from high-throughput measurements of thousands of systematically designed promoters. *Nat Biotechnol*. 2012;30(6):521-530. doi:10.1038/nbt.2205.

80. Reich L "Luther," Dutta S, Keating AE. Generating High-Accuracy Peptide-Binding Data in High Throughput with Yeast Surface Display and SORTCERY. In: ; 2016:233-247. doi:10.1007/978-1-4939-3569-7_14.

81. Sirin S, Apgar JR, Bennett EM, Keating AE. AB-Bind: Antibody binding mutational database for computational affinity predictions. *Protein Sci*. 2016;25(2):393-409. doi:10.1002/pro.2829.

82. Moal IH, Fernández-Recio J. SKEMPI: a Structural Kinetic and Energetic database of Mutant Protein Interactions and its use in empirical models. *Bioinformatics*. 2012;28(20):2600-2607. doi:10.1093/bioinformatics/bts489.

83. Kortemme T, Baker D. A simple physical model for binding energy hot spots in protein-protein complexes. *Proc Natl Acad Sci U S A*. 2002;99(22):14116-14121. doi:10.1073/pnas.202485799.

84. Moretti R, Fleishman SJ, Agius R, et al. Community-wide evaluation of methods for predicting the effect of mutations on protein-protein interactions. *Proteins*. 2013;81(11):1980-1987. doi:10.1002/prot.24356.

85. Rocklin GJ, Chidyausiku TM, Goreshnik I, et al. Global analysis of protein folding using massively parallel design, synthesis, and testing. *Science*. 2017;357(6347):168-175. doi:10.1126/science.aan0693.

86. Chevalier A, Silva D-A, Rocklin GJ, et al. Massively parallel de novo protein design for targeted therapeutics. *Nature*. 2017;550(7674):74-79. doi:10.1038/nature23912.

87. Wiedemann U, Boisguerin P, Leben R, et al. Quantification of PDZ domain specificity, prediction of ligand affinity and rational design of super-binding peptides. *J Mol Biol*. 2004;343(3):703-718. doi:10.1016/j.jmb.2004.08.064.

88. Gfeller D, Butty F, Wierzbicka M, et al. The multiple-specificity landscape of modular peptide recognition domains. *Mol Syst Biol*. 2011;7(1):484. doi:10.1038/msb.2011.18.

89. Dutta S, Ryan J, Chen TS, Kougentakis C, Letai A, Keating AE. Potent and specific peptide inhibitors of human pro-survival protein Bcl-xL. *J Mol Biol*. 2015;427(6 Pt B):1241-1253. doi:10.1016/j.jmb.2014.09.030.

90. Sio CF, Riemens AM, van der Laan J-M, Verhaert RMD, Quax WJ. Directed evolution of a glutaryl acylase into an adipyl acylase. *Eur J Biochem*. 2002;269(18):4495-4504. http://www.ncbi.nlm.nih.gov/pubmed/12230561. Accessed April 16, 2018.

91. Chaparro-Riggers JF, Polizzi KM, Bommarius AS. Better library design: data-driven protein engineering. *Biotechnol J*. 2007;2(2):180-191. doi:10.1002/biot.200600170.

92. Habibi N, Mohd Hashim SZ, Norouzi A, Samian M. A review of machine learning methods to predict the solubility of overexpressed recombinant proteins in Escherichia coli. *BMC Bioinformatics*. 2014;15(1):134. doi:10.1186/1471-2105-15-134.

93. Wilkinson DL, Harrison RG. Predicting the solubility of recombinant proteins in Escherichia coli. *Biotechnology (N Y)*. 1991;9(5):443-448. http://www.ncbi.nlm.nih.gov/pubmed/1367308. Accessed April 3, 2018.

94. Bedbrook CN, Yang KK, Rice AJ, Gradinaru V, Arnold FH. Machine learning to design integral membrane channelrhodopsins for efficient eukaryotic expression and plasma membrane localization. Maranas CD, ed. *PLOS Comput Biol*. 2017;13(10):e1005786. doi:10.1371/journal.pcbi.1005786.

95. Chang CCH, Li C, Webb GI, Tey B, Song J, Ramanan RN. Periscope: quantitative prediction of

soluble protein expression in the periplasm of Escherichia coli. *Sci Rep.* 2016;6(1):21844. doi:10.1038/srep21844.

96. Wang H, Feng L, Zhang Z, Webb GI, Lin D, Song J. Crysalis: an integrated server for computational analysis and design of protein crystallization. *Sci Rep.* 2016;6(1):21383. doi:10.1038/srep21383.

97. Radivojac P, Clark WT, Oron TR, et al. A large-scale evaluation of computational protein function prediction. *Nat Methods.* 2013;10(3):221-227. doi:10.1038/nmeth.2340.

98. Potapov V, Kaplan JB, Keating AE. Data-driven prediction and design of bZIP coiled-coil interactions. *PLoS Comput Biol.* 2015;11(2):e1004046. doi:10.1371/journal.pcbi.1004046.

99. Opferman JT. Attacking cancer's Achilles heel: antagonism of anti-apoptotic BCL-2 family members. *FEBS J.* August 2015. doi:10.1111/febs.13472.

100. Moldoveanu T, Follis AV, Kriwacki RW, Green DR. Many players in BCL-2 family affairs. *Trends Biochem Sci.* 2014;39(3):101-111. doi:10.1016/j.tibs.2013.12.006.

101. Montero J, Sarosiek KA, DeAngelo JD, et al. Drug-Induced Death Signaling Strategy Rapidly Predicts Cancer Response to Chemotherapy. *Cell.* 2015;160(5):977-989. doi:10.1016/j.cell.2015.01.042.

102. Ni Chonghaile T, Sarosiek KA, Vo T-T, et al. Pretreatment mitochondrial priming correlates with clinical response to cytotoxic chemotherapy. *Science.* 2011;334(6059):1129-1133. doi:10.1126/science.1206727.

103. Jenson JM, Ryan JA, Grant RA, Letai A, Keating AE. Epistatic mutations in PUMA BH3 drive an alternate binding mode to potently and selectively inhibit anti-apoptotic Bfl-1. *Elife.* 2017;6:e25541. doi:10.7554/eLife.25541.

104. Roberts AW, Seymour JF, Brown JR, et al. Substantial susceptibility of chronic lymphocytic leukemia to BCL2 inhibition: results of a phase I study of navitoclax in patients with relapsed or refractory disease. *J Clin Oncol.* 2012;30(5):488-496. doi:10.1200/JCO.2011.34.7898.

105. Rudin CM, Hann CL, Garon EB, et al. Phase II Study of Single-Agent Navitoclax (ABT-263) and Biomarker Correlates in Patients with Relapsed Small Cell Lung Cancer. *Clin Cancer Res.* 2012;18(11).

106. Schoenwaelder SM, Jarman KE, Gardiner EE, et al. Bcl-xL–inhibitory BH3 mimetics can induce a transient thrombocytopathy that undermines the hemostatic function of platelets. *Blood.* 2011;118(6).

107. Souers AJ, Leverson JD, Boghaert ER, et al. ABT-199, a potent and selective BCL-2 inhibitor, achieves antitumor activity while sparing platelets. *Nat Med.* 2013;19(2):202-208. doi:10.1038/nm.3048.

108. Kotschy A, Szlavik Z, Murray J, et al. The MCL1 inhibitor S63845 is tolerable and effective in diverse cancer models. *Nature.* 2016;538(7626):477-482. doi:10.1038/nature19830.

109. Foight GW, Ryan JA, Gullá S V, Letai A, Keating AE. Designed BH3 Peptides with High Affinity and Specificity for Targeting Mcl-1 in Cells. *ACS Chem Biol.* 2014;9(9):1962-1968. doi:10.1021/cb500340w.

110. Dutta S, Chen TS, Keating AE. Peptide ligands for pro-survival protein Bfl-1 from computationally guided library screening. *ACS Chem Biol.* 2013;8(4):778-788. doi:10.1021/cb300679a.

111. Berger S, Procko E, Margineantu D, et al. Computationally designed high specificity inhibitors delineate the roles of BCL2 family proteins in cancer. *Elife.* 2016;5:1422-1432. doi:10.7554/eLife.20352.

112. Mathieu A-L, Sperandio O, Pottiez V, et al. Identification of Small Inhibitory Molecules Targeting the Bfl-1 Anti-Apoptotic Protein That Alleviates Resistance to ABT-737. *J Biomol Screen.* 2014;19(7):1035-1046. doi:10.1177/1087057114534070.

113. Cashman JR, MacDonald M, Ghirmai S, et al. Inhibition of Bfl-1 with N-aryl maleimides. *Bioorg*

Med Chem Lett. 2010;20(22):6560-6564. doi:10.1016/j.bmcl.2010.09.046.

114. Zhai D, Jin C, Shiau C-W, Kitada S, Satterthwait AC, Reed JC. Gambogic acid is an antagonist of antiapoptotic Bcl-2 family proteins. *Mol Cancer Ther.* 2008;7(6):1639-1646. doi:10.1158/1535-7163.MCT-07-2373.

115. Zhai D, Godoi P, Sergienko E, et al. High-throughput fluorescence polarization assay for chemical library screening against anti-apoptotic Bcl-2 family member Bfl-1. *J Biomol Screen.* 2012;17(3):350-360. doi:10.1177/1087057111429372.

Chapter 2

Epistatic mutations in PUMA BH3 drive an alternate binding mode to potently and selectively inhibit anti-apoptotic Bfl-1

Jenson JM, Ryan JA, Grant RA, Letai A, Keating AE. Epistatic mutations in PUMA BH3 drive an alternate binding mode to potently and selectively inhibit anti-apoptotic Bfl-1. Elife. 2017;6:e25541. doi:10.7554/eLife.25541.

J.M.J. and A.E.K. designed and wrote the study. J.A.R. performed the BH3 profiling assays. J.M.J and R.A.G solved the x-ray crystal structures. J.M.J. did all remaining experiments.

Abstract

Overexpression of anti-apoptotic Bcl-2 family proteins contributes to cancer progression and confers resistance to chemotherapy. Small molecules that target Bcl-2 are used in the clinic to treat leukemia, but tight and selective inhibitors are not available for Bcl-2 paralog Bfl-1. Guided by computational analysis, we designed variants of the native BH3 motif PUMA that are > 150-fold selective for Bfl-1 binding. The designed peptides potently trigger disruption of the mitochondrial outer membrane in cells dependent on Bfl-1, but not in cells dependent on other anti-apoptotic homologs. High-resolution crystal structures show that designed peptide FS2 binds Bfl-1 in a shifted geometry, relative to PUMA and other binding partners, due to a set of epistatic mutations. FS2 modified with an electrophile reacts with a cysteine near the peptide-binding groove to augment specificity. Designed Bfl-1 binders provide reagents for cellular profiling and leads for developing enhanced and cell-permeable peptide or small-molecule inhibitors.

Introduction

Anti-apoptotic members of the Bcl-2 family are broadly recognized as promising cancer therapeutic targets. Human anti-apoptotic proteins Bcl-2, Bcl-x_L, Bcl-w, Mcl-1, and Bfl-1 have a globular, helical fold and function by binding to short, α-helical Bcl-2 homology 3 (BH3) motifs in pro-apoptotic proteins, as shown in Figure 2.1A. Competition for binding among BH3-containing proteins regulates mitochondrial outer membrane permeabilization (MOMP), which is an irreversible step towards caspase activation and cell death. The appropriate balance of interactions between pro-survival and pro-death Bcl-2 family members in healthy cells is often disrupted in cancer cells, where overexpression of anti-apoptotic Bcl-2 proteins can promote oncogenesis and confer resistance to chemotherapeutic agents[1].

There has been considerable progress developing BH3 mimetic peptides and small molecules to inhibit the function of anti-apoptotic Bcl-2 proteins by blocking their interactions. One outstanding example is the small molecule venetoclax, which targets Bcl-2 and was recently approved by the FDA for treatment of chronic lymphocytic leukemia[2,3]. A major challenge in developing venetoclax was achieving specificity, which is important because Bcl-2 family members support survival of healthy cells. For example, the small molecule ABT-263 inhibits both Bcl-2 and Bcl-x_L, but Bcl-x_L cross-reactivity leads to dose-limiting thrombocytopenia[4–6]. In the laboratory, highly selective inhibitors of anti-apoptotic proteins are used for profiling experiments that can establish which anti-apoptotic proteins are essential for cancer cell survival in individual patients and predict chemotherapeutic response *in vivo*[7–9]. There has been progress towards creating a panel of reagents specific for each mammalian anti-apoptotic protein that can

advance such diagnostic assays. Useful reagents for this purpose include peptides and small molecules that are selective for Mcl-1[10] or Bcl-x_L[11,12].

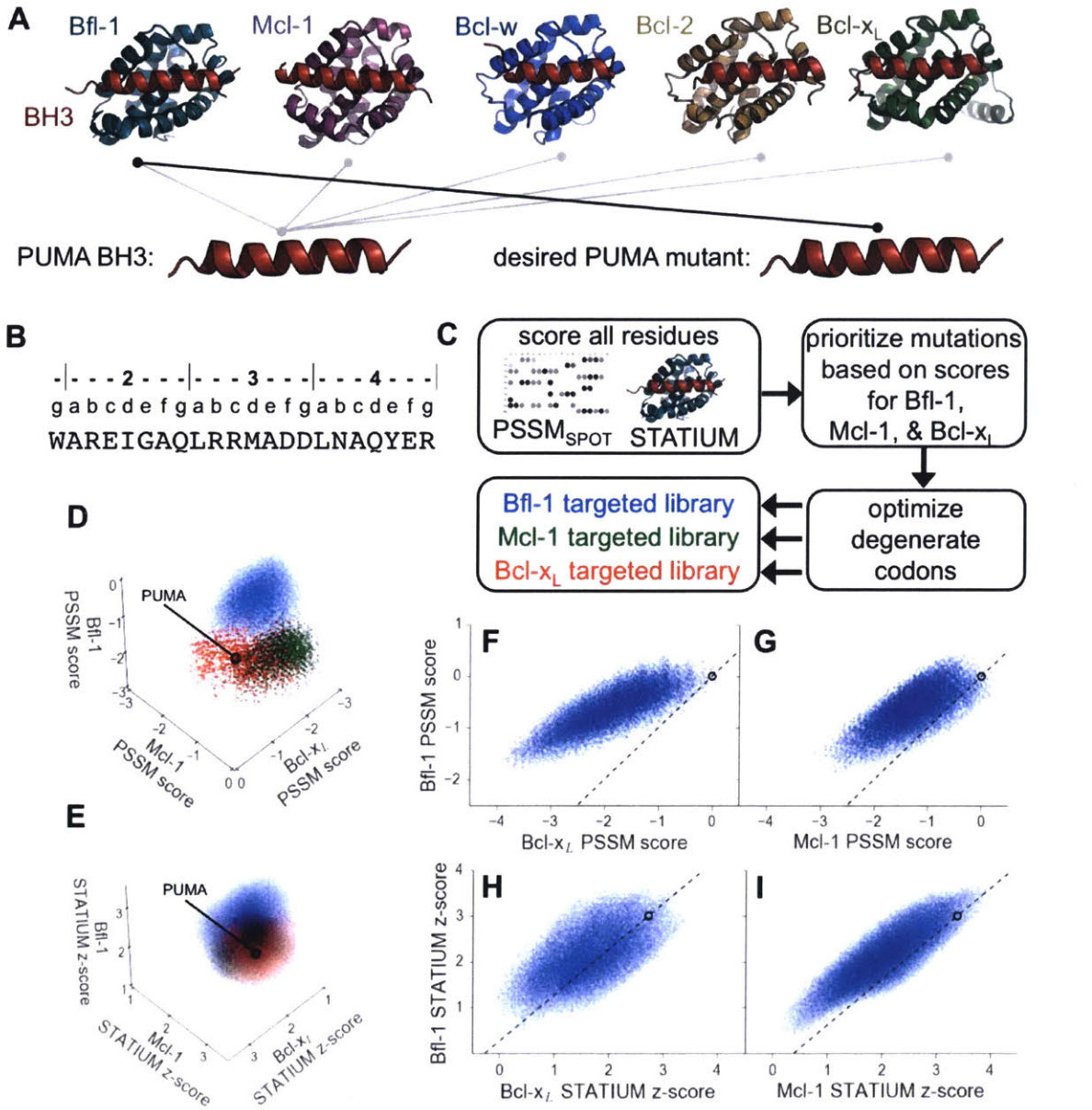

Figure 2.1. Computational design of a library of PUMA BH3 variants selective for Bfl-1. (A) PUMA BH3 is pan-selective; the design objective was a peptide that binds tightly only to Bfl-1. (B) Sequence of PUMA BH3 showing the heptad numbering convention used in this paper. (C) Overview of the computational library design procedure. (D-E) Scores for members of three libraries designed to target Bfl-1 (blue), Mcl-1 (green), or Bcl-x_L (red). (D) $PSSM_{SPOT}$ scores (E) STATIUM z-scores. (F-I) The affinities of library peptides for different Bcl-2 proteins were predicted to be strongly correlated. (F) $PSSM_{SPOT}$ scores for binding to Bcl-x_L versus Bfl-1, (G) $PSSM_{SPOT}$ scores for binding to Mcl-1 versus Bfl-1, (H) STATIUM z-scores for binding to Bcl-x_L versus Bfl-1, (I) STATIUM z-scores for binding to Mcl-1 versus Bfl-1. For (D-I), each point represents one peptide sequence and higher scores correspond to higher predicted affinities for the indicated target. Points on the dashed line have the same low specificity as PUMA BH3 (which is shown with a black open circle).

The role of anti-apoptotic protein Bfl-1 in cancer is less characterized than that of Mcl-1 or Bcl-x_L, but many lines of evidence suggest that Bfl-1 is also a critical target. In melanoma, Bfl-1 overexpression confers resistance to BRAF inhibitors, and siRNA mediated knockdown of Bfl-1 induces cell death in melanoma cell lines but not non-malignant cells[13–15]. Mis-regulation of Bfl-1 is also implicated in hematological malignancies, where elevated levels of Bfl-1 confer resistance to common chemotherapeutic agents. Bfl-1 knockdown suppresses resistance and sensitizes malignant B-cells to chemotherapy[16]. Bfl-1 expression can also counteract the effects of inhibitors of other anti-apoptotic family members (e.g. Mcl-1, Bcl-2) in leukemia and lymphoma[17]. Bfl-1 mRNA is over-expressed in myriad malignancies including solid tumor samples from breast, colon, ovary, and prostate tissues[18]. Thus, Bfl-1 is an intriguing therapeutic target and biomarker for resistance to cytotoxic anticancer drugs.

Identifying Bfl-1-selective interaction inhibitors has proven difficult. Small molecules must compete with an extended protein-peptide interface, and development of small-molecule inhibitors of Bcl-x_L, Bcl-2, and Mcl-1 required years of work, guided by intensive NMR studies of fragment binding[2,19,20]. Screening has identified small-molecule inhibitors of Bfl-1, but these compounds have IC_{50} values in the high nanomolar to low micromolar range and exhibit only modest specificity for Bfl-1 relative to other Bcl-2 family members[21–24]. Recently, helical bundle proteins that incorporate a BH3 motif have been designed to inhibit Bfl-1 and other anti-apoptotic proteins. These proteins are tight and selective binders, but their function relies on them being folded, and delivering proteins of molecular weight > 13 kDa into cells is problematic given current technologies[25].

An attractive strategy for inhibiting Bcl-2 family proteins is to develop short peptides that mimic the interaction geometry of native Bcl-2 protein complexes (Figure 2.1A). Screening BH3-like peptide libraries previously led to identification of a molecule with ~50 nM affinity for Bfl-1 and 30-fold specificity for Bfl-1 over Mcl-1,[26] but this peptide was not shown to induce mitochondrial depolarization in cell-based assays. Identifying Bfl-1 selective peptides is complicated by the extremely large sequence space of short BH3-like helical binders. There are more than 10^{29} possible peptides of length 23 residues. This sequence space is too large to exhaustively search experimentally. Furthermore, the BH3 motif is a weak motif (only three positions are strongly conserved) that does little to restrict possible binders. Another confounding factor is that Bfl-1 interacts with fewer BH3-like peptides than other anti-apoptotic Bcl-2 family paralogs do[27,28], and no native interaction partners are known to be selective for Bfl-1, suggesting that there may be limited opportunities for achieving specificity.

The results described here showcase our computational/experimental roadmap for designing selective peptide inhibitors. We used computational models to design a focused library of ~10^7 candidate binders and screened it to identify three peptides, FS1, FS2, and FS3, that bind tightly and specifically to Bfl-1. Mutational studies and high-resolution structures revealed that the high specificity comes from a BH3 binding mode that is markedly different from what has been seen in prior structures of Bfl-1:BH3 complexes[29,30]. Importantly, FS1, FS2, and FS3 are specific in BH3 profiling, an assay that tests for MOMP in cells. Subsequent rational introduction of an acrylamide moiety to covalently react with Bfl-1 further enhanced Bfl-1 inhibitor specificity. FS1, FS2, FS3

and their chemical derivatives provide new reagents with utility for studying Bfl-1 biology and a launching point for developing Bfl-1 targeting therapeutics.

Results

Computational analysis prioritizes mutations for targeted library design

To reduce the enormous space of possible 23-mer sequences to < 10^7 candidates that could be tested experimentally, we used computational modeling to design focused combinatorial libraries. We first scored mutations throughout the BH3 motif using: (1) a position-specific scoring matrix (PSSM) derived from SPOT peptide array data ($PSSM_{SPOT}$) and (2) STATIUM, a structure-based statistical potential that previously showed good performance evaluating Bcl-2 protein binding to BH3-like peptides (2. 1B,C)[28,31]. Mutations were modeled in the BIM BH3 motif, with the intention of testing the mutations in the context of both BIM and PUMA BH3 motifs. These two BH3-only proteins, as well as tBID, interact tightly with Bfl-1. BIM and PUMA bind with low nanomolar affinity to Bfl-1, but also to anti-apoptotic paralogs Bcl-2, Bcl-x_L, Mcl-1, and Bcl-w[26,27]. Thus, our design challenge was to introduce mutations that eliminate off-target binding without destabilizing Bfl-1 binding. Bfl-1 shares 38% binding-groove sequence identity with Mcl-1 and 30% binding-groove identity to Bcl-x_L. Bcl-2 and Bcl-w are closely related to Bcl-x_L, with 60% sequence identity in the binding groove[27]. To model cross-reactivity, we compared how mutations in BIM were predicted to affect binding to Bfl-1 relative to Bcl-x_L and Mcl-1, for which high quality structures of complexes are available. The predicted binding scores of diverse sequences for the three proteins were highly correlated, and most single mutations were predicted to weaken Bfl-1 binding compared to the wild-type sequence (Figure 2.2).

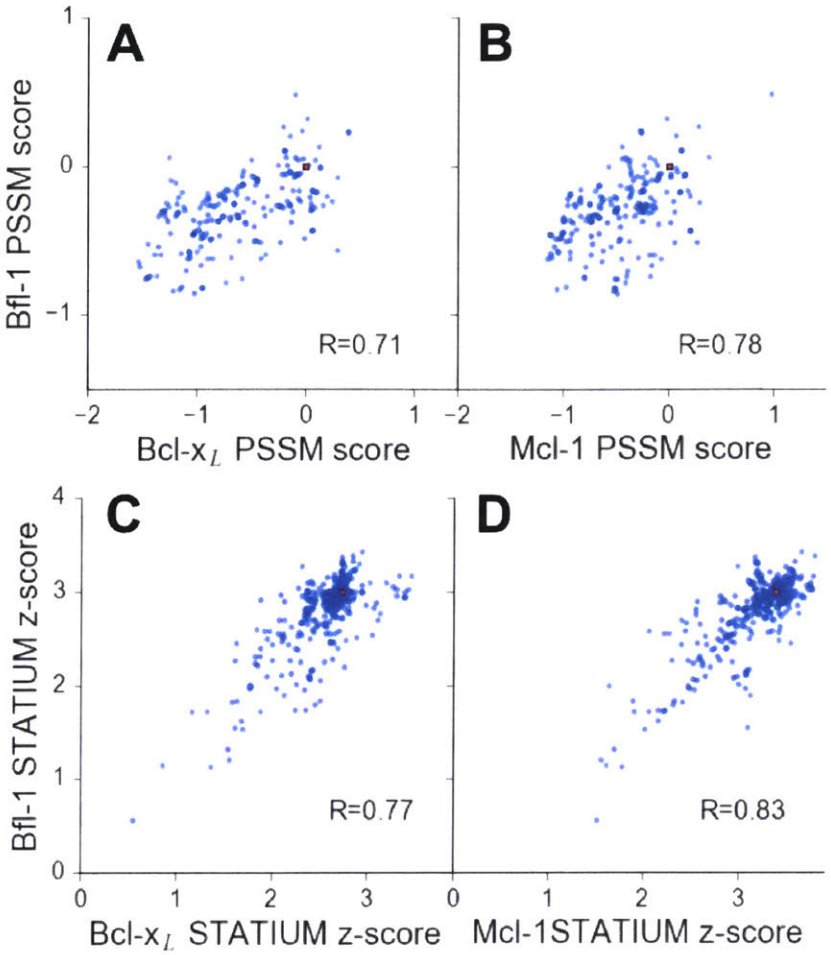

Figure 2.2. Affinities of BIM point mutants for different Bcl-2 proteins are predicted to be strongly correlated. Larger scores predict tighter binding. Red points represent wt PUMA BH3. (A) $PSSM_{SPOT}$ scores for binding to Bcl-x_L versus Bfl-1, (B) $PSSM_{SPOT}$ scores for binding to Mcl-1 versus Bfl-1, (C) STATIUM z-scores for binding to Bcl-x_L versus Bfl-1, (D) STATIUM z-scores for binding to Mcl-1 versus Bfl-1. Single point mutations to all residues other than cysteine and methionine were measured at positions 2d, 2e, 2g-3b, and 3d-4a for $PSSM_{SPOT}$ (A, B). Single point mutations to all residues were calculated for positions 1g, 2a, 2c-2e, 2g-3b, 3d-3f, 4a, 4b, 4e, and 4f for STATIUM (C, D). Pearson correlation coefficients are indicated.

Mutational scoring identified promising positions for introducing sequence variation (helix positions are defined in Figure 2.1B above the sequence of PUMA BH3). Bfl-1, Bcl-x_L, and Mcl-1 were predicted to have distinct residue preferences at conserved hydrophobic positions 3d and 4a, consistent with previous observations[32]. Many mutations at position 4e were predicted to be strongly Bfl-1 selective, which is supported by the observation that peptide binding by both Bcl-x_L, and Mcl-1 is

weakened by mutations at this position[33]. Mutations at positions 2a and 3g were also predicted to confer Bfl-1 specificity. In native BH3 motifs, these sites are generally occupied by small charged or polar residues that can form hydrogen bonds/salt-bridges with Bcl-x_L and Mcl-1 groups that are absent in Bfl-1. Finally, the region around sites 2e and 2g has local structural differences in Bfl-1, Mcl-1 and Bcl-x_L.

We used in-house software to select degenerate codons at variable sites that optimized the predicted Bfl-1 binding affinity and specificity and that provided chemical diversity in the resulting library[26,34]. The final library design included > $6.8*10^6$ unique sequences (Table 2.1), most of which were predicted to be Bfl-1 selective by $PSSM_{SPOT}$ and STATIUM (2.1 F-I). As a control, we designed similarly sized libraries to be selective for Bcl-x_L and Mcl-1 (Table 2.1). $PSSM_{SPOT}$ predicted each library to be enriched in peptides selective for the appropriate target, as shown in Figure 2.1D. In contrast, STATIUM predicted significantly more cross-reactivity for library members (Figure 2.1E, Figure 2.3).

Table 2.1. Composition of the Bcl-x_L, Mcl-1, and Bfl-1 targeted libraries

Position	BIM	PUMA	Bfl-1 Specific Library	Bcl-x_L Specific Library	Mcl-1 Specific Library
1g	P	W			AGPRSTW
2a	E	A	AEIKLPQTV	DEGHIKLMNQRSV	
2b	I	R			ACDFGHLPRSVY
2c	W	E			DEHQ
2d	I	I			AITV
2e	A	G	ACDGSY		AGISTV
2f	Q	A			
2g	E	Q	CDFGHILNRSVY		
3a	L	L			
3b	R	R		ADEGKNRST	AEGIKRTV
3c	R	R			
3d	I	M	ACFGILPRSTV	ADFHILNPSTVY	
3e	G	A		AG	
3f	D	D			
3g	E	D	DEHIKLMNQV		
4a	F	L	ADFHILNPSTVY		ADFHILNPSTVY
4b	N	N		ADHILNPTV	DEHKNQ
4c	A	A		ADEGKNRST	
4d	Y	Q			
4e	Y	Y	AFILPSTV	ACDGHNPRSTY	
4f	A	E			
4g	R	R			
5a	R	R			

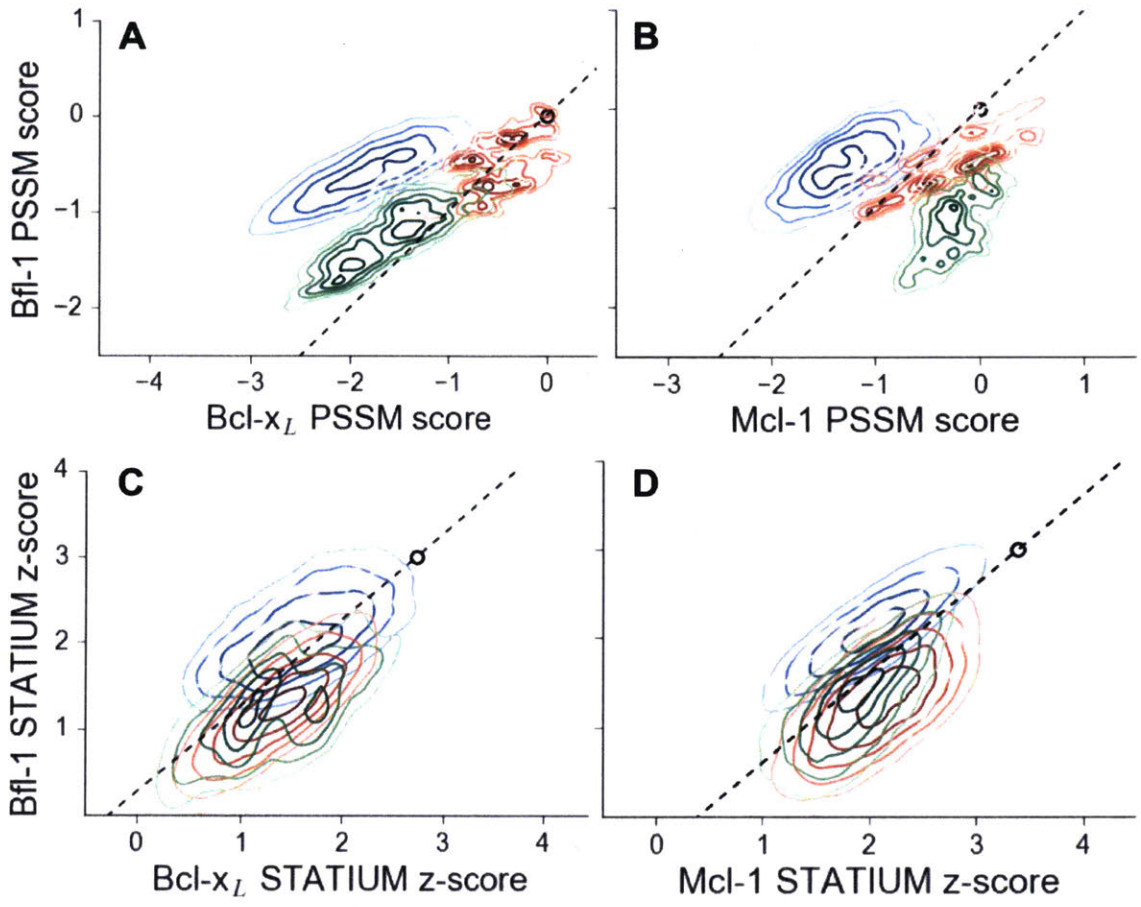

Figure 2.3. Scores for members of three libraries designed to target Bfl-1 (blue), Mcl-1 (green), or Bcl-x_L (red). Scores show predicted affinities of peptides in each library for each target. Larger scores predict tighter binding. (A) $PSSM_{SPOT}$ scores for binding to Bcl-x_L versus Bfl-1, (B) $PSSM_{SPOT}$ scores for binding to Mcl-1 versus Bfl-1, (C) STATIUM z-scores for binding to Bcl-x_L versus Bfl-1, (D) STATIUM z-scores for binding to Mcl-1 versus Bfl-1. Points on the dashed line have the same low specificity as PUMA BH3 (open black circle).

Experimental Library screening

Oligonucleotides encoding the peptide libraries designed to be specific for Bfl-1, Bcl-x_L, and Mcl-1 were synthesized in the context of BIM and PUMA BH3 sequences. Pooled BIM-based libraries and pooled PUMA-based libraries were then screened separately for tight and selective binding to Bfl-1. Screening the libraries designed for Mcl-1 and Bcl-x_L for binding to Bfl-1, in addition to the library designed to target Bfl-1, provided an opportunity to evaluate the utility of computational library focusing.

We used yeast-surface display to identify selective Bfl-1-binding peptides from our mixed libraries (Figure 2.4A). FACS analysis revealed that the initial libraries had a modest number of cells expressing peptides that bound to Bfl-1 at 100 nM (Figure 2.4B). This is consistent with predictions that less than 6.5% or 4% of the theoretical library would bind as well or better than PUMA, according to $PSSM_{SPOT}$ or STATIUM, respectively.

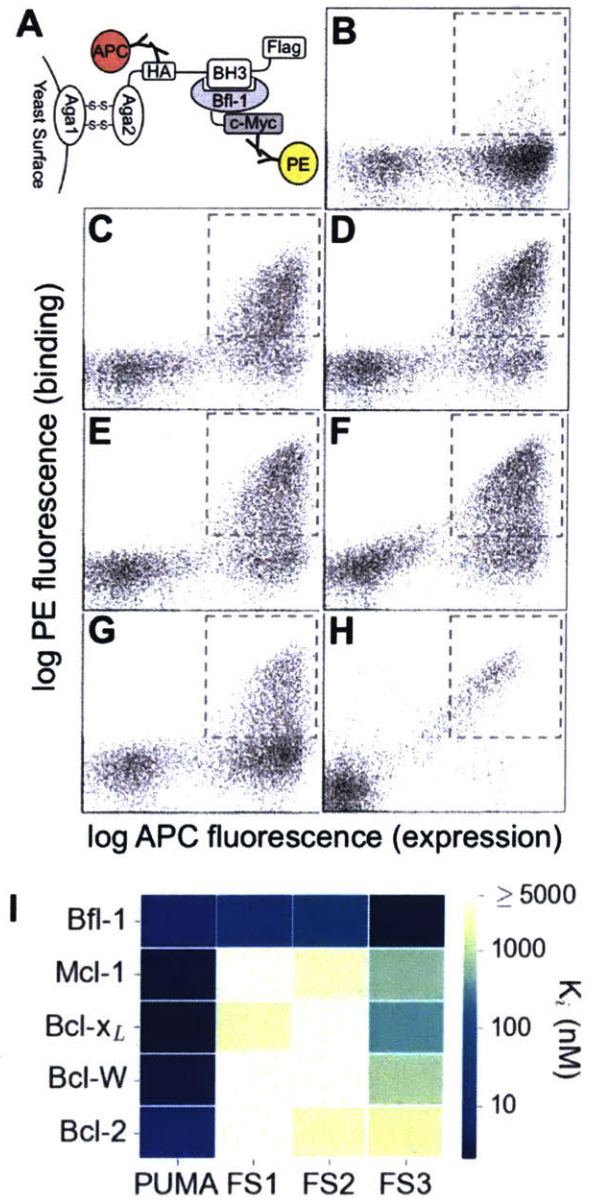

Figure 2.4. Experimental library screening for Bfl-1 affinity and selectivity. (A) Yeast-surface display configuration. BH3 peptides were expressed as fusions to Aga2; HA tag expression was detected with APC and Bfl-1 binding was detected with PE. (B) FACS analysis showed that only ~5 % of cells in the unsorted PUMA libraries bound to Bfl-1 at 100 nM. (C) Library binding to 100 nM Bfl-1 after one round of enrichment. (D-G) Library binding to off-target proteins (100 nM) after one round of enrichment: (D) Bcl-x_L (E) Bcl-2 (F) Bcl-w (G) Mcl-1. (H) Library binding to 100 nM Myc-tagged Bfl-1 in the presence of excess unlabeled competitor (Mcl-1, Bcl-2, Bcl-w, and Bcl-x_L; 1 μM each) after six rounds of enrichment. (I) Inhibition constants determined using fluorescence anisotropy for 23-residue peptides corresponding to PUMA BH3, FS1, FS2 and FS3.

Most of the peptides that bound Bfl-1 were cross-reactive with one or more other Bcl-2 family proteins (Figure 2.4C-G). This cross-reactivity was expected based on the high correlation of predicted binding scores for Bfl-1, Mcl-1, and Bcl-x_L and highlights the challenge of identifying specific binders (Figure 2.1D-E, Figure 2.2). Six rounds of positive, negative, and/or competition FACS screening were used to isolate cells that expressed the tightest and most Bfl-1-selective peptides (Figure 2.5). Mcl-1, Bcl-x_L, Bcl-2, and Bcl-w were included in the screen as untagged competitors. Early screening provided many Bfl-1 selective hits from the PUMA libraries, but few from the BIM libraries, so the BIM libraries were not pursued (Figure 2.6). After several rounds of competition screening, the PUMA library was enriched in cells displaying peptides that bound to Bfl-1 at 100 nM in the presence of 40-fold excess unlabeled competitor (Figure 2.4H).

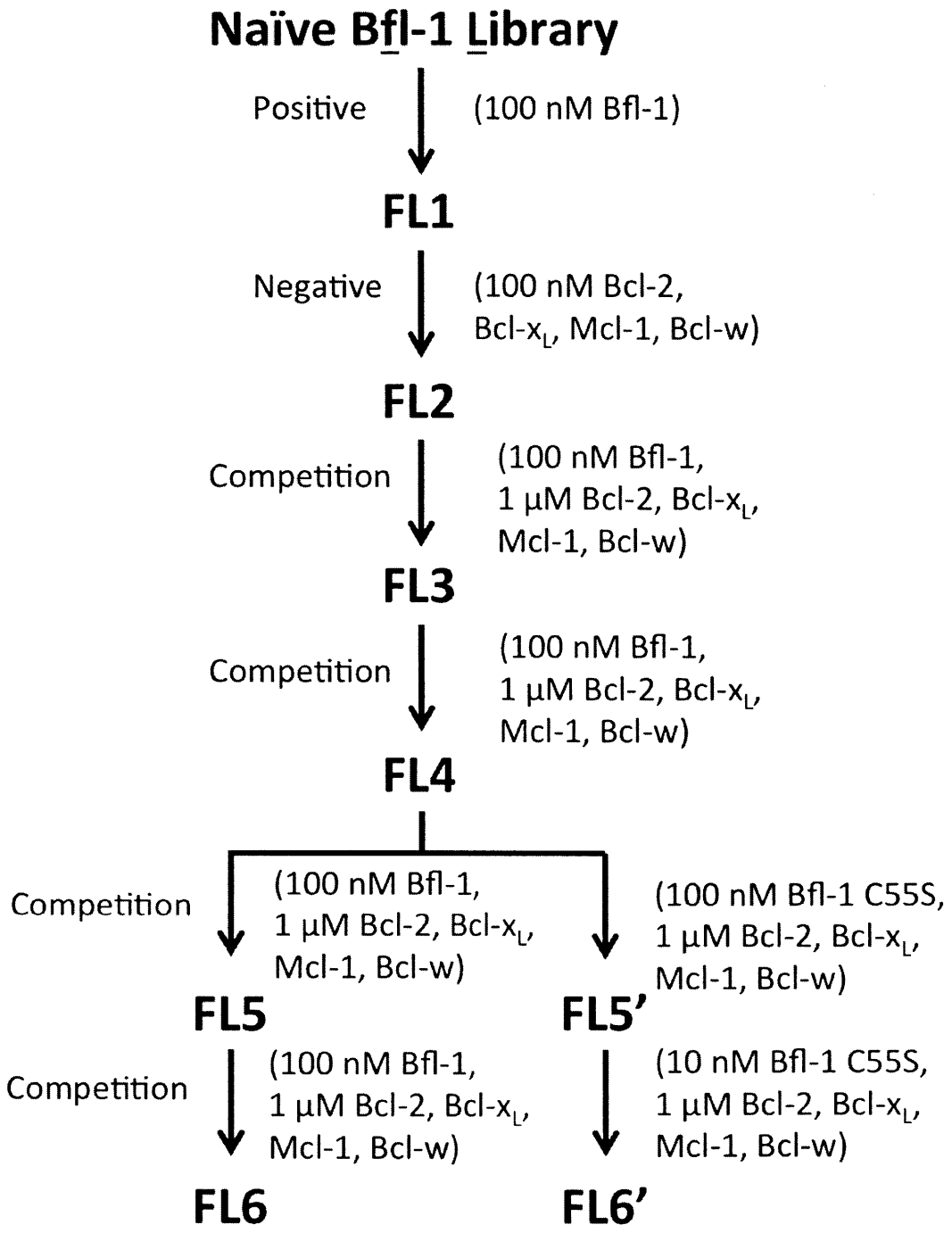

Figure 2.5. The PUMA BH3 library was screened to enrich for selective binders of Bfl-1. Several positive, negative, and competition screens were used to identify tight and selective Bfl-1 binders. Competition screens included unlabeled competitors at the indicated concentrations. In negative screens, cells that did not bind to the indicated labeled proteins were collected. Nearly all clones sequenced from pools FL5 and FL6 contained a cysteine in positions 1g-2e. Sorts FS5 and FS6 were repeated with the cysteine-to-serine point mutant of Bfl-1, C55S.

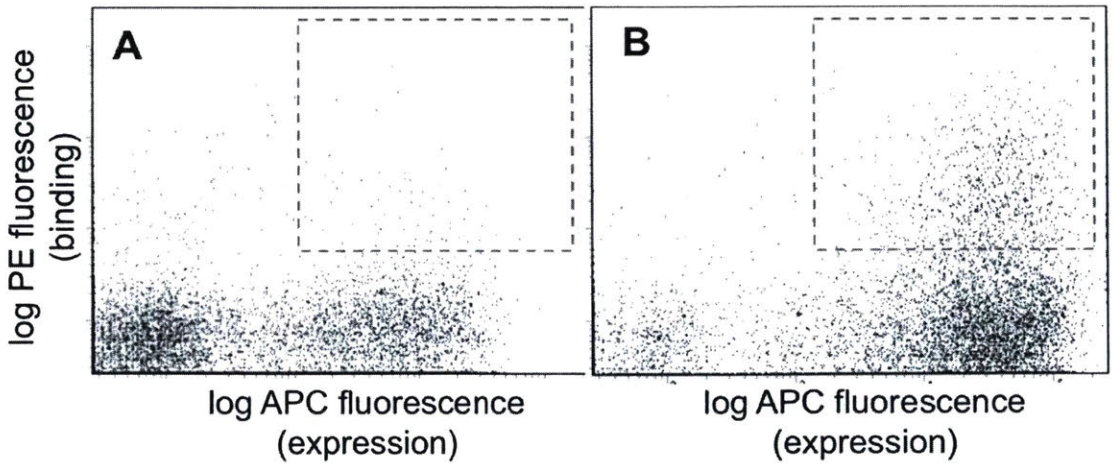

Figure 2.6. FACS analysis of the designed libraries after first two rounds of sorting (FL2, see Figure 2.5). Plots show binding of library peptides to 100 nM Myc-tagged Bfl-1 in the presence of excess unlabeled competitor (Mcl-1, Bcl-2, Bcl-w, and Bcl-x_L; 1 μM each) when encoded in (A) a BIM background or (B) a PUMA background. Cells displaying Bfl-1 selective peptides fall in the region outlined by dotted lines.

50 colonies isolated in the final round of screening were sequenced, providing 13 unique sequences. 9 sequences were from the Bfl-1 specific library, 2 were from the Bcl-x_L library, and 2 were from the Mcl-1 library (Table 2.2). We tested three Bfl-1 selective peptides that were recovered two or more times (FS1, FS2, and FS3). FS1, FS2, and FS3 were all derived from the Bfl-1 targeted library, although FS1 also contained one mutation caused by a spurious single-base pair mutation. FS1, FS2, and FS3 each had reduced affinity for Bfl-1 relative to PUMA, but significantly increased specificity (Figure 2.4I and Table 2.3). FS1 bound Bfl-1 with K_i = 15 nM and at least 150-fold specificity for Bfl-1 relative to Bcl-x_L, Bcl-2, Bcl-w, and Mcl-1.

Table 2.2. Conventionally sequenced clones from pool FL6'.

name	sequence	library	count
FS1	QWVREIAAGLRLAADNVNAQLER	Bfl-1	25
FS2	QWVREIAAGLRRAADDVNAQVER	Bfl-1	10
FS3	QWIREIAAGLRRFADILNAQVER	Bfl-1	5
	QWVREIGAGLRRIADNANAQLER	Bfl-1	1
	QWVRELGAQLRRYGDDLNKQDER	Bcl-x_L	1
	QWLREIGAGLRRSADDANAQPER	Bfl-1	1
	QWVREIGAQLRRTGDDLDEQDER	Bcl-x_L	1
	QWIREIDAFLRRFADQNNAQFER	Bfl-1	1
	QWIREIDAFLRPFADQNNAQFER	Bfl-1	1
	QWVREIAAGLRRAADKANAQPER	Bfl-1	1
	QRASEAGAQLGRMADDVEAQYER	Mcl-1	1
	QWAREIAAGLRRAADKVNAQVER	Bfl-1	1
	QSAAHTIAQLGRMADDAKAQYER	Mcl-1	1

Table 2.3. Peptide affinities for Bfl-1, Bcl-x_L, Mcl-1, Bcl-2, and Bcl-w. K_i obtained from competition assays with fluoresceinated BIM peptide. Data are mean ± SD of three replicates.

Peptide	Sequence ----2------3-----4--- fgabcdefgabcdefgabcdefg	K_i (nM) Bfl-1	Mcl-1	Bcl-x_L	Bcl-w	Bcl-2
PUMA	QWAREIGAQLRRMADDLNAQYER	4.8 ± .6	2.4 ± .8	2.3 ± 1.9	3 ± 2	6 ± 4
FS1	QWVREIAAGLRLAADNVNAQLER	15 ± 3	> 5000	2400 ± 400	> 5000	> 5000
FS2	QWVREIAAGLRRAADDVNAQVER	21 ± 6	3200 ± 300	> 5000	> 5000	2400 ± 500
FS3	QWIREIAAGLRRFADILNAQVER	2.1 ± .3	550 ± 150	320 ± 90	770 ± 80	2000 ± 300

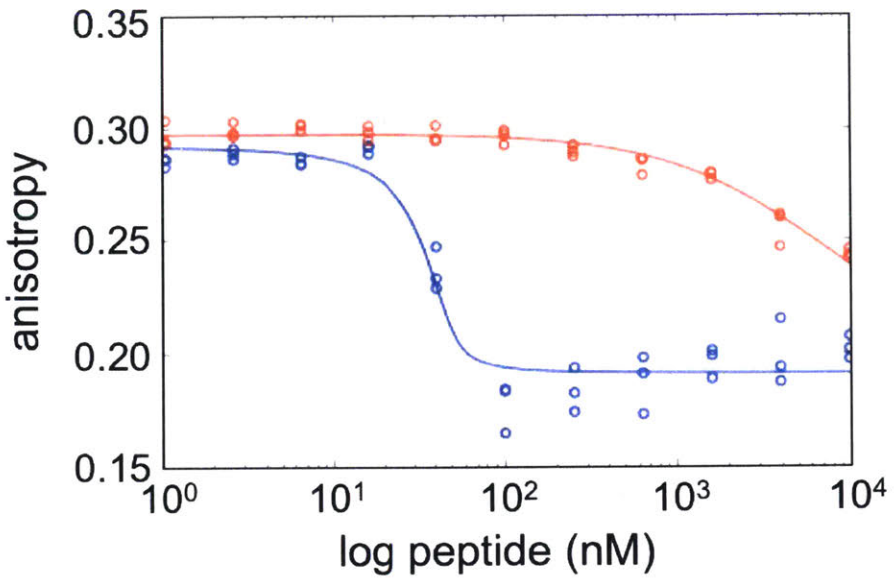

Figure 2.7. FS2 mutations made in a BIM background generate a weak binder of Bfl-1. Fluorescence anisotropy competition experiments for unlabeled BIM (blue) vs. BIM including mutations from FS2 (BIM-FS2; E2bV, A2eA, E2gG, I3dA, F4aV, Y4eV; red). BIM-FS2 (K_i = 720 ± 110 nM) binds > 1000-fold more weakly than native BIM (K_i < 0.1 nM). Data from are 3 independent measurements. K_i values are mean ± SD at least three replicates.

To analyze enrichment trends and to assess the success of our library design, we deep sequenced samples from the naïve pool and from pools collected after 3, 4, 5, and 6 rounds of sorting (sorting conditions are detailed in Figure 2.5). The naïve pool was diverse and not dominated by any particular subset of sequences. In contrast, FS1 (38% of sequences, the most prevalent library member), FS2 (25% of sequences), and many other peptides from the Bfl-1 targeted library were prominent in the final screening pool. Analysis of sequential pools showed that peptides from the Bfl-1 targeted library were substantially enriched relative to peptides from the Bcl-x_L and Mcl-1 targeted libraries (Figure 2.8A). 73.9% of the unique sequences in the final pool were from the Bfl-1 targeted library (Figure 2.8B).

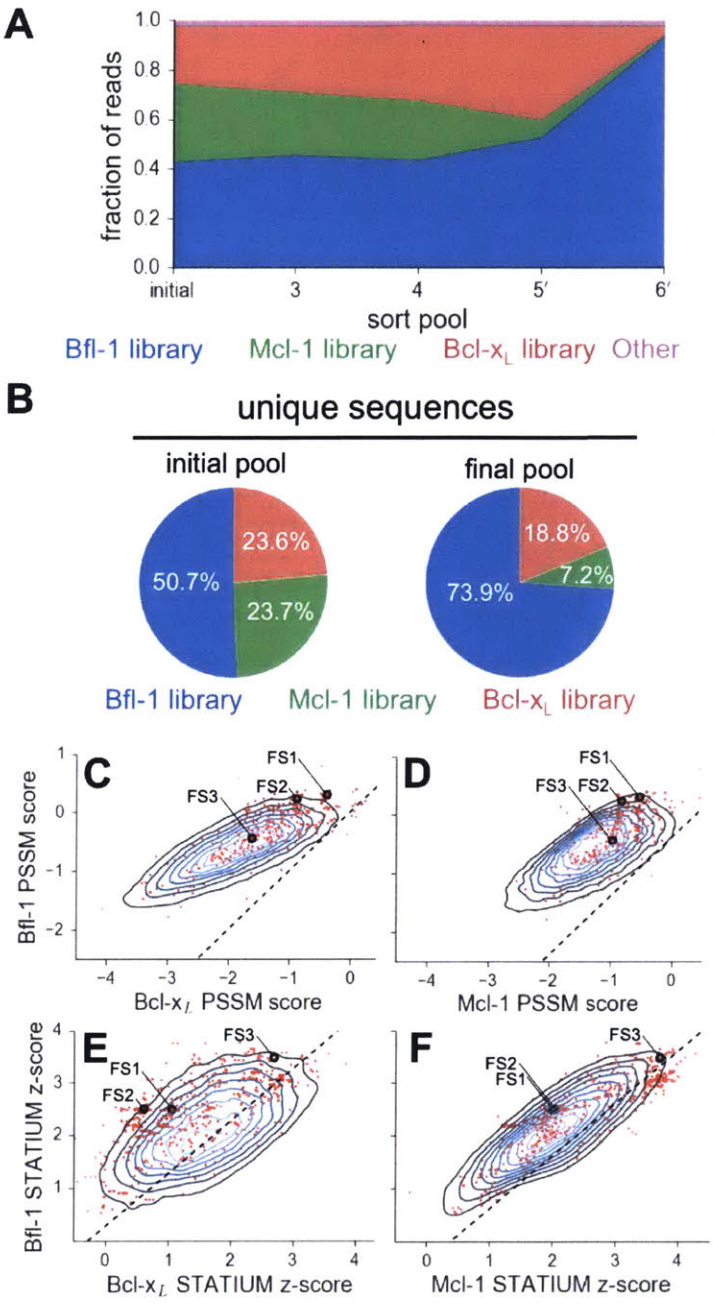

Figure 2.8. Evaluation of the library design. (A) Sequences from the Bfl-1 library were preferentially enriched during sorting. Sequences with no more than 1 amino-acid mutation from the Bfl-1 (blue), Mcl-1 (green), or Bcl-x_L (red) targeted libraries are plotted. Other sequences are shown in magenta. (B) The large majority of unique sequences in the final pool originated from the Bfl-1 library (colors as in part a). (C-F) Comparison of $PSSM_{SPOT}$ and STATIUM scores for the library before and after sorting. Peptides from the final sorted pool (red dots) are superimposed on the distribution of scores for the theoretical library (blue contour plots). Points to the left of the dotted lines correspond to peptides predicted to bind more selectively to Bfl-1 than does PUMA, with respect to the indicated competitor protein (Bcl-x_L in C and E, Mcl-1 in D and F). Scores for FS1, FS2 and FS3 are indicated.

We scored peptides from the Bfl-1 targeted library that passed all rounds of screening with the STATIUM and $PSSM_{SPOT}$ models used in library design (Figure 2.8 C-F). Most sequences were predicted to have improved selectivity for Bfl-1 relative to PUMA (98-99% with improved specificity over Bcl-x_L or Mcl-1 by $PSSM_{SPOT}$, and 95% or 62% with improved specificity over Bcl-x_L or Mcl-1, respectively, by STATIUM). The selected sequences were not among those predicted by either model to be the tightest or most Bfl-1 selective in the theoretical library.

The binding mode of Bfl-1-selective peptides

FS1, FS2, and FS3 included mutations to larger residues than those in PUMA at their N-termini (red in Figure 2.9B,C), and smaller residues at their C-termini (blue in Figure 2.9B,C). Deep sequencing of additional selective sequences supported this trend: Of 612 unique peptide sequences from the final round of sorting that originated from the Bfl-1 targeted library sequences, 364 showed this type of residue size patterning at the same sites (sequence logo in Figure 2.9A).

To assess whether the combination of large and small residues played a role in establishing binding specificity, we tested PUMA/FS2 chimeric peptides for binding to all five anti-apoptotic proteins. Mutating PUMA to introduce smaller residues at positions 2g, 3d, 4a, and 4e differentially impaired binding to all receptors and resulted in weak yet specific binding to Bfl-1 (Table 2.4). Mutating residues at the N-terminus of PUMA to larger residues at positions 2a and 2e gave a modest 2.3-fold increase in affinity for Bfl-1. But the same mutations in the context of smaller residues at positions 2g, 3d, 4a, and 4e improved affinity for Bfl-1 by 28.6-fold (Figure 2.9D). The different effects of these

mutations, when made in different contexts, indicates an energetic coupling consistent with a structural repositioning of the designed peptides in the groove of Bfl-1.

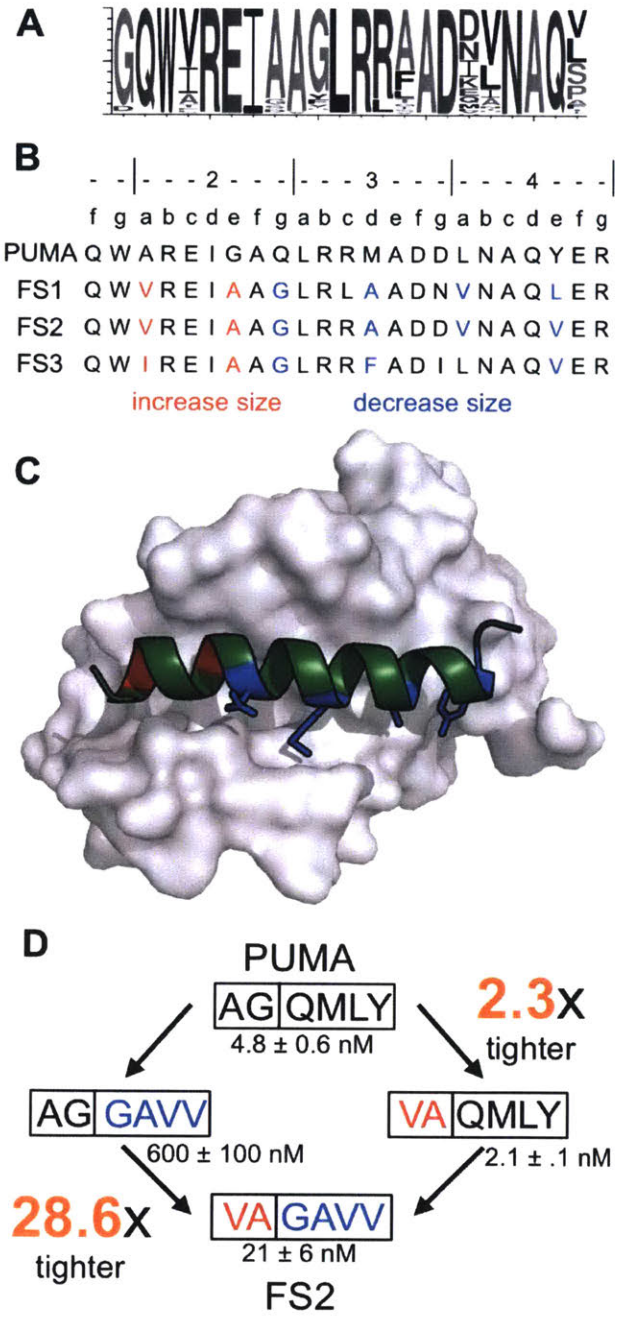

Figure 2.9. Epistatic mutations in PUMA confer Bfl-1 binding specificity. (A) Sequence logo of unique peptide sequences in the final sorted pool from the Bfl-1 targeted library. (B) Location of mutated sites in FS1, FS2, and FS3. Mutations at positions 2a and 2e are in red and positions 2g, 3d, 4a, and 4e are in blue. (C) Structure of Bfl-1 (gray surface) bound to PUMA (green, this work) with residues at positions 2a and 2e in red and those at 2g, 3d, 4a, and 4e in blue. (D) Non-additive mutational energies for PUMA/FS2 chimeric proteins indicate coupling between N- and C-terminal mutations. Data are K_i ± SD of 3 or more independent fluorescence anisotropy competition experiments.

Table 2.4. Affinities of FS2 chimeric proteins binding to Bfl-1, Bcl-x_L, Mcl-1, Bcl-2, and Bcl-w. K_i obtained from competition assays with fluoresceinated BIM peptide. Data are mean ± SD of three replicates.

Peptide	Sequence ----2------3-----4--- fgabcdefgabcdefgabcdefg	K_i (nM)[a]				
		Bfl-1	Mcl-1	Bcl-x_L	Bcl-w	Bcl-2
Puma	QWAREIGAQLRRMADDLNAQYER	4.8 ± .6	2.4 ± .8	2.3 ± 1.9	3 ± 2	6 ± 4
FS2_N/Puma_C	QWVREIAAQLRRMADDLNAQYER	2.1 ± .1	.3 ± .3	2.4 ± 1.2	1.2 ± .3	14 ± 2
Puma_N/FS2_C	QWAREIGAGLRRAADDVNAQVER	600 ± 100	> 5000	1100 ± 300	> 5000	2000 ± 160
FS2	QWVREIAAGLRRAADDVNAQVER	21 ± 6	3200 ± 300	> 5000	> 5000	2400 ± 500

To better understand the structural basis for the epistasis, we solved X-ray crystal structures of Bfl-1 bound to PUMA, at 1.33 Å resolution, and of Bfl-1 bound to FS2 at 1.2 Å resolution (Table 2.5). In comparison with all available X-ray structures of BH3 peptides bound to human or murine Bfl-1, PUMA and FS2 each adopt new, distinct positions in the binding groove (Figure 2.10A and Figure 2.11). FS2 is shifted 1.2 Å and rotated 17° in the binding groove compared to its parent peptide PUMA. The peptide C-terminus, which harbors the large-to-small mutations, is repositioned more dramatically than the N-terminus (Figure 2.10B). Despite the shifts in peptide binding geometry, the structures of Bfl-1 in these newly solved complexes are highly similar. The all-atom RMSD for residues in the binding pocket (within 5 Å of the BH3 peptide) of Bfl-1:FS2 vs. Bfl-1:PUMA is < 0.7 Å and is 1.05 Å for Bfl-1:FS2 vs. Bfl-1:BIM[29].

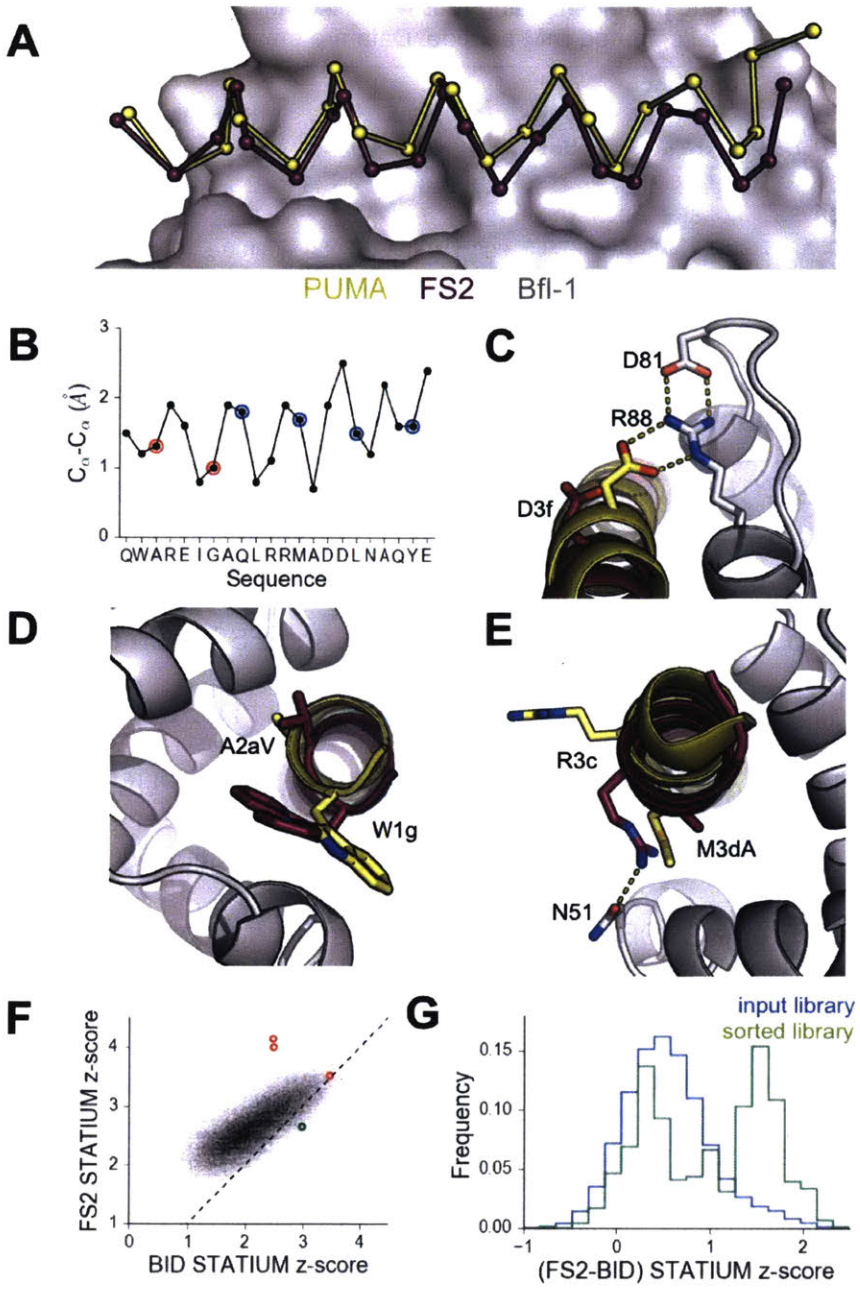

Figure 2.10. High-resolution structures of PUMA and FS2 bound to human Bfl-1. (A) Binding groove of Bfl-1 (gray, surface) with PUMA (yellow) and FS2 (purple). (B) C_α- C_α shifts between FS2 and PUMA. Sites with larger/smaller residues in FS2 are indicated in red/blue. (C) The canonical Bfl-1:BH3 salt bridge between D3f and R88 is observed in the Bfl-1:PUMA complex but not the Bfl-1:FS2 complex. (D) Tryptophan at 1g is rotated into the Bfl-1 binding groove in the Bfl-1:FS2 complex and away from the binding groove in the Bfl-1:PUMA complex. (E) In contrast with the solvent exposed arginine at position 3c of the Bfl-1:PUMA complex, R3c is oriented into the BH3 binding groove in the Bfl-1:FS2 complex, forming a hydrogen bond with N51 of Bfl-1. (F) Bfl-1 targeted library sequences score better on the Bfl-1:FS2 structure than on the Bfl-1:BID structure used for the initial library design; higher scores predict tighter binding. STATIUM z-scores for the Bfl-1 targeted library are in blue. FS1, FS2, and FS3 are indicated in red and PUMA in green. (G) Sorting enriched sequences that score better on the Bfl-1:FS2 template than on the Bfl-1:BID template. STATIUM z-scores for the input Bfl-1 library are in blue and scores for sequences identified after the final round of screening are in green.

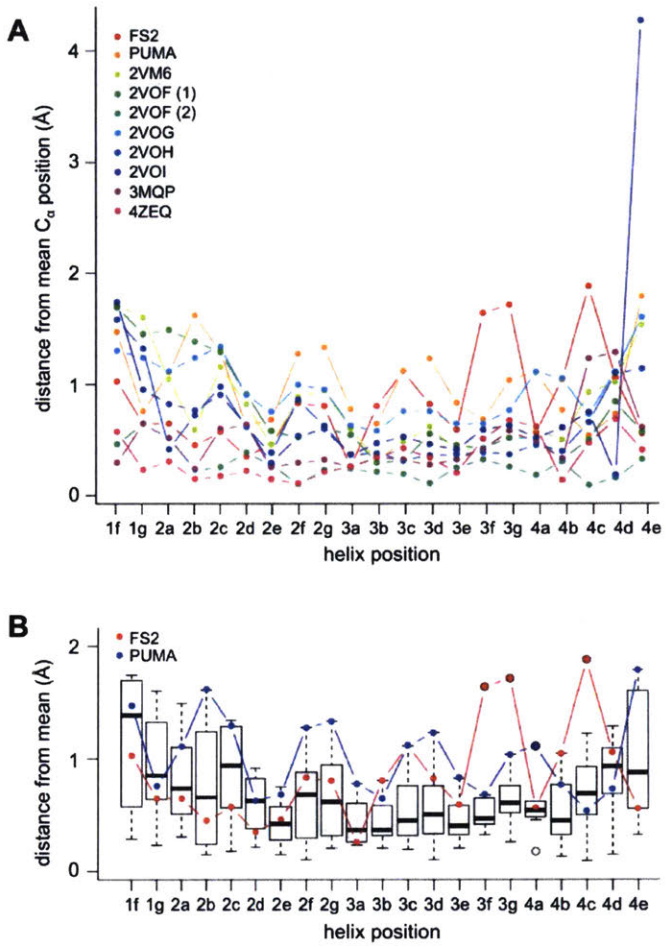

Figure 2.11. Comparison of PUMA and FS2 binding poses with crystal structures of BH3:Bfl-1 deposited in the PDB. All Bfl-1:peptide structures were aligned to Bfl-1 and the mean C-alpha positions were calculated for each BH3 peptide position. Mean distances were calculated separately for all complexes in the asymmetric unit. (A) The C-alpha distance deviation from the mean is plotted for all structures. (B) Box plots illustrate the positional variability at each site. FS2 is significantly shifted at peptide positions 3f, 3g, and 4c. The following structures from the PDB were included in this comparison: 2VM6[29], 2VOF[30], 2VOG[30], 2VOH[30], 2VOI[30], 3MQP[53], and 4ZEQ[64].

Table 2.5. Summary of X-ray data collection and refinement statistics.

	Bfl-1:Puma	Bfl-1:FS2	Bfl-1:FS2_1fX	Mcl-1:FS2
Data Collection				
Space Group	P 1 21 1	P 1 21 1	P 1 21 1	C 1 2 1
Cell parameters				
a, b, c	43.21, 43.43, 47.38	43.25, 43.33, 45.74	43.40, 43.50, 47.07	132.62, 62.76, 48.79
α, β, γ	90, 114.40, 90	90, 110.90, 90	90, 114.78, 90	90, 98.142, 90
Rmeas	0.066 (0.328)	.075 (534)	.083 (.357)	.164 (1.007)
Rpim	0.026 (0.166)	.022 (.196)	.035 (.185)	.067(.493)
Mean I/σ(I)	35.0 (3.0)	58.6 (3.8)	21.0 (2.4)	19.8 (2.5)
Completeness (%)	97 (75)	95 (89)	94 (52)	99 (96)
Redundancy	5.8 (3)	10.2 (5.5)	5.0 (2.6)	5.8 (3.6)
Refinement				
Resolution (Å)	43-1.33 (1.36-1.33)	36.59-1.199 (1.24 -1.199)	39.4-1.726 (1.788-1.726)	27.33-2.35 (2.41-2.35)
No. Reflections	35893 (2869)	47325 (4377)	15892 (974)	16697 (1625)
Rwork/Rfree	0.1325/0.1555 (0.1692/0.2385)	0.1435/0.1629 (0.2054/0.2287)	0.1802/0.2060 (0.3157/0.3360)	0.2162/0.2508 (0.2840/0.3594)
Number of non-hydrogen atoms	1597	1608	1529	3011
Average B-factors	21.68	27.32	29.24	48.77
Rmsd				
Bond lengths (Å)	0.006	0.008	0.003	0.003
Bond angles (°)	0.778	0.9	0.49	0.5

Values in parentheses are for the highest-resolution shell.

Further structural analysis showed that the Bfl-1:FS2 complex supports several key side-chain interactions that are absent in Bfl-1:PUMA and that may be important for selective binding. Surprisingly, aspartate at position 3f (D3f) in FS2, which is strongly conserved in known BH3 motifs, makes different interactions than what is observed in numerous previously solved Bcl-2 complex structures. D3f typically forms a salt bridge with arginine 88 (R88) in helix 4 in Bfl-1 or the corresponding arginine in Bcl-x_L, Mcl-1, Bcl-w, or Bcl-2 (Figure 2.10C). In the Bfl-1:FS2 structure, the carboxylate of D3f is shifted 5.6 Å away from the guanidinium group of R88, and is highly solvent exposed (Figure 2.10C). Because D3f does not form the canonical D3f:R88 interaction and is solvent exposed, we reasoned that FS2 should tolerate mutations at this site. This was confirmed by the tight binding of 6 peptides with alanine, serine, asparagine, glutamate, histidine or tyrosine at this position (Figure 2.12). Disruption of the D3f:R88 salt bridge

would be expected to reduce affinity for Bfl-1 and for all of the other anti-apoptotic receptors. However, in the Bfl-1:FS2 complex this change may be partially compensated by hydrogen bonding on the opposite side of the FS2 helix between arginine at position 3c (R3c) of FS2 and asparagine 51 (N51) of Bfl-1 (Figure 2.10E). In Bfl-1:FS2, position 3c is positioned closer to helix 2 of Bfl-1 than in Bfl-1:PUMA, allowing R3c to fill the space left by an adjacent methionine-to-alanine mutation at 3d when it adopts this hydrogen-bonded position. N51 at this position of helix 2 is unique to Bfl-1 among the human anti-apoptotic proteins (Figure 2.13).

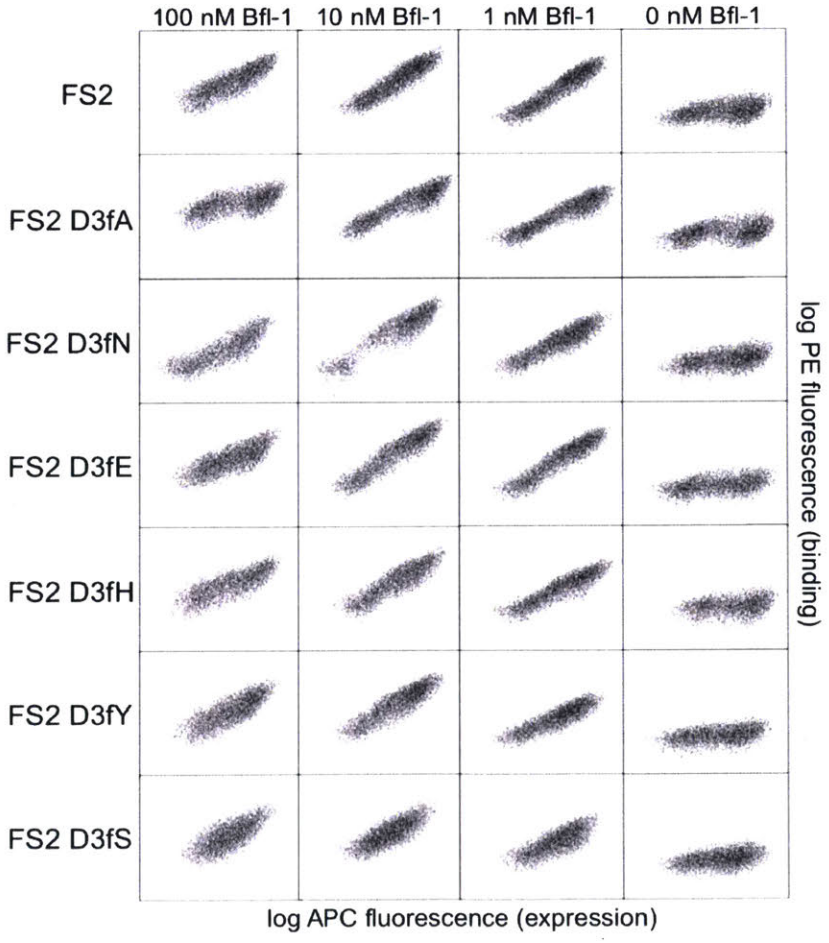

Figure 2.12. FACS analysis of cells displaying FS2 or FS2 with single point mutants at position 3f. FACS profiles for mutants are nearly indistinguishable from that of FS2. Data were collected the same day with the same settings, and all plots use the same scale of arbitrary units.

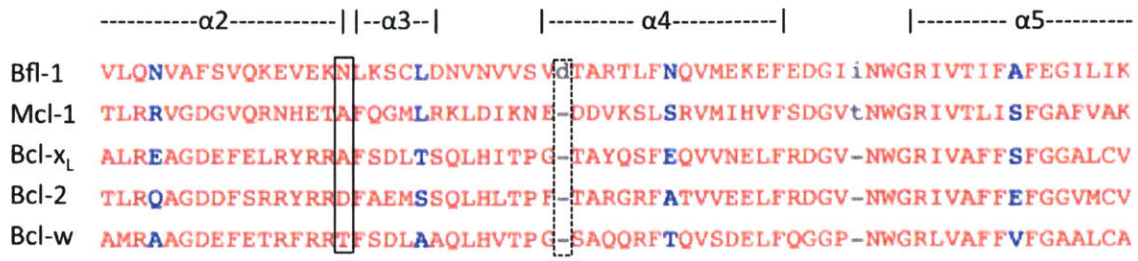

Figure 2.13. Multiple-sequence alignment of helices 2-4 of human anti-apoptotic Bfl-1 homologs. Bfl-1 has an amino-acid insertion that may contribute to the widened binding groove between helices 3 and 4 (dotted box). Additionally, there is an asparagine that is unique to Bfl-1 at the elbow between helix 2 and 3 that forms a hydrogen bond with FS2 (solid box). This interaction may contribute to the Bfl-1 specificity of FS2. Sequence alignment made using Cobalt[65].

Other structural differences between PUMA and FS2 binding are apparent near the N-terminal end of the peptide. Modeling FS2 mutations in the Bfl-1:PUMA structure suggested that the small-to-large mutation of alanine at position 2a in PUMA to the valine in FS2 would result in steric clashes with helix 4 of Bfl-1 for all backbone-dependent rotamers (Figure 2.14). This change is accommodated by the shift in the Bfl-1:FS2 structure. Also, a rotation of FS2 in the Bfl-1 binding groove partially buries the phenylalanine at position 1g that is solvent-exposed in the PUMA complex, which may be energetically favorable (Figure 2.10D).

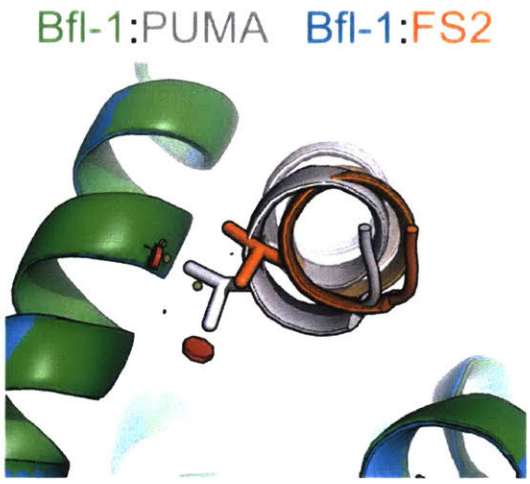

Figure 2.14. Residues in FS2 are not readily accommodated in the PUMA binding geometry. Modeling on a fixed backbone indicates that all valine rotamers would clash (red spheres) with Bfl-1 (green) when modeled in to position 2a of PUMA (gray). Shown here is the most preferred rotamer. The shifted binding mode of FS2 accommodates valine at position 2a. Model made using Pymol. Red lozenge indicates a steric clash as detected by the program.

Because the altered binding mode of FS2 is expected to impact predictions made using structure-based models, we re-scored the designed Bfl-1 library on the shifted Bfl-1:FS2 structure using STATIUM. FS1 and FS2 scored much better (higher) on the shifted model than on the original model, whereas PUMA scored better on the original model (Figure 2.10F). Analysis of the entire pool of sequences that passed screening showed that these peptides were enriched in sequences that scored better on the shifted model, compared to the input library, consistent with our observation of size patterning in the majority of these sequences (Figure 2.10G).

Structural analysis of off-target binding to Mcl-1

To better understand the structural basis of FS2 binding specificity, we solved the X-ray crystal structure of FS2 bound to Mcl-1 at 2.35 Å resolution. FS2 binding to Mcl-1 is > 100-fold weaker than binding to Bfl-1. Similar to the way FS2 binds to Bfl-1, FS2

engages Mcl-1 in a shifted orientation relative to BIM (Figure 2.15A, B). As is the case for FS2 binding to Bfl-1, this shift re-positions the highly conserved aspartate at peptide position 3f to a location 4.8 Å away from Mcl-1, disrupting the canonical salt bridge with arginine 92 (Figure 2.15C). This disruption would be expected to reduce affinity for Mcl-1, but it doesn't account for the specificity of FS2 for Bfl-1, because the salt bridge is lost in both complexes. There are other differences between the Bfl-1:FS2 and Mcl-1:FS2 structures that may account for some of the affinity difference. For example, R3c in FS2 forms a hydrogen bond with N51 of Bfl-1, but does not form an equivalent interaction with Mcl-1 and is instead solvent exposed (Figure 2.15D). In Mcl-1, there is an alanine (A55) at this site, and an adjacent histidine (H53) would be expected to clash with R3c if it adopted this conformation. The N-terminus of FS2 is also buried further into the binding groove of Bfl-1 than Mcl-1 (Figure 2.15E). The Bfl-1 binding groove is wider in this region than the Mcl-1 binding groove, as illustrated by aligning many Bfl-1 and Mcl-1 structures (Figure 2.16). This region of the groove is formed by helices 3 and 4. There is an amino acid insertion in the loop between helices 3 and 4 that is unique to Bfl-1 that likely contributes to the distinct structural environment of Bfl-1 in this region (Figure 2.13).

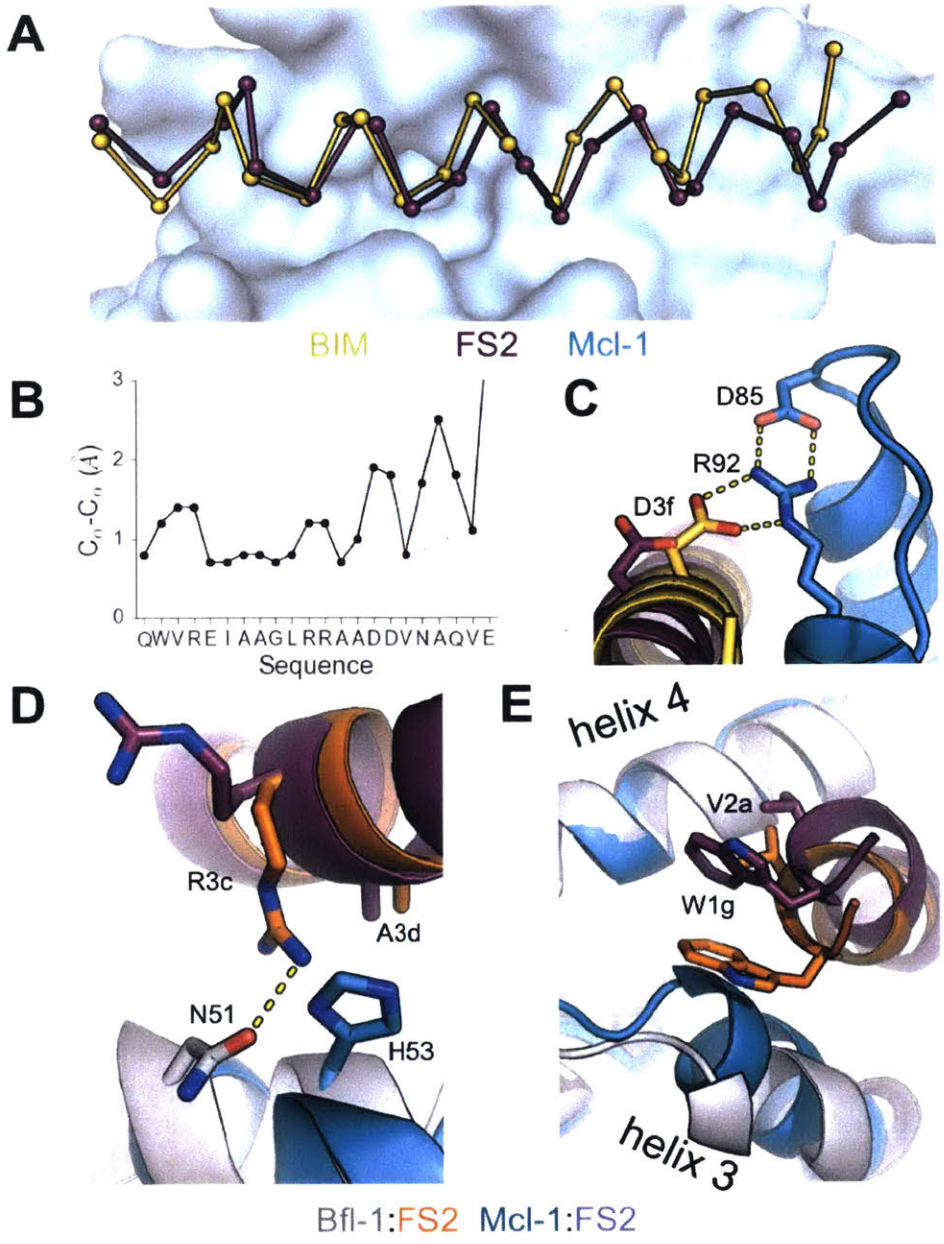

Figure 2.15. Crystal structure of FS2 bound to human Mcl-1. (A) Binding groove of Mcl-1 (blue, surface) with BIM (yellow, 2PQK[66]) and FS2 (purple). (B) C_α- C_α shifts between FS2 and BIM when bound to Mcl-1. (C) The canonical Bfl-1:BH3 salt bridge between D3f and R92, formed in Mcl-1:BIM, is not observed in the Mcl-1:FS2 complex. (D) In contrast with the arginine at position 3c of the Bfl-1:FS2 complex, which makes packing and hydrogen-bond interactions the interface, R3c is oriented away from the BH3 binding groove in the Mcl-1:FS2 complex. (E) The Mcl-1 binding groove between helix 3 and helix 4 is narrower than the Bfl-1 binding groove, and the N-terminus of FS2 is shifted in the Mcl-1:FS2 structure in comparison with the Bfl-1:FS2 complex.

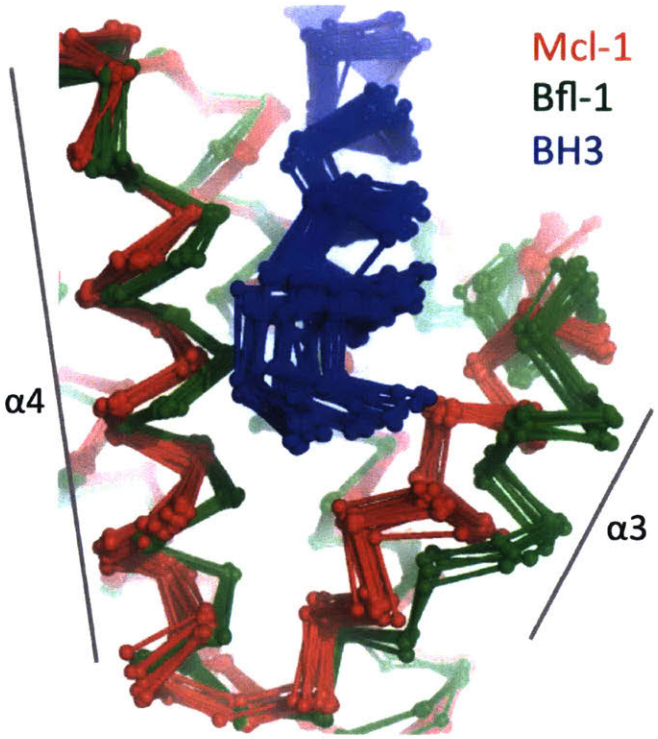

Figure 2.16. Alignment of all crystal structures in the PDB of Bfl-1/Mcl-1 bound to BH3 peptides. Helix 3 in Bfl-1 is shifted relative to Mcl-1, resulting in a widened binding groove.

Biological Activity of Designed Bfl-1 inhibitors

We tested our designed peptides for Bfl-1 selective targeting by carrying out BH3 profiling of cells with known dependencies on anti-apoptotic proteins. In this assay, peptides are titrated into permeabilized cells, and mitochondrial depolarization is measured using the voltage-sensitive dye JC-1 (Figure 2.17A)[8]. We tested the apoptotic sensitivity of BCR-ABL-expressing B-lineage acute lymphoblastic leukemia cell lines engineered to depend on Bcl-2, Bcl-x_L, Mcl-1, or Bfl-1 overexpression for survival[35]. The percent depolarization from these assays is shown in Figure 2.17B. In comparison with a shorter, truncated PUMA BH3 (PUMA1e-4c, $PUMA_{sh}$), which promoted mitochondrial depolarization in all of the cell lines tested, at 100 nM the Bfl-1 selective inhibitors FS1, FS2, and FS3 promoted depolarization only in Bfl-1 dependent cells. An inactive

$PUMA_{sh}$ mutant, PUMA L3aA;D3fA (PUMA 2A) was used as a negative control[36]. EC_{50} values for inducing mitochondrial permeabilization in the engineered cell lines agreed well with trends in Bfl-1 binding affinities, as expected based on the mechanism of action (Figure 2.17C). As an additional test for on-pathway activity, we measured cytochrome c release in the same engineered cell lines in response to peptide treatment, using iBH3 profiling[37]. The specificity pattern observed when monitoring cytochrome c release was consistent with that obtained by BH3 profiling read out using JC-1 (Figure 2.17D, Figure 2.18). A Mcl-1 selective peptide, MS1 was used as a control[10]. In both assays, FS3 promoted mitochondrial depolarization more potently than FS1 or FS2, but was less selective, with significant cross reactivity at 30 μM peptide concentration.

FS1, FS2, and FS3 were based on the sequence of PUMA BH3, which has been proposed to directly activate apoptosis through interactions with BAK and BAX[38,39]. To test the possibility that FS1, FS2, or FS3 may directly activate BAK and BAX, we measured cytochrome c release in two "unprimed" cell lines (PC-3 and SF295). Unprimed cells require BAK/BAX activators to release cytochrome c[40]. We observed cytochrome c release in cells treated with BIM or PUMA BH3 but not in cells treated with as much as 100 μM FS1 or FS2 (Figure 2.19). Treatment with FS3 or $PUMA_{sh}$ peptide led to cytochrome c release at 32 and 100 μM (Figure 2.19). This may indicate that FS3 and $PUMA_{sh}$ have very weak activator function. Taken together, our data show that FS1 and FS2 are not themselves activators, but that they instead act as apoptotic sensitizers by competing with activators or with BAX or BAK for binding to anti-apoptotic proteins, as intended in our design scheme.

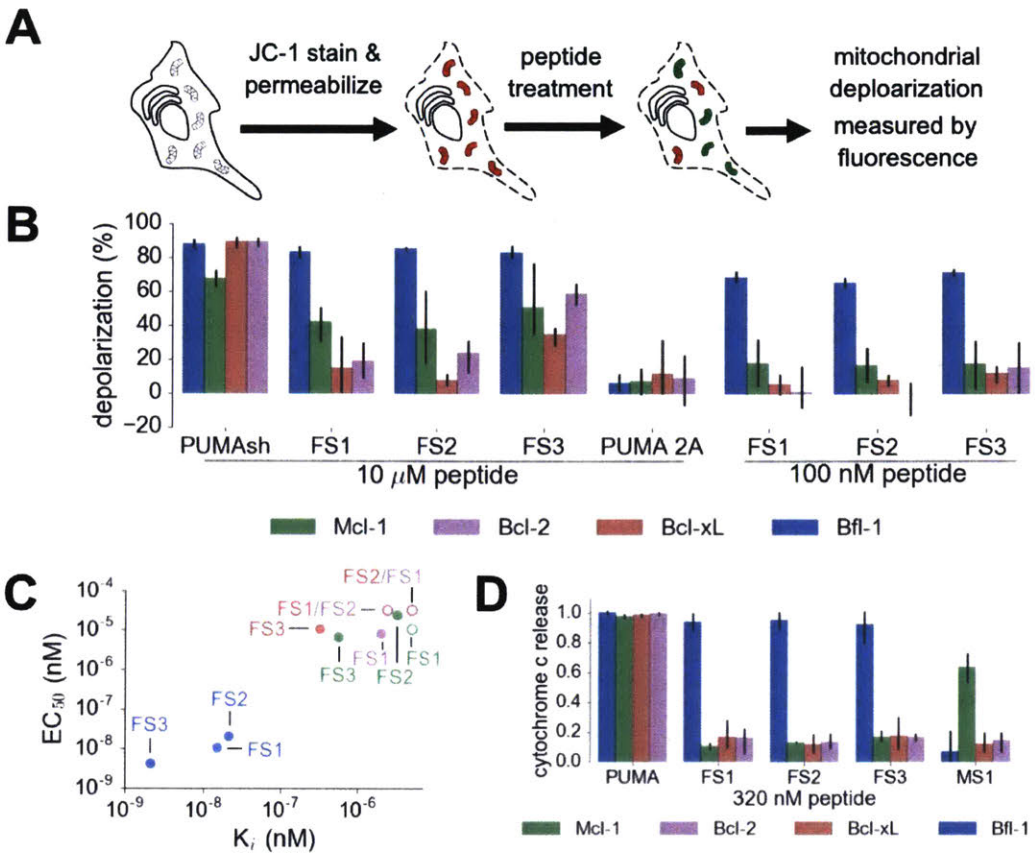

Figure 2.17. Designed Bfl-1 inhibitors selectively induce MOMP in Bfl-1 dependent cells. (A) The BH3 profiling assay detects MOMP by monitoring JC-1 fluorescence in permeabilized cells treated with different peptides. (B-C) Depolarization of mitochondria induced by designed peptides in four cell lines that depend on ectopic expression of Mcl-1, Bcl-2, Bcl-x_L, or Bfl-1 for survival. (C) Correlation between K_i in solution studies and EC_{50} values in BH3 profiling. Open circles indicate lower bound estimates of EC_{50} or K_i. (D) Cytochrome c release from the same cell lines in b and c. Data are mean ± SD of 3 or more independent measurements.

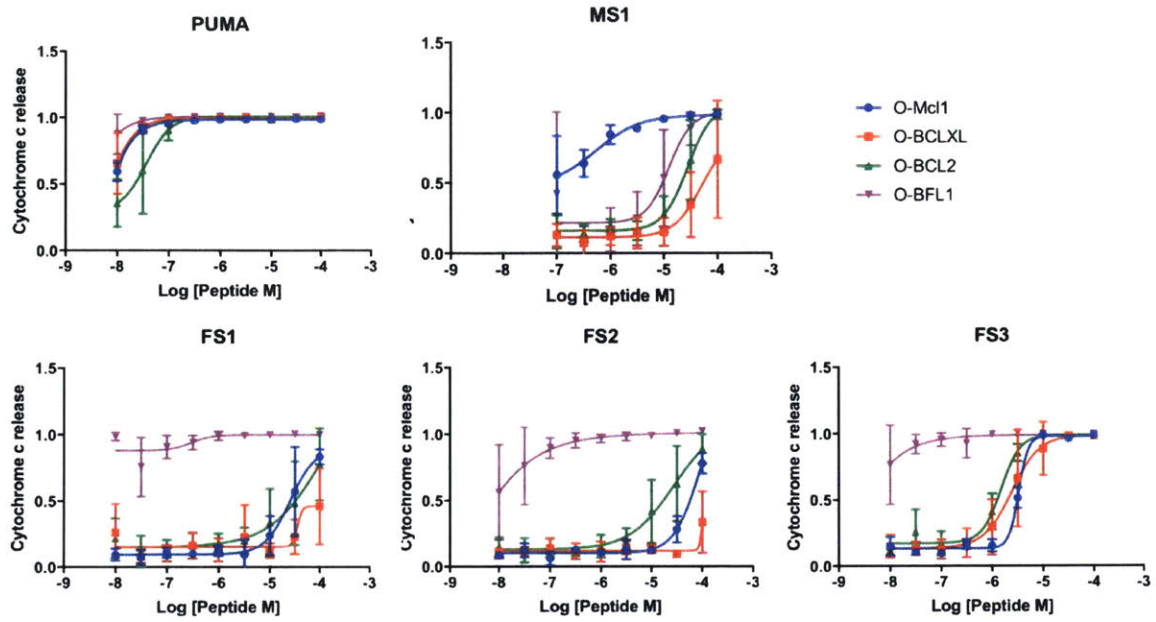

Figure 2.18. At low concentrations, FS1, FS2, and FS3 selectively induced cytochrome c release only in Bfl-1 dependent cell lines. iBH3 was performed on highly primed cells of known anti-apoptotic dependency. Data are mean ± SD of 3 or more independent measurements.

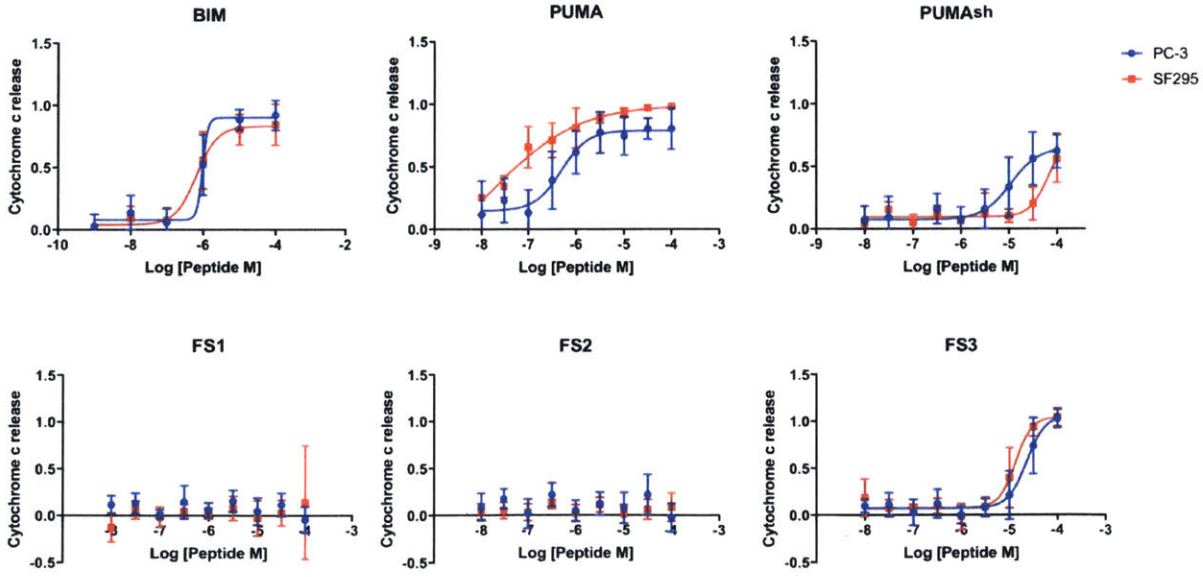

Figure 2.19. iBH3 was performed on unprimed cells to test for activation function. These cells require a BAK/BAX activator to release cytochrome c. Cytochrome c release is stimulated by the known activator peptides BIM and PUMA BH3. Truncated PUMA (1e-4c), $PUMA_{sh}$, and FS3 have reduced capacity to promote cytochrome c release. FS1 and FS2 show no cytochrome c release up to 100 μM. Data are mean ± SD of 3 or more independent measurements.

Covalent Inhibitors of Bfl-1 Enhance Specificity

Our initial sorts for Bfl-1 selective binders identified many sequences that included cysteine at position 1g or 2b (Table 2.6). Interestingly, cysteines encoded at several other positions along the BH3 motif were not enriched. Furthermore, cysteine was not enriched in previous screens for Bfl-1 binding[26]. This observation led us to hypothesize that Bfl-1 binding selectivity could be improved in non-reducing conditions if the peptide ligand formed a disulfide bond with cysteine 55 (C55) of Bfl-1, which is adjacent to the binding cleft of Bfl-1 and unique to Bfl-1 among Bcl-2 family paralogs (Figure 2.20). Testing yeast-displayed peptides for binding to a Bfl-1 cysteine-to-serine (C55S) mutant confirmed that PUMA and BIM bound to Bfl-1 C55S, whereas the majority of the peptides in the cysteine-enriched pool bound to wild type Bfl-1 but not to Bfl-1 C55S (Figure 2.21). Rescreening our library using Bfl-1 C55S led to the identification of FS1, FS2 and FS3, as described above. But, in addition, the discovery that BH3 peptides in our library could access a unique, reactive cysteine in Bfl-1 led us to design covalent inhibitors based on these peptides.

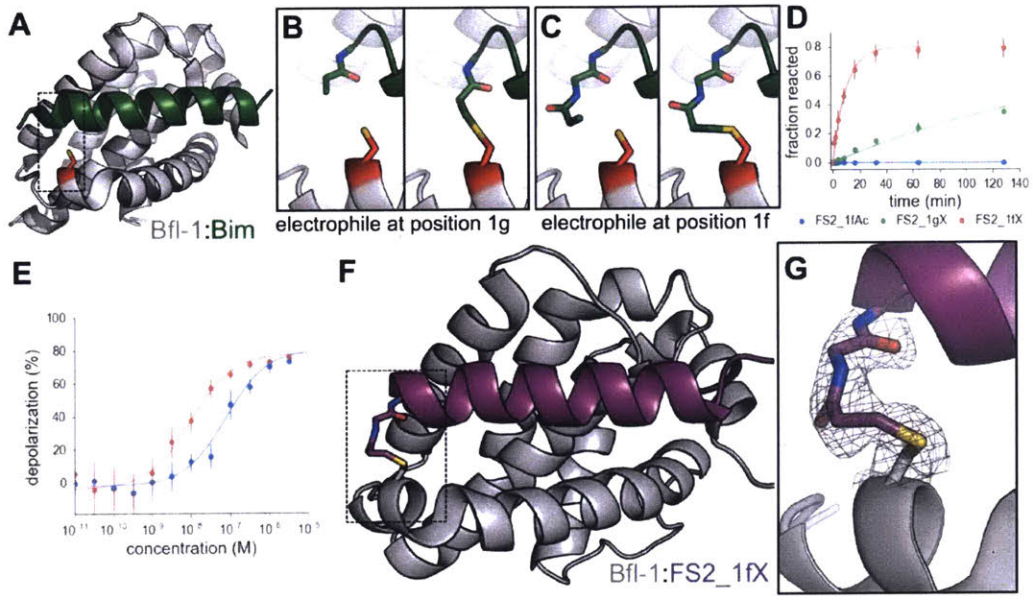

Figure 2.20. An electrophilic variant of FS2 reacts covalently with Bfl-1. (A) C55 in Bfl-1 is close to the BH3 binding groove in BIM:Bfl-1 structure 2VM6[29]. (B-C) Modeling suggested two ways in which an N-terminal acrylamide group could be incorporated into a BH3 peptide with good reaction geometry, leading to peptides FS2_1gX (modification shown in B) or FS2_1fX (modification shown in C) (D) FS2_1fX (red) reacted more rapidly with Bfl-1 than FS2_1gX (green). Bfl-1 crosslinking as a function of reaction time was measured using gel-shift assays; data are mean ± SD of 2 or more independent measurements. Crosslinking did not occur with the acetylated control peptide FS2_1fAc (blue). (E) FS2_1fX (red) was more potent than FS2_1fAc (blue) in BH3 profiling assays of Bfl-1 dependent cells. Data are mean ± SD of 3 or more independent measurements. (F) X-ray structure of Bfl-1 covalently cross-linked to FS2_1fX. (G) Electron density map of covalent crosslink between FS2_1fX and Bfl-1.

Table 2.6. Conventionally sequenced clones from pool FL6 and their frequencies.

sequence	count
GQAACDIGAQLGRMADDHDAQYERRR	1
GQAACDVGAQLGRMADDVEAQYERRR	1
GQAACQIGAQLGRMADDVEAQYERRR	1
GQCLREFGAQLARSGDDQDTQGERRR	1
GQCLREFGAQLIRLGDDLVKQGERRR	1
GQCVREIGAQLARSADDMTEQAERRR	1
GQGACDIGAQLGRMADDVDAQYERRR	2
GQGACDIGAQLGRMADDVEAQYERRR	3
GQGACDIGAQLTRMADDIDAQYERRR	1
GQGACDVGAQLGRMADDVEAQYERRR	1
GQGACEIGAQLGRMADDVEAQYERRR	2
GQGACHIGAQLGRMADDVEAQYERRR	1
GQGGCDVGAQLGRMADDIEAQYERRR	1
GQPACDIAAQLGRMADDVDAQYERRR	1
GQPACDIGAQLARMADDADAQYERRR	1
GQPACDIGAQLGRMADDAEAQYERRR	1
GQPACDIGAQLGRMADDTEAQYERRR	1
GQPACDVGAQLGRMADDVEAQYERRR	1
GQPACHIGAQLGRMADDVDAQYERRR	2
GQRACDIGAQLGRMADDVEAQYERRR	3
GQRACDVGAQLGRMADDVDAQYERRR	1
GQRACQIGAQLGRMADDVEAQYERRR	3
GQSACDIGAQLGRMADDVEAQYERRR	1
GQSACEIGAQLGRMADDVEAQYERRR	1
GQSACHIGAQLGRMADDVDAQYERRR	1
GQSACQIGAQLGRMADDVEAQYERRR	1
GQTACHIGAQLGRMADDVEAQYERRR	1
GQWACDIGAQLGRMADDTDAQYERRR	2
GQWACDIGAQLGRMADDVEAQYERRR	1
GQWQREIGAGLRRIADDTNAQLERRR	1
GQWVREIAAYLRRSADMINAQIERRR	1

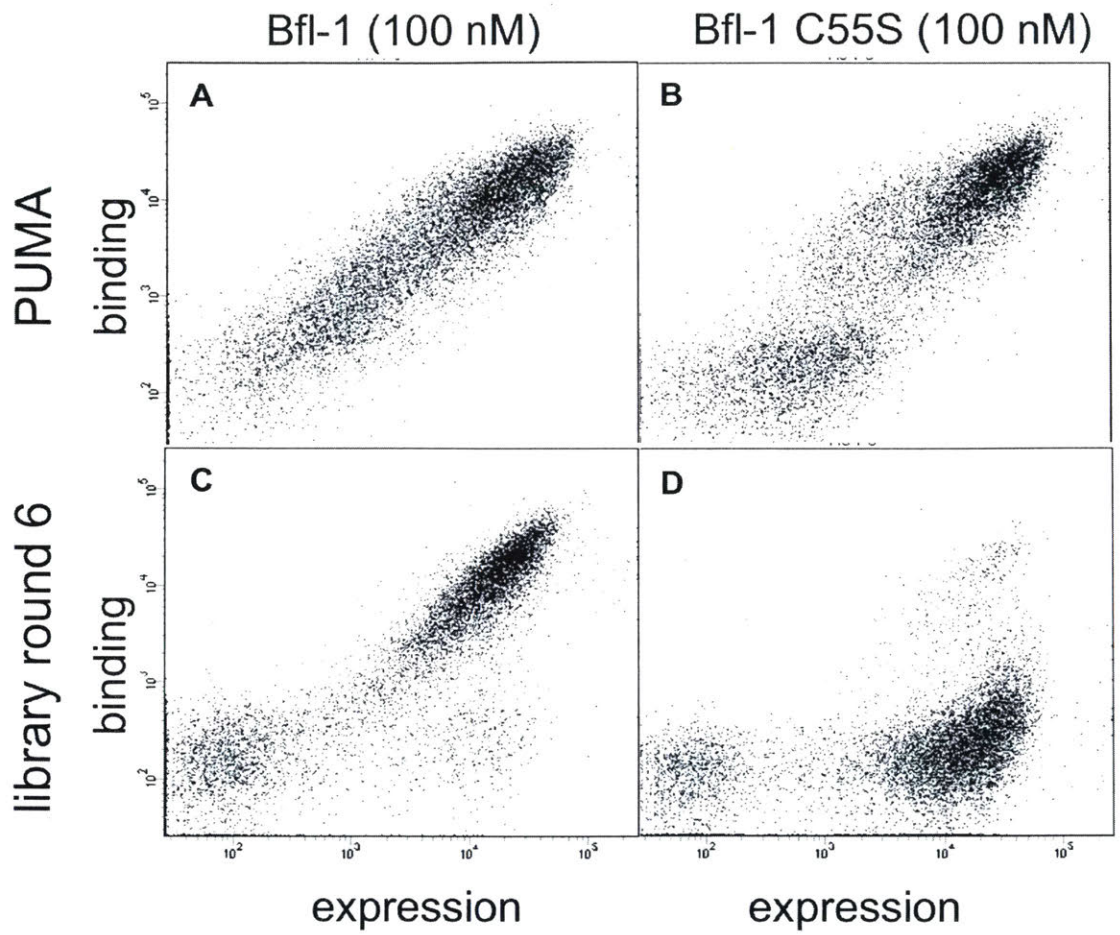

Figure 2.21. Library members bind covalently to Bfl-1 cysteine 55. FACS analysis of yeast cells displaying (A) PUMA in the presence of Bfl-1, (B) PUMA in the presence of the cysteine-to-serine point mutant Bfl-1 C55S, (C) the FL6 library pool in the presence of Bfl-1, and (D) the FL6 library pool in the presence of Bfl-1 C55S.

We used structure-based modeling to choose appropriate cysteine-reactive electrophiles and optimize their placement in different BH3 positions in the 2VM6 structure of Bfl-1 bound to BIM BH3[29]. Our two most promising designs featured N-terminal Michael acceptors at position 1g (FS2_1gX; Figure 2.20B) or 1f (FS2_1fX; Figure 2.20C) of peptide FS2. We tested our designs for covalent modification of Bfl-1 and Bfl-1 C55S using gel-shift assays. Both FS2_1gX and FS2_1fX modified Bfl-1 once or less when applied at micromolar concentrations, whereas Bfl-1 C55S (which contains

2 other solvent-exposed cysteine residues) did not react with these electrophilic peptides for at least 6 hours (Figure 2.22). Using densitometry, we measured the fraction of Bfl-1 reacted as a function of time for both designs. FS2_1fX reacted with Bfl-1 with a half-life of 6.5 min and FS2_1gX reacted more slowly with a half-life of 138 min (Figure 2.20D). We tested FS2_1fX in BH3 profiling and found that it improved on-pathway targeting of Bfl-1 compared to N-terminally acetylated control (Figure 2.20E) and was selective for Bfl-1 (Figure 2.23). We solved a crystal structure of FS2_1fX bound to Bfl-1 that showed clear electron density consistent with a covalent bond to C55, as designed (Figure 2.20F,G).

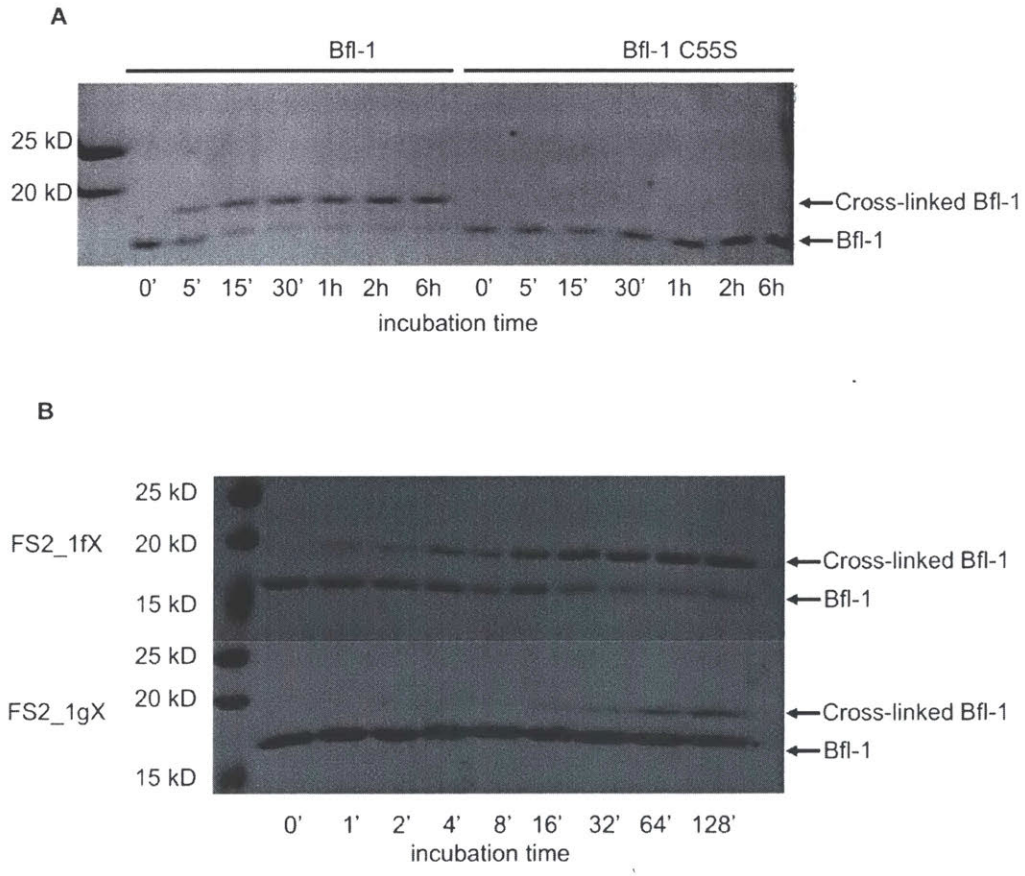

Figure 2.22. Kinetics of the reaction of Bfl-1 with electrophilic peptides. (A) There is a time-dependent shift in apparent molecular weight, as assessed by SDS-PAGE, when Bfl-1 is incubated with FS2_1fX but not when Bfl-1 C55S 1 is incubated with FS2_1gX, consistent with covalent modification of Bfl-1 at cysteine 55. (B) Time course of FS2_1gX and FS2_1fX crosslinking with Bfl-1.

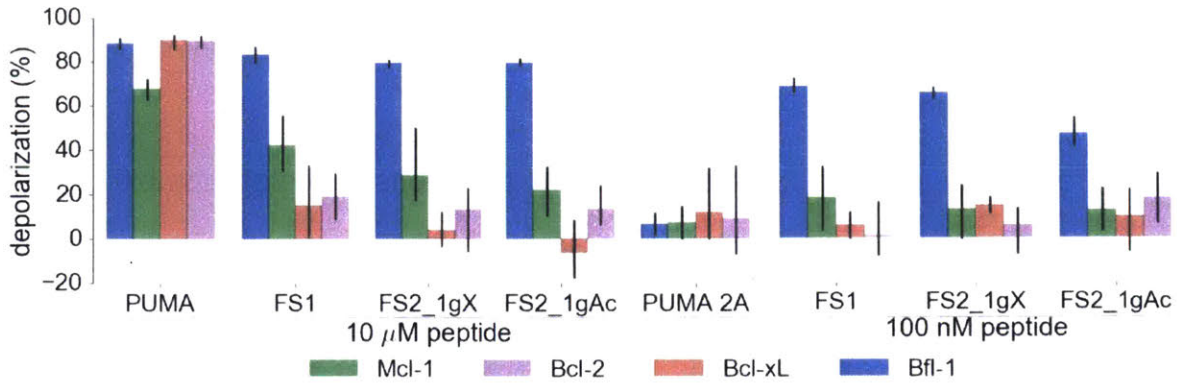

Figure 2.23. Depolarization of mitochondria induced by designed peptides, including covalent inhibitor FS2_1gX, in four cell lines that depend on ectopic expression of Mcl-1, Bcl-2, Bcl-x_L, or Bfl-1 for survival. Data are mean ± SD of 3 or more independent measurements.

Discussion

Bfl-1 is implicated in cancer progression, and inhibiting its anti-apoptotic function may be therapeutically beneficial. Because the role of Bfl-1 in disease is less characterized than that of Mcl-1 or Bcl-2, selective targeting agents will likely be critical for disentangling the roles of different anti-apoptotic proteins. Prior efforts to identify Bfl-1 selective inhibitors provided molecules with only modest binding affinity and/or selectivity[21–24,26]. More recent work has shown, as we demonstrate here, that reaction of an electrophilic group on a Bfl-1 inhibitor with a cysteine near the BH3 binding site confers both infinitely tight and covalently selective interactions with Bfl-1 in preference to other Bcl-2 protein family members. This strategy has been used to target Bfl-1 with a BIM peptide chemically modified to react with cysteine[41–43]. But BIM is a promiscuous binder of Bcl-2, Bcl-x_L, Bcl-w and Mcl-1, as well as an activator of BAX and BAK[44]. Thus, although Bfl-1 is the only covalent target of electrophilic BIM, this approach does not provide an optimal strategy for dissecting the contributions of Bfl-1 to cell survival, because BIM peptides are expected to have many effects on the apoptotic protein-

interaction network. Here, we addressed this by successfully re-engineering PUMA, a promiscuous binder of anti-apoptotic proteins, to make it highly selective for Bfl-1 both as a non-covalent and as a covalent inhibitor.

In re-designing PUMA, we confronted the enormous space of possible mutational variants. The challenge was to identify combinations of mutations that would reduce binding to Bcl-2, Bcl-x_L, Bcl-w, and Mcl-1, while not substantially weakening Bfl-1 interaction. We used computational modeling and existing experimental data to guide our design of focused libraries of peptides predicted to provide the desired specificity. We tested libraries of combinations of the best-ranked mutations both in the context of BIM and in the context of PUMA.

Interestingly, our experimental results showed stark differences in binding behavior between two libraries that introduced the same mutations into BIM vs. PUMA BH3 peptides. Our carefully designed library was rich in Bfl-1 selective binders when tested in a PUMA background, but poor in binders when encoded in a BIM BH3 sequence. This was not because PUMA is a tighter or more selective binder of Bfl-1 than is PUMA; published data indicate that BIM BH3 binds at least as tightly to Bfl-1 as does PUMA BH3[26]. Also, deep sequencing of the two input libraries indicated that they were of similar quality; each had only a small percentage of sequences that were not designed (6.6% for the BIM library and 4.4% for the PUMA library). Given that dramatic differences were observed between the libraries early in screening (pool FL2, Figure 2.6), and that the PUMA library still contained just 5.9% non-designed mutations in pool FL3, it is unlikely that random mutations were the source of the observed differences.

We think it likely that the difference between the PUMA vs. BIM libraries arose because background sequence differently influenced the contributions of library mutations, or combinations of mutations, to binding. For example, this could be the case if PUMA variants but not BIM variants could undergo the conformational shifts we observed in our structures. Consistent with this, we found that introducing the 6 mutations of FS2 into BIM BH3 rather than PUMA BH3, giving BIM-FS2, weakened BIM BH3 binding to Bfl-1 by >1000-fold; Figure 2.7. Differential effects of mutations based on BH3 context were also observed by DeBartolo et al., who reported modest correlation between the influence of point mutations on Mcl-1 binding tested in the context of BIM vs. NOXA BH3 (Pearson r ~0.55), and between the effect on Bcl-x_L binding of mutations made in BIM vs. BAD (r ~ 0.78)[31]. Our results are also consistent with the experiments of Dutta et al., who studied Bfl-1 binding selectivity in BIM-based libraries but identified only modestly selective peptides in screening[26]. Other groups have reported similarly dramatic background effects of context in protein engineering, e.g. in antibody libraries, and have obtained different success rates from screens and selections that started with different framework sequences[45].

Epistasis between mutations contributed to selective Bfl-1 binding (Figure 2.9D). Crystal structures of Bfl-1 bound to PUMA vs. FS2 show that epistasis arises from a substantial alteration of the Bfl-1-binding mode. FS2 binds in a shifted and rotated orientation relative to PUMA (Figure 2.10A), and does not make a key salt bridge that is conserved in nearly all structures of Bcl-2 protein complexes. Interestingly, sorting for Bfl-1 selective binders enriched sequences that score better when modeled using the FS2 binding conformation than with the BIM or PUMA binding geometry (Figure 2.10G),

suggesting that this structural shift may be a common feature of many sequences that we identified and a general strategy for achieving Bfl-1 specificity. The FS2 structures now provide a springboard to permit the design of further improvements in Bfl-1 selectivity, affinity, cell permeability, and other physicochemical properties. For example, the structures of FS2 bound to Bfl-1 can be used to design chemical crosslinks to reinforce helicity and promote cellular uptake[46–49], the structure of FS2 bound to Mcl-1can be used to further reduce Mcl-1 binding, and the structure of FS2_1fX can be used as a platform for the design of therapeutic peptides and small molecules that covalently target Bfl-1.

By combining the strengths of computational design and library screening, we successfully identified rare peptides with desired binding specificities. It is unlikely that computational approaches alone could have identified FS1, FS2, or FS3 in the absence of structural templates for the FS2 binding mode. Also, library sequences that were predicted to give the best Bfl-1 affinity and specificity over Bcl-x_L and Mcl-1 (the top/left edge of the score distribution for sequences in Figure 2.1F-I) were not among the hits recovered in screening. This could be because of deficiencies in the models, or because the experiments included competitor homologs Bcl-w and Bcl-2, which were not modeled in library design. A structure of Bcl-w bound to a BH3 peptide was not available when we deigned our libraries, so designing specificity against Bcl-w would have been subject to the inaccuracies of homology models. It is also possible that even the highest affinity sequences that bind in the geometry that we modeled cannot match the tight binding or specificity that can be achieved with a conformational shift.

Conversely, unguided library approaches (including random mutagenesis) would probably not generate FS1, FS2, or FS3. More than 6×10^{12} sequences are 6 mutations away from 23-residue PUMA BH3, and most mutations are predicted to weaken binding. Furthermore, our models predict that most mutations will have correlated effects on binding to different Bcl-2 family members (Figure 2.2), which dramatically reduces the random chance of finding mutations that confer specificity. Library approaches that take advantage of iterative randomization would have difficulty finding sequences that contain synergistic mutations like those in FS2.

Random mutagenesis is a powerful tool for exploring a local sequence space (e.g. by error-prone PCR), and this could be a strategy for further improving peptides identified in library screens such as this one. The low frequency of non-designed mutations in our libraries introduced a random sampling element, but this did not appear to be important for success in this study. FS2 and FS3 were included in the designed library, and FS1 had only a single non-designed mutation, at a solvent-exposed site.

The peptides we designed in this work have immediate value as biochemical reagents and tools for therapeutic development. FS1, FS2, and FS3 selectively trigger apoptosis of Bfl-1 dependent cells in a BH3 profiling assay, and given that Bcl-2, Mcl-1, and Bcl-x_L dependencies are predictive of therapeutic response to cytotoxic anticancer drugs[7–9], we speculate that diagnosing Bfl-1 dependence using these peptides will provide additional predictive power to guide the use of existing treatments[50]. Furthermore, recent studies with an electrophilic variant of BIM show that targeting Bfl-1 enhances cytotoxicity and caspase 3/7 activity in at least 3 Bfl-1 expressing melanoma cell lines[41]. Finally, the high affinity and selectivity of these peptides, along with the

available structural data, make them promising starting points for the development of peptide- or small-molecule therapeutics directly targeting Bfl-1. Therapeutic applications using peptides require a solution to the cell delivery problem. But chemical modification by hydrocarbon stapling, carefully optimized, has proven effective for delivering other helical BH3 peptides into cells[46–49]. We are optimistic that similar modifications will be effective for FS1, FS2, and/or FS3, and we predict rapid development of a range of cell-deliverable Bfl-1 targeting agents that draws on lessons learned from Bcl-x_L and Mcl-1 inhibitor design as well as the new structural insights that we provide here.

Methods

Peptide synthesis and purification

Library peptides, the PUMA BH3 peptide, and PUMA BH3 peptide mutants had N-terminal acetlyation and C-terminal amidation. Fluoresceinated BIM (fluorescein-IWIAQELRRIGDEFNAYY) BH3 was synthesized with N-terminal 5/6-fluorescein amidite and C-terminal amidation. Covalent peptide inhibitors had N-terminal acrylamide and C-terminal amidation. Peptides were synthesized by the MIT Biopolymers Laboratory. The crude synthesis product was purified by HPLC on a C18 column with a linear gradient of acetonitrile in water. Peptides were verified by mass spectrometry.

Fluorescence polarization assay

Competition fluorescence polarization experiments were performed by titrating 0-10 μM of unlabeled peptide into 50 nM receptor plus 25 nM fluoresceinated BIM (fluorescein-IWIAQELRRIGDEFNAYY) in FP buffer (25 mM Tris pH 7.8, 50 mM NaCl, 1 mM EDTA, 5% DMSO, 0.001% v/v Triton-X). C-myc-tagged receptors were used for all Bcl-2 homologs, as previously described[31,32]. Plates were mixed at 23 °C for 3 h. Plates

were read again at 24 to check equilibration. Experiments were done in at least triplicate. Data were fit, as described for competition fluorescence anisotropy experiments in Foight *et al.*[10], to a complete competitive binding model (equation 17 in Roehrl et al., 2004)[51] using a Python script.

Library design

Position-specific scoring matrices based on SPOT array intensities ($PSSM_{SPOT}$) were described previously[31,32,52]. $PSSM_{SPOT}$ scores were normalized to wild-type BIM BH3, as described by Dutta et al[32]. The structure-based statistical potential STATIUM was used to predict and score the effect of mutations in BH3 peptides on binding to Bfl-1, Mcl-1, Bcl-x_L[28,31]. The crystal structures used to create the STATIUM models were the same as those used in previous studies[28,31]: 3MQP (Bfl-1:Noxa)[53], 3PK1 (Mcl-1:BAX)[54], and 3I08 (Bcl-x_L:BIM3aF)[55]. STATIUM z-scores were normalized using the score distribution for the human proteome, as described by DeBartolo et al[28].

Libraries were constructed using degenerate codons chosen by a computational optimization protocol[56]. To guide codon selection, we divided residue substitutions into three categories: *preferred*, *required*, and *disruptive*. Preferred substitutions were those that scored higher than the median of all point mutants of BIM at positions 2a–4e on either $PSSM_{SPOT\_Bfl\text{-}1}$ or $STATIUM_{Bfl\text{-}1}$. Additionally, some substitutions that did not meet these criteria but that had large specificity scores from either $PSSM_{SPOT\_Bfl\text{-}1}$ or $STATIUM_{Bfl\text{-}1}$ were included. Required substitutions, designated manually, were a subset of the most promising preferred residues, particularly those predicted to be highly selective for Bfl-1 or BIM/PUMA wild-type residues. Specificity for Bfl-1 over Bcl-x_L or Mcl-1 was determined by the difference of $PSSM_{SPOT}$ scores or the difference in

STATIUM z-scores. Disruptive residues included mutations with $PSSM_{SPOT}$ or STATIUM scores for Bfl-1 that were more than 1 standard deviation worse than wild-type BIM. Degenerate codons were considered as possibilities for design if they included all of the required residues at a site and none of the disruptive residues. Codons that encoded 3 or fewer variants were eliminated, to decrease the likelihood that a large percentage of the library would be "poisoned" by a disruptive substitution that wasn't identified by our models. Combinations of degenerate codons were optimized with integer linear programming, as previously described, to maximize the number of sequences composed of preferred residues[56]. The library was limited to at most 1×10^7 DNA sequences. The final Bfl-1 targeted library contained a large number of protein sequences (6.84×10^6), many of which were predicted to be tight and selective Bfl-1 binders by the $PSSM_{SPOT}$ and STATIUM models. The entire design process was repeated to produce libraries selective for Bcl-x_L and Mcl-1.

Construction of the yeast-display vector and the combinatorial library

DNA encoding PUMA-BH3 (residues 132-172 from human PUMA, UniProt # Q9BXH1-1) with a carboxy-terminal FLAG tag was subcloned into the plasmid pCTCON2[57] between Nhe1 and Xho1 restriction digest sites (5' NheI-GGTACCGGATCCGGTGGC-PUMA BH3-GGCGGCCGCGATTATAAAGATGATGATGATAAATAA-Xho1-3'). The BH3 peptide library was constructed with homologous recombination. The inserts were constructed using the PUMA-BH3 yeast display vector as a template, a reverse primer (5' CTAAAAGTACAGTGGGAACAAAGTCG 3'), and forward primers with degenerate bases (PUMA Bfl-1 targeted library: 5' C GGA TCC GGT GGC CAA TGG **VHA** CGT

GAA ATT **KVT** GCC **NDC** CTG CGT CGC **NBC** GCG GAT **VWK NHT** AAT GCC CAA **NYT** GAA CGT CGT CGC CAG GAG GAA C 3'; BIM Bfl-1 targeted library: 5' GGA TCC GGT GGC CGT CCG **VHA** ATT TGG ATT **KVT** CAG **NDC** CTG CGT CGT **NBC** GGC GAT **VWK NHT** AAT GCG TAT **NYT** GCG CGT CGC GTG TTT CTG AAT 3'; PUMA Bcl-x_L targeted library: 5' C GGA TCC GGT GGC CAA TGG **VWS** CGT GAA **NWT** GGC GCC CAA CTG **RBA** CGC **NNC GSC** GAT GAT CTG **VHC RMA** CAA **NVC** GAA CGT CGT CGC CAG GAG GAA C 3'; BIM Bcl-x_L targeted library: 5' GGA TCC GGT GGC CGT CCG **VWS** ATT TGG **NWT** GCG CAG GAA CTG **RBA** CGT **NNC GSC** GAT GAA TTT **VHC RMA** TAT **NVC** GCG CGT CGC GTG TTT CTG AAT 3'; PUMA Mcl-1 targeted library: 5' GT ACC GGA TCC GGT GGC CAA **NSG** GCG **BNC SAW RYC RBT** GCC CAA CTG **RNA** CGC ATG GCG GAT GAT **NHT VAK** GCC CAA TAT GAA CGT CGT CGC C 3'; BIM Mcl-1 targeted library: 5' TACCGGATCCGGTGGCCGT **NSG** GAA **BNC SAW RYC RBT** CAGGAACTG **RNA** CGTATTGGCGATGAA **NHT VAK** GCGTATTATGCGCGTCGCGT 3'). To complete insert construction, the 5' ends of these PCR products were further extended until there was at least 40 bp of homology to the acceptor vector on both ends of the library inserts. The acceptor vector was prepared by cleaving the yeast display vector with the endonucleases Xho1 and Nhe1 and purifying the cleavage product with a gel purification kit (Qiagen). The library inserts and acceptor vector were mixed and transformed into yeast following the procedure of Gietz *et al.*[58]. 20 electroporations produced > 10 fold more transformants than the theoretical size of each library with vector background estimated at < 0.01%. DNA from transformed cells was PCR amplified to check for randomization.

Flow cytometric analysis and sorting

The yeast-displayed Bfl-1 library was grown and sorted using fluorescence activated cell sorting (FACS) according to a protocol adapted from Reich *et al*[59]. The libraries were grown from glycerol stocks that were inoculated to a final OD_{600} of 0.05 in a volume sufficient to oversample the estimated library diversity by at least 10-fold in selective media containing glucose (SD+CAA: 5 g/L casamino acids, 1.7 g/L yeast nitrogen base, 5.3 g/L ammonium sulfate, 10.2 g/L Na_2HPO_4-$7H_2O$ and 8.6 g/L NaH_2PO_4-H_2O, 2% glucose). Cultures were grown for 12 h at 30 °C and then cells were diluted to OD_{600} of 0.005-0.01 in SD+CAA and grown to OD_{600} of 0.1–0.6 (~12h) at 30 °C. To induce expression, cultured were diluted (40 mL inoculate/L) into selective media containing galactose (SG+CAA: 5 g/L casamino acids, 1.7 g/L yeast nitrogen base, 5.3 g/L ammonium sulfate, 10.2 g/L Na_2HPO_4-$7H_2O$ and 8.6 g/L NaH_2PO_4-H_2O, 2% glucose) and grown to OD_{600} of 0.2–0.5 (16-24h) at 30 °C. Induced yeast cells were filtered with 0.45 µm filter plates or bottle-top filters and washed twice with BSS (50 mM Tris, 100 mM NaCl, pH 8, 1 mg/ml BSA). Sufficient cells to oversample the library diversity at least 10-fold were resuspended in BSS with at least 10-fold molar excess target protein and incubated for 2 h at room temperature with gentle shaking. Cells were filtered, washed twice in chilled BSS, and incubated with a mixture of primary antibodies (anti-HA mouse, Roche, RRID:AB_514505, and anti-c-myc rabbit, Sigma, RRID:AB_439680) at 1:100 dilution in a volume of 20 µl per 10^6 cells for 15 min at 4 °C in BSS. Cells were filtered, washed twice in chilled BSS, and incubated in a mixture of secondary antibodies (1:40 APC rat anti-mouse, BD, RRID:AB_398465, and 1:100 PE goat anti-rabbit, Sigma, RRID:AB_261257) in BSS at 4 °C in the dark for 15 min. The

filtering and washing steps were repeated and the labeled cells were resuspended in BSS and analyzed on a BD FACSCanto flow cytometer or sorted on a BD FACSAria using FACSDiva software. The sorted cells were collected in selective media containing glucose (SD+CAA) and grown to an OD_{600} of 6-10 for ~48 hours in the presence of streptomycin/penicillin to prevent bacterial growth, then pelleted, washed, and stored as glycerol stocks in SD+CAA+20% glycerol. A series of positive, negative, and competition sorts were used to enrich Bfl-1 selective binders. The detailed sorting scheme is given in Figure 2.5.

Illumina sequencing and data processing

Glycerol stocks from each pool isolated during sorting were grown overnight in SD+CAA, using sufficient stock to oversample the estimated library diversity by at least 10-fold. 1×10^8 cells from each pool were pelleted in a microcentrifuge tube at 300 × g for 1 min and washed twice with PBS. The plasmid DNA from yeast was extracted using the Zymoprep Yeast Plasmid Miniprep II (Zymo Research) reagents and Qiagen miniprep columns. The DNA was eluted in water. The BH3 library was amplified with PCR using primers that encoded an MmeI restriction enzyme binding site at 5′ end and a universal Illumina sequencing region on the 3′ end. After purification with the Qiagen PCR purification kit, the PCR products were digested with MmeI (3.45 pmol DNA:2 µL MmeI, NEB) for 1 h at 37 °C before being heat inactivated at 80 °C for 20 min. Each digestion product was then ligated by treatment with T4 DNA ligase (NEB) for 30 min at 20 °C to double-stranded DNA fragments containing Illumina adapters, with the adapter containing a unique barcode, and heat inactivated for 10 min at 65 °C. Barcodes were varied by at least two bases and were used to assign Illumina reads to the appropriate

pool. A final PCR amplified the ligation product and extended the 5' and 3' regions to include adaptor sequences for Illumina sequencing. Samples were then multiplexed and run in one lane on an Illumina Nextseq with paired-end reads of 75 bp using the universal Illumina forward sequencing primer and a PUMA construct-specific Illumina read primer reverse (5' CGCCTTGTTCCTCCTGGCGACGACGTTCATATTGGGC 3'). Illumina deep sequencing data was processed in python. The data was filtered for sequences with barcodes that had high Phred Scores (> 20). Sequences were reconstructed by aligning pair end reads. Sequences observed fewer than 20 times were removed from the data set.

Crystallography

Crystals of Bfl-1 in complex with PUMA, FS2 or FS2_1fX peptides were grown in hanging drops over a reservoir containing 1.8 M ammonium sulfate, 0.1 M MES pH 7.0 at room temperature. Crystals were seeded with drops containing parent crystals grown in higher ammonium sulfate (2.2-2.4 M) using a cat whisker. The protein was mixed with peptide at a 1:1 molar ratio and concentrated to 4 mg/ml in 20 mM Tris, 150 mM NaCl, 1% glycerol, 1 mM DTT, pH 8.0. The hanging drops contained 1.5 µL of complex mixed with 1.5 µL of reservoir solution. Crystals were cryo-protected by transferring into 2.0 M lithium sulfate with 10% glycerol prior to flash freezing. Diffraction data were collected at the Advanced Photon Source at the Argonne National Laboratory, NE-CAT beamline 24-ID-C. The Bfl-1:FS2 data were integrated and scaled to 1.2 Å using HKL2000 and phased using PHENIX ridged body refinement of chain A of structure 4ZEQ using PHENIX[60,61]. The peptide was built into the difference density from the rigid body

refinement and the structure was refined with iterative rounds of refinement and model building using PHENIX and COOT[61,62]. The PUMA and FS2_1fX complex data sets extended to 1.33 Å and 1.73 Å respectively and were phased with the Bfl-1 chain of the FS2 complex model[63].

Crystals of the Mcl-1/FS2 peptide complex were grown at room temperature in hanging drops over a reservoir containing 0.2 M zinc sulfate, 0.1 M imidazole (pH 6.5), and 3% 6-aminohexanoic acid. The protein was mixed with peptide at a 1:1 molar ratio and diluted to 2 mg/ml in 20 mM Tris, 150 mM NaCl, 1% glycerol, 1 mM DTT, pH 8.0. The hanging drops contained 1.5 µL of complex mixed with 1.5 µL of reservoir solution. Crystals were cryoprotected by transferring into 15% glycerol, 0.2 M zinc sulfate, 0.1 M imidazole (pH 6.5), and 3% 6-aminohexanoic acid prior to flash freezing. Diffraction data were collected at the Advanced Photon Source at the Argonne National Laboratory, NE-CAT beamline 24-ID-E. The data to were processed to 2.35 Å and phased using molecular replacement with chain A of structure 3PK1[54] using PHASER and refined using PHENIX and COOT[60–63].

Gel shift assays

Myc-tagged Bfl-1 (5 µM) was incubated with BH3 peptide (25 µM) in 200 µL of FP in 200 µL FP buffer (see above). 20 µL subsamples were taken at 0, 1, 2, 4, 8, 16, 32, 64, and 128 minutes and quenched in 7 µL loading buffer. Samples were immediately flash frozen in liquid nitrogen, and stored at -80 °C. Samples were run on a 14% acrylamide SDS-PAGE gel and visualized with Coomassie Brilliant Blue. Bands were quantified with ImageJ. Data were fit in python to the equation $y=C^*(1-e^{-kt})$, where

y is the fraction of cross-linked Bfl-1, C is the upper limit, t is time, and k is the decay constant.

Cell lines

The creation and characterization of the BCR-ABL-expressing B-lineage acute lymphoblastic leukemia suspension cell lines with engineered dependencies on human versions of anti-apoptotic genes is detailed in Koss *et al*[35] and was grown in RPMI (Life Technologies, CA) with 10% fetal bovine serum, 2 mM L-glutamine, 100 I.U./mL penicillin, 100 µg/mL streptomycin, 25 mM HEPES, and 1 mM non-essential amino acids. The adherent cell lines PC-3 and SF295 are from the NCI60 panel and were grown in RPMI (Life Technologies, CA) with 10% fetal bovine serum, 2 mM L-glutamine, penicillin, and streptomycin.

BH3 profiling assays

Peptides were titrated by serial dilution in MEB buffer (150 mM Mannitol, 10 mM HEPES-KOH pH 7.5, 50 mM KCl, 0.02 mM EGTA, 0.02 mM EDTA, 0.1% BSA, and 5 mM Succinate) containing 20 µg/mL oligomycin, 50 µg/mL digitonin, 2 µM JC-1, and 10 mM 2-mercaptoethanol in 384-well plates. Controls for no depolarization (1% DMSO) and complete depolarization with the mitochondrial oxidative phosphorylation uncoupler FCCP (20 µM) were included for data normalization. Cells were suspended at 1.67 x 10^6 cells/mL in MEB. 15 µL of cell suspension was added to each well containing 15 µL of treatment solution. Fluorescence emission was measured every 5 minutes for 3 hours at 590 nM with 525 nM excitation on a Tecan Safire2. To produce percent depolarization, the area under the resultant curve was calculated and normalized to the

assay controls. Peptide titration curves were fit to sigmoidal dose-response curves using Graphpad PRISM 7 to obtain EC_{50} values.

iBH3 assays

Cells were suspended in MEB buffer (150 mM mannitol, 50mM KCl, 10 mM HEPES, 5 mM succinic acid, 20 µM EGTA, 20 µM EDTA, 0.1% BSA, final pH 7.4) at $0.5*10^6$ cells/mL (adherent lines) or $2*10^6$ cells/mL (suspension lines). Cell suspension was added to a 384 non-binding well plate (10 µL/well) containing peptides at 2X final concentration in MEB with 20 µg/mL digitonin. Plates were incubated at 25 °C for 1 hr. To terminate exposure, 10 µL of 4% formaldehyde in PBS was added to each well, plates were incubated for 10 min before addition of 10 µL N2 buffer (1.7M Tris, 1.25M glycine, pH 9.1) for 5 min. 10 µL of staining buffer (2% Tween20, 10% BSA, PBS) containing 10 µg/mL Hoechst 33342 and 1.25 µg/mL anti-cytochrome c Alexa647 conjugate (BioLegend clone 6H2.B4) was added to each well before sealing the plate and shaking overnight. The median fluorescence of the cytochrome c channel of Hoechst positive singlets was recorded by an IntelliCyt iQue Screener Plus. Cytochrome c release was determined by normalizing the median fluorescence intensity (MFI) data to positive control wells (Alamethicin) and negative control wells (DMSO) as follows:

Cytochrome c release = $1 - (MFI_{Sample} - MFI_{Alamethicin}) / (MFI_{DMSO} - MFI_{Alamethicin})$

Acknowledgements

We thank the Koch Institute Bioploymers and Proteomics Facility for peptide synthesis, the Koch Institute Flow Cytometry Core Facility for assistance with FACS sorting, and the MIT Structural Biology Core Facility for assistance with X-ray crystallography. We thank L.R.F. Backman for help with x-ray data collection. We thank members of the Keating lab, especially T. Hwang for performing gel shift assays, R. Rezaei Araghi for performing mass spec, V. Xue for help processing Illumina sequencing reads, V. Frappier for helping with structural analysis, and G. Foight for help with library design. We thank the laboratory of J. Opferman for providing the cell lines of defined anti-apoptotic dependence used in the BH3 profiling assays. Part of this work was conducted at the Northeastern Collaborative Access Team beamlines, which are funded by the National Institute of General Medical Sciences from the National Institutes of Health (P41 GM103403). The Pilatus 6M detector on 24-ID-C beam line is funded by a NIH-ORIP HEI grant (S10 RR029205). This research used resources of the Advanced Photon Source, a U.S. Department of Energy (DOE) Office of Science User Facility operated for the DOE Office of Science by Argonne National Laboratory under Contract No. DE-AC02-06CH11357. The content is solely the responsibility of the authors and does not necessarily represent the official views of the National Institutes of Health or the U.S. Department of Energy.

References

1. Opferman JT. Attacking cancer's Achilles heel: antagonism of anti-apoptotic BCL-2 family members. *FEBS J.* August 2015. doi:10.1111/febs.13472.
2. Souers AJ, Leverson JD, Boghaert ER, et al. ABT-199, a potent and selective BCL-2 inhibitor, achieves antitumor activity while sparing platelets. *Nat Med.* 2013;19(2):202-208. doi:10.1038/nm.3048.
3. Roberts AW, Davids MS, Pagel JM, et al. Targeting BCL2 with Venetoclax in Relapsed Chronic Lymphocytic Leukemia. *N Engl J Med.* 2016;374(4):311-322. doi:10.1056/NEJMoa1513257.
4. Rudin CM, Hann CL, Garon EB, et al. Phase II Study of Single-Agent Navitoclax (ABT-263) and Biomarker Correlates in Patients with Relapsed Small Cell Lung Cancer. *Clin Cancer Res.* 2012;18(11).
5. Roberts AW, Seymour JF, Brown JR, et al. Substantial susceptibility of chronic lymphocytic leukemia to BCL2 inhibition: results of a phase I study of navitoclax in patients with relapsed or refractory disease. *J Clin Oncol.* 2012;30(5):488-496. doi:10.1200/JCO.2011.34.7898.
6. Schoenwaelder SM, Jarman KE, Gardiner EE, et al. Bcl-xL–inhibitory BH3 mimetics can induce a transient thrombocytopathy that undermines the hemostatic function of platelets. *Blood.* 2011;118(6).
7. Ryan JA, Brunelle JK, Letai A. Heightened mitochondrial priming is the basis for apoptotic hypersensitivity of CD4+ CD8+ thymocytes. *Proc Natl Acad Sci U S A.* 2010;107(29):12895-12900. doi:10.1073/pnas.0914878107.
8. Deng J, Carlson N, Takeyama K, Dal Cin P, Shipp M, Letai A. BH3 profiling identifies three distinct classes of apoptotic blocks to predict response to ABT-737 and conventional chemotherapeutic agents. *Cancer Cell.* 2007;12(2):171-185. doi:10.1016/j.ccr.2007.07.001.
9. Montero J, Sarosiek KA, DeAngelo JD, et al. Drug-Induced Death Signaling Strategy Rapidly Predicts Cancer Response to Chemotherapy. *Cell.* 2015;160(5):977-989. doi:10.1016/j.cell.2015.01.042.
10. Foight GW, Ryan JA, Gullá S V, Letai A, Keating AE. Designed BH3 Peptides with High Affinity and Specificity for Targeting Mcl-1 in Cells. *ACS Chem Biol.* 2014;9(9):1962-1968. doi:10.1021/cb500340w.
11. Dutta S, Ryan J, Chen TS, Kougentakis C, Letai A, Keating AE. Potent and specific peptide inhibitors of human pro-survival protein Bcl-xL. *J Mol Biol.* 2015;427(6 Pt B):1241-1253. doi:10.1016/j.jmb.2014.09.030.
12. Lessene G, Czabotar PE, Sleebs BE, et al. Structure-guided design of a selective BCL-XL inhibitor. *Nat Chem Biol.* 2013;9(6):390-397. doi:10.1038/nchembio.1246.
13. Hind CK, Carter MJ, Harris CL, Chan HTC, James S, Cragg MS. Role of the pro-survival molecule Bfl-1 in melanoma. *Int J Biochem Cell Biol.* 2015;59:94-102. doi:10.1016/j.biocel.2014.11.015.
14. Haq R, Yokoyama S, Hawryluk EB, et al. BCL2A1 is a lineage-specific antiapoptotic melanoma oncogene that confers resistance to BRAF inhibition. *Proc Natl Acad Sci U S A.* 2013;110(11):4321-4326. doi:10.1073/pnas.1205575110.
15. Senft D, Berking C, Graf SA, Kammerbauer C, Ruzicka T, Besch R. Selective induction of cell death in melanoma cell lines through targeting of Mcl-1 and A1. Sanchis D, ed. *PLoS One.* 2012;7(1):e30821. doi:10.1371/journal.pone.0030821.
16. Brien G, Trescol-Biemont M-C, Bonnefoy-Bérard N. Downregulation of Bfl-1 protein expression sensitizes malignant B cells to apoptosis. *Oncogene.* 2007;26(39):5828-5832. doi:10.1038/sj.onc.1210363.
17. Fan G, Simmons MJ, Ge S, et al. Defective ubiquitin-mediated degradation of antiapoptotic Bfl-1 predisposes to lymphoma. *Blood.* 2010;115(17):3559-3569. doi:10.1182/blood-2009-08-236760.

18. Beverly LJ, Varmus HE. MYC-induced myeloid leukemogenesis is accelerated by all six members of the antiapoptotic BCL family. *Oncogene*. 2009;28(9):1274-1279. doi:10.1038/onc.2008.466.

19. Oltersdorf T, Elmore SW, Shoemaker AR, et al. An inhibitor of Bcl-2 family proteins induces regression of solid tumours. *Nature*. 2005;435(7042):677-681. doi:10.1038/nature03579.

20. Kotschy A, Szlavik Z, Murray J, et al. The MCL1 inhibitor S63845 is tolerable and effective in diverse cancer models. *Nature*. 2016;538(7626):477-482. doi:10.1038/nature19830.

21. Mathieu A-L, Sperandio O, Pottiez V, et al. Identification of Small Inhibitory Molecules Targeting the Bfl-1 Anti-Apoptotic Protein That Alleviates Resistance to ABT-737. *J Biomol Screen*. 2014;19(7):1035-1046. doi:10.1177/1087057114534070.

22. Zhai D, Godoi P, Sergienko E, et al. High-throughput fluorescence polarization assay for chemical library screening against anti-apoptotic Bcl-2 family member Bfl-1. *J Biomol Screen*. 2012;17(3):350-360. doi:10.1177/1087057111429372.

23. Cashman JR, MacDonald M, Ghirmai S, et al. Inhibition of Bfl-1 with N-aryl maleimides. *Bioorg Med Chem Lett*. 2010;20(22):6560-6564. doi:10.1016/j.bmcl.2010.09.046.

24. Zhai D, Jin C, Shiau C-W, Kitada S, Satterthwait AC, Reed JC. Gambogic acid is an antagonist of antiapoptotic Bcl-2 family proteins. *Mol Cancer Ther*. 2008;7(6):1639-1646. doi:10.1158/1535-7163.MCT-07-2373.

25. Berger S, Procko E, Margineantu D, et al. Computationally designed high specificity inhibitors delineate the roles of BCL2 family proteins in cancer. *Elife*. 2016;5:1422-1432. doi:10.7554/eLife.20352.

26. Dutta S, Chen TS, Keating AE. Peptide ligands for pro-survival protein Bfl-1 from computationally guided library screening. *ACS Chem Biol*. 2013;8(4):778-788. doi:10.1021/cb300679a.

27. Foight GW, Keating AE. Locating Herpesvirus Bcl-2 Homologs in the Specificity Landscape of Anti-Apoptotic Bcl-2 Proteins. *J Mol Biol*. 2015;427(15):2468-2490. doi:10.1016/j.jmb.2015.05.015.

28. DeBartolo J, Taipale M, Keating AE. Genome-wide prediction and validation of peptides that bind human prosurvival Bcl-2 proteins. *PLoS Comput Biol*. 2014;10(6):e1003693. doi:10.1371/journal.pcbi.1003693.

29. Herman MD, Nyman T, Welin M, et al. Completing the family portrait of the anti-apoptotic Bcl-2 proteins: Crystal structure of human Bfl-1 in complex with Bim. *FEBS Lett*. 2008;582(25-26):3590-3594. doi:10.1016/j.febslet.2008.09.028.

30. Smits C, Czabotar PE, Hinds MG, Day CL. Structural Plasticity Underpins Promiscuous Binding of the Prosurvival Protein A1. *Structure*. 2008;16(5):818-829. doi:10.1016/j.str.2008.02.009.

31. DeBartolo J, Dutta S, Reich L, Keating AE. Predictive Bcl-2 family binding models rooted in experiment or structure. *J Mol Biol*. 2012;422(1):124-144. doi:10.1016/j.jmb.2012.05.022.

32. Dutta S, Gullá S, Chen TS, Fire E, Grant RA, Keating AE. Determinants of BH3 binding specificity for Mcl-1 versus Bcl-xL. *J Mol Biol*. 2010;398(5):747-762. doi:10.1016/j.jmb.2010.03.058.

33. Boersma MD, Sadowsky JD, Tomita YA, Gellman SH. Hydrophile scanning as a complement to alanine scanning for exploring and manipulating protein-protein recognition: application to the Bim BH3 domain. *Protein Sci*. 2008;17(7):1232-1240. doi:10.1110/ps.032896.107.

34. Foight GW, Chen TS, Richman D, Keating AE. Enriching Peptide Libraries for Binding Affinity and Specificity Through Computationally Directed Library Design. In: Schueler-Furman O, London N, eds. *Modeling Peptide-Protein Interactions: Methods and Protocols, Methods in Molecular Biology, Vol. 1561*. Springer Science+Business Media LLC; 2017. doi:DOI 10.1007/978-1-4939-6798-8_13.

35. Koss B, Ryan J, Budhraja A, et al. Defining specificity and on-target activity of BH3-mimetics using engineered B-ALL cell lines. *Oncotarget*. February 2016. doi:10.18632/oncotarget.7204.

36. Ryan J, Letai A. BH3 profiling in whole cells by fluorimeter or FACS. *Methods*. 2013;61(2):156-164. doi:10.1016/j.ymeth.2013.04.006.

37. Ryan J, Montero J, Rocco J, Letai A. iBH3: simple, fixable BH3 profiling to determine apoptotic

priming in primary tissue by flow cytometry. *Biol Chem*. 2016;397(7):671-678. doi:10.1515/hsz-2016-0107.

38. Dai H, Pang Y-P, Ramirez-Alvarado M, Kaufmann SH. Evaluation of the BH3-only protein Puma as a direct Bak activator. *J Biol Chem*. 2014;289(1):89-99. doi:10.1074/jbc.M113.505701.

39. Edwards AL, Gavathiotis E, LaBelle JL, et al. Multimodal interaction with BCL-2 family proteins underlies the proapoptotic activity of PUMA BH3. *Chem Biol*. 2013;20(7):888-902. doi:10.1016/j.chembiol.2013.06.007.

40. Certo M, Moore VDG, Nishino M, et al. Mitochondria primed by death signals determine cellular addiction to antiapoptotic BCL-2 family members. *Cancer Cell*. 2006;9(5):351-365. doi:10.1016/j.ccr.2006.03.027.

41. Huhn AJ, Guerra RM, Harvey EP, Bird GH, Walensky LD. Selective Covalent Targeting of Anti-Apoptotic BFL-1 by Cysteine-Reactive Stapled Peptide Inhibitors. *Cell Chem Biol*. 2016;23(9):1123-1134. doi:10.1016/j.chembiol.2016.07.022.

42. Barile E, Marconi GD, De SK, et al. hBfl-1/hNOXA Interaction Studies Provide New Insights on the Role of Bfl-1 in Cancer Cell Resistance and for the Design of Novel Anticancer Agents. *ACS Chem Biol*. December 2016:acschembio.6b00962. doi:10.1021/acschembio.6b00962.

43. de Araujo AD, Lim J, Good AC, Skerlj RT, Fairlie DP. Electrophilic Helical Peptides That Bond Covalently, Irreversibly, and Selectively in a Protein–Protein Interaction Site. *ACS Med Chem Lett*. November 2016:acsmedchemlett.6b00395. doi:10.1021/acsmedchemlett.6b00395.

44. Letai A, Bassik MC, Walensky LD, Sorcinelli MD, Weiler S, Korsmeyer SJ. Distinct BH3 domains either sensitize or activate mitochondrial apoptosis, serving as prototype cancer therapeutics. *Cancer Cell*. 2002;2(3):183-192. doi:10.1016/S1535-6108(02)00127-7.

45. Boyer S, Biswas D, Kumar Soshee A, Scaramozzino N, Nizak C, Rivoire O. Hierarchy and extremes in selections from pools of randomized proteins. *Proc Natl Acad Sci U S A*. 2016;113(13):3482-3487. doi:10.1073/pnas.1517813113.

46. Rezaei Araghi R, Keating AE. Designing helical peptide inhibitors of protein–protein interactions. *Curr Opin Struct Biol*. 2016;39:27-38. doi:10.1016/j.sbi.2016.04.001.

47. Rezaei Araghi R, Ryan JA, Letai A, Keating AE. Rapid Optimization of Mcl-1 Inhibitors using Stapled Peptide Libraries Including Non-Natural Side Chains. *ACS Chem Biol*. 2016;11(5):1238-1244. doi:10.1021/acschembio.5b01002.

48. Bird GH, Mazzola E, Opoku-Nsiah K, et al. Biophysical determinants for cellular uptake of hydrocarbon-stapled peptide helices. *Nat Chem Biol*. 2016;12(10):845-852. doi:10.1038/nchembio.2153.

49. Walensky LD, Kung AL, Escher I, et al. Activation of apoptosis in vivo by a hydrocarbon-stapled BH3 helix. *Science*. 2004;305(5689):1466-1470. doi:10.1126/science.1099191.

50. Ni Chonghaile T, Sarosiek KA, Vo T-T, et al. Pretreatment mitochondrial priming correlates with clinical response to cytotoxic chemotherapy. *Science*. 2011;334(6059):1129-1133. doi:10.1126/science.1206727.

51. Roehrl MHA, Wang JY, Wagner G. A General Framework for Development and Data Analysis of Competitive High-Throughput Screens for Small-Molecule Inhibitors of Protein−Protein Interactions by Fluorescence Polarization †. *Biochemistry*. 2004;43(51):16056-16066. doi:10.1021/bi048233g.

52. London N, Gullá S, Keating AE, Schueler-Furman O. In silico and in vitro elucidation of BH3 binding specificity toward Bcl-2. *Biochemistry*. 2012;51(29):5841-5850. doi:10.1021/bi3003567.

53. Guan R, Xiao R, Zhao L, Acton T., Gelinas C, Montelione GT. Crystal Structure of human BFL-1 in complex with NOXA BH3 peptide. *To be Publ*. doi:10.2210/PDB3MQP/PDB.

54. Czabotar PE, Lee EF, Thompson G V, Wardak AZ, Fairlie WD, Colman PM. Mutation to Bax beyond the BH3 domain disrupts interactions with pro-survival proteins and promotes apoptosis. *J*

Biol Chem. 2011;286(9):7123-7131. doi:10.1074/jbc.M110.161281.

55. Lee EF, Czabotar PE, Yang H, et al. Conformational changes in Bcl-2 pro-survival proteins determine their capacity to bind ligands. *J Biol Chem.* 2009;284(44):30508-30517. doi:10.1074/jbc.M109.040725.

56. Chen TS, Palacios H, Keating AE. Structure-based redesign of the binding specificity of anti-apoptotic Bcl-x(L). *J Mol Biol.* 2013;425(1):171-185. doi:10.1016/j.jmb.2012.11.009.

57. Chao G, Lau WL, Hackel BJ, Sazinsky SL, Lippow SM, Wittrup KD. Isolating and engineering human antibodies using yeast surface display. *Nat Protoc.* 2006;1(2):755-768. doi:10.1038/nprot.2006.94.

58. Gietz RD, Woods RA. Transformation of yeast by lithium acetate/single-stranded carrier DNA/polyethylene glycol method. *Methods Enzymol.* 2002;350:87-96. http://www.ncbi.nlm.nih.gov/pubmed/12073338. Accessed July 6, 2016.

59. Reich L "Luther," Dutta S, Keating AE. Generating High-Accuracy Peptide-Binding Data in High Throughput with Yeast Surface Display and SORTCERY. In: ; 2016:233-247. doi:10.1007/978-1-4939-3569-7_14.

60. Otwinowski Z, Minor W. [20] Processing of X-ray diffraction data collected in oscillation mode. *Methods Enzymol.* 1997;276:307-326. doi:10.1016/S0076-6879(97)76066-X.

61. Adams PD, Afonine P V, Bunkóczi G, et al. PHENIX: a comprehensive Python-based system for macromolecular structure solution. *Acta Crystallogr D Biol Crystallogr.* 2010;66(Pt 2):213-221. doi:10.1107/S0907444909052925.

62. Emsley P, Lohkamp B, Scott WG, Cowtan K. Features and development of Coot. *Acta Crystallogr D Biol Crystallogr.* 2010;66(Pt 4):486-501. doi:10.1107/S0907444910007493.

63. McCoy AJ, Grosse-Kunstleve RW, Adams PD, Winn MD, Storoni LC, Read RJ. Phaser crystallographic software. *J Appl Crystallogr.* 2007;40(Pt 4):658-674. doi:10.1107/S0021889807021206.

64. Guan R, Xiao R, Mao L, Gelinas C, Montelione GT. Crystal Structure of human BFL-1 in complex with tBid BH3 peptide. *To Be Publ.* doi:10.2210/PDB4ZEQ/PDB.

65. Papadopoulos JS, Agarwala R. COBALT: constraint-based alignment tool for multiple protein sequences. *Bioinformatics.* 2007;23(9):1073-1079. doi:10.1093/bioinformatics/btm076.

66. Fire E, Gullá S V, Grant RA, Keating AE. Mcl-1-Bim complexes accommodate surprising point mutations via minor structural changes. *Protein Sci.* 2010;19(3):507-519. doi:10.1002/pro.329.

Chapter 3

Peptide design by optimization on a high-dimensional, data-parameterized protein interaction landscape

V. Xue, J.M. Jenson, and A.E. Keating designed and wrote the study. L. Stretz performed the titrations of the standards. V. Xue did the computational work and J.M. Jenson did all remaining experiments.

Abstract

Many applications in biotechnology require optimizing protein or peptide binding affinity and specificity for one target among many similar, evolutionarily related family members. For example, this is necessary to make specific detection reagents, or to inhibit one paralog that is implicated in disease without affecting others that are important for the maintenance of healthy cells. The underlying problem is that of navigating a high-dimensional landscape in both sequence variables (L dimensions, where L is the protein length) and target affinities (N dimensions, if there are N paralogs of interest). Because the protein designer begins a problem with no understanding of this complex landscape, the problem is typically treated by screening large, libraries of candidate solutions that are often generated randomly and addressing each design challenge with a new set of experiments. This is inefficient. Furthermore, because functional protein sequences are rare, most screens only explore the local sequence spaces around known binders, and therefore discover just a few function-enhancing mutations at a time. A knowledge of the underlying protein landscape could open new avenues for design and ways to access functional regions in sequence space that are otherwise difficult to discover. We developed a protocol for using thousands of protein-peptide binding affinities, measured with SORTCERY, to parameterize models in a landscape where N = 3 members of the Bcl-2 family of apoptosis regulating proteins. We showed that models trained on experimental data have predictive ability on unobserved peptide sequences, and that optimization on a landscape defined by these models generates new peptides that are distinct from any previously known binders and have highly optimized interaction affinities and specificities. We generated 36 peptides

that bind with high affinity and specificity to just one of Bcl-x_L, Mcl-1 or Bfl-1, and additional peptides that can bind selectively to two out of three of these proteins. The successful designs demonstrate the power of this landscape-based design approach, and the resulting peptides have potential for use as diagnostics or therapeutic leads.

Introduction

Protein-protein interactions (PPIs) play an essential role in all cellular functions, including transcription, translation, signaling, homeostasis, and the regulation of enzymatic activity. Protein interaction affinity and specificity are encoded in sequence and structure in a complex mapping that we do not completely understand. A long-standing goal in protein science is to describe the underlying relationships accurately enough to inform studies of disease mechanisms, for example by predicting the effects of mutations on function. Models that accurately link sequence to function can also enable discovery of new binding partners and direct the engineering of proteins with new functions.

Families of structurally similar protein domains that share an evolutionary history provide intriguing, and often biomedically compelling, examples of how subtle details of the protein sequence-structure relationship impact biological function. Diverged protein paralogs often have distinct functions, e.g. distinct binding specificities, that can be accommodated in a common structural scaffold. For example, the PDZ domain fold has been evolved into proteins with at least 16 distinct specificity classes[1]. Many biomedical applications require reagents that can bind or inhibit the function of just a single family member within a larger family. Computational and experimental strategies for

engineering selective inhibitors can be effective, but most methods treat each target design as a new problem. A driving need for custom, selective, protein-binding molecules has compelled our pursuit of new methods for modeling sequence-function relationships that consider a wider swath of the protein sequence landscape for a given type of domain.

Proteins of the B-cell lymphoma 2 (Bcl-2) family are critical regulators of apoptosis that have emerged as promising therapeutic targets for the treatment of many different cancers. Overexpression of human anti-apoptotic proteins Bcl-2, Mcl-1, Bfl-1, Bcl-x_L, and Bcl-w contribute to oncogenesis and resistance to chemotherapy[2]. These five proteins are highly similar in structure and 18 - 53% identical in sequence[3]. Molecules that bind and block the functions of anti-apoptotic proteins have shown great promise in pre-clinical and clinical studies[4–7]. It would be useful to design Bcl-2 family member-selective inhibitors, rather than pan-family inhibitors, because off-target binding can lead to cytotoxic effects[5,8]. The small molecule ABT-263, which binds and inhibits the function of Bcl-2, Bcl-x_L and Bcl-w, was identified as a potential therapeutic for treatment of acute lymphoblastic leukemia[5]. However, ABT-263 inhibition of Bcl-x_L leads to dose-limiting thrombocytopenia[8,9]. Venetoclax, an FDA approved therapeutic for treating chronic lymphocytic leukemia, inhibits only Bcl-2 and not Bcl-x_L or Bcl-w; fewer side effects helped advance this molecule to the clinic[4,6]. Selective inhibitors of Bcl-2 family proteins also have utility for research and for cancer patient cell profiling[10,11]. The Bcl-2 family is just one example out of many protein families where understanding and managing binding specificity is important for developing effective and safe therapeutics.

Many native binding partners of Bcl-2, Mcl-1, Bfl-1, Bcl-x_L, and Bcl-w contain a ~23-residue Bcl-2 homology 3 (BH3) motif that forms an amphipathic helix upon complex formation[12]. Synthetic peptides with BH3 motif sequences can compete with native interaction partners and function as inhibitors. Mapping how sequence determines the binding profiles of BH3-like peptides could support the design of selective inhibitors with applications as probes, diagnostics and therapeutics leads, but the $>10^{28}$ possible sequences for a 23-mer peptide pose a daunting challenge. Systematic mutational analyses have provided information about the effects of single mutations in BH3 peptides, and library screening has uncovered functional sequences distinct from wild-type examples[3,13–15]. However, as for most proteins, the biophysical study of BH3 structure-function relationships is hampered by the sparsity of available data in an enormous sequence space. Ideally, computational methods would fill this gap, but physical, structure-based modeling has limited accuracy for predicting folding or binding energy differences among related protein complexes, especially in high-throughput[16]. Previous computational design of Bcl-2 inhibitors installed known "hot-spot" residues at the protein interface to stabilize binding, and used computation to generate a stabilized scaffold to accommodate these residues[17]. Basing inhibitor design on known residue interactions limits the novelty of solutions that can be obtained.

Experimental library screening is an effective method for discovering peptides ligands that bind protein targets, including anti-apoptotic Bcl-2 proteins. Such experiments typically consider only a single design objective (e.g. identify a tight and selective binder of protein Bfl-1), and for every design objective, a new experiment must be performed. The experiments usually focus on identifying a "winner," or a small set of

the best binders out of an input library. Advances in technology have now made it possible to use deep sequencing to obtain large amounts of phenotypic data from a library screen, for example, readouts for all single-point and residue-pair mutations in a modest-sized protein[18]. This information is now available to guide protein design, and the field can potentially advance faster by using it effectively.

A few exciting examples illustrate the potential of large amounts of experimental data, treated in a systematic way, to improve design. An early example was the use of peptide arrays to measure the effects of peptide point mutations on PDZ domain binding[19]. This led to a simple model of what was important for binding that, in turn, guided the design of PDZ "super-binder" peptides that would have been difficult to identify without the underlying experimental dataset. More recently, the Baker Lab has demonstrated how using high-throughput screening to assay the effects of all possible point mutations in a designed protein can provide insights into limitations of computational models and lead to their improvement[20]. Rocklin et al. showed that computationally designing and testing thousands of novel mini-proteins, and applying computational analyses to capture trends in folding stability, led to improvements in computational design outcomes[21]. Bedbrook et al. used activity data for hundreds of variants of channel rhodopsins to train a model to captures the sequence features important for expression and membrane localization, and used this model to predict the best members in a library and also improve the behavior of poorly localizing protein[22].

With increasing amounts of experimental data becoming more routinely accessible, the synergistic application of high-throughput binding assays with data-driven modeling holds great potential for advancing rational design. Here, we

demonstrate the possibilities of this type of approach by applying the high-throughput SORTCERY assay to generate quantitative protein-peptide interaction data for the Bcl-2 protein family members Bfl-1, Mcl-1, and Bcl-x_L. The data allowed us to develop family-specific computational models that provide insight into the determinants of binding affinity and specificity. We applied our models to peptide design, showing that this data-driven approach rapidly and reliably provides peptides with custom desired binding properties. Our success illustrates a new approach for integrating data collection and modeling to map high-dimensional protein binding landscapes and guide exploration of novel sequence spaces. This can enable discovery of novel peptides with high potential utility.

Results

SORTCERY is a protocol for measuring the relative affinities of hundreds or thousands of peptide binders in parallel[23,24]. Yeast cells displaying different peptide ligands are separated into pools based the binding signal using fluorescence activated cell sorting (FACS). By deep sequencing the library DNA from cells in different pools, it is possible to assign relative binding affinities on the cell surface. In previous work, SORTCERY was used to rank-order ligands by affinity[23]. We improved on the original pipeline, as described below, by using the binding profiles of standards of known affinity to convert quantitative SORTCERY outputs into binding affinities in standard units (e.g. kcal/mol). This allowed us to directly compare the binding of ligands measured at different target protein concentrations and also compare peptide binding affinities for different target proteins. We call this elaboration of the original SORTCERY protocol *amped* (affinity mapped) *SORTCERY* (Figure 3.1A).

We applied amped SORTCERY to measure binding of the three Bcl-2 family proteins Bcl-x_L, Mcl-1, and Bfl-1 to members of a small yet diverse library of BH3-like peptides (Figure 3.1A). Approximately 10,000 peptides to be measured were selected from much larger combinatorial libraries that were previously designed to be enriched in selective binders of Bcl-x_L, Mcl-1 or Bfl-1[25].The input libraries contained peptides with up to 8 amino-acid mutations compared to human Bim or Puma BH3 motifs and had a theoretical diversity of 27,696,384 possible members; we refer to this set of sequences as the *input library* (Figure 3.1A). Clones to be assayed by amped SORTCERY were selected from the input library by pre-sorting to include peptides with a range of binding affinities for Bcl-x_L, Mcl-1, and Bfl-1 (see Methods). SORTCERY assays were then run at 1 nM, 1 nM, or 100 nM of Bcl-x_L, Mcl-1, or Bfl-1, respectively, generating six datasets (Table 3.1). Bfl-1 binding was assayed at a higher protein concentration than was used for Bcl-x_L or Mcl-1 because few peptides in this library bound detectably at 1 nM. After computational filtering, each experiment generated binding profiles for between 1292 and 3489 unique peptides.

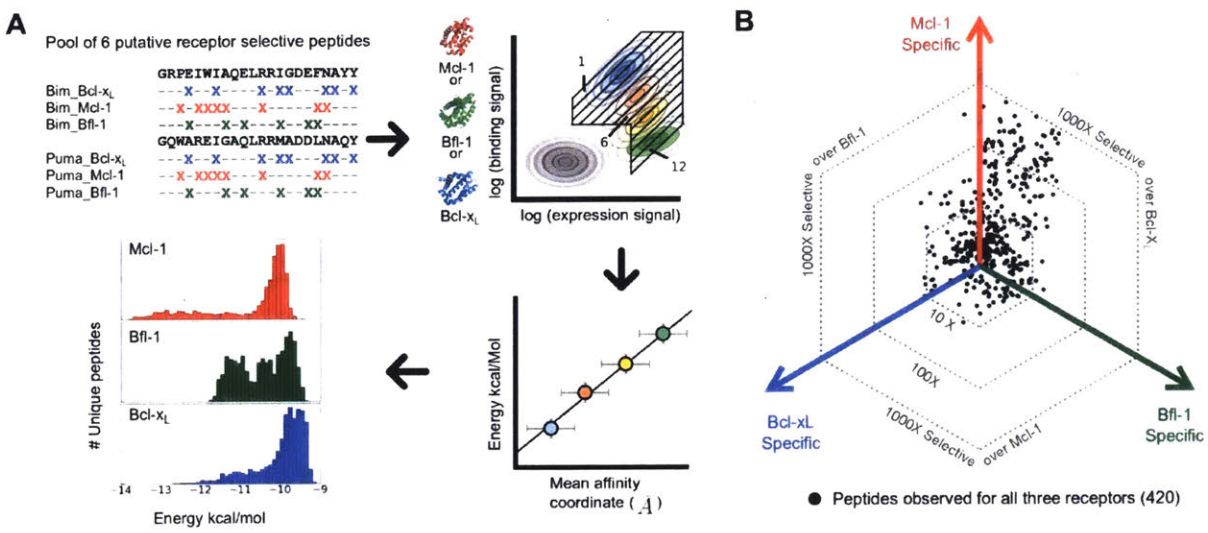

Figure 3.1. High-throughput measurement of thousands of BH3 mutant affinities for Bfl-1, Bcl-x_L, and Mcl-1 with amped SORTCERY. A) Schematic of data collection and modeling pipeline. Three computationally designed libraries targeting Mcl-1 (red), Bfl-1 (green) and Bcl-x_L (blue) were synthesized in the context of Bim and Puma BH3 scaffolds. In the left-most panel, "X" symbols indicate the positions that were varied in each library. The six libraries were expressed on the yeast cell surface, cell populations were pooled, and a subset of ~10^4 clones was evaluated for binding to the three receptors via a 12 gate FACS scheme. Deep sequencing and computational analysis were applied to reconstruct the individual peptide binding profiles across the 12 gates and determine mean affinity coordinates for each peptide. Standards were measured to calibrate the mean affinity coordinate of each peptide to binding free energy in kcal/mol. Experimentally determined receptor binding energies for 2679, 1292 or 3480 peptides binding to Bcl-x_L, Bfl-1, and Mcl-1 were identified, respectively. A histogram of the binding free energies show that the peptides have cell-surface affinities between -14 and -9 kcal/mol. B) The binding energies for 420 sequences with experimentally measured affinities for Mcl-1, Bfl-1, and Bcl-x_L are plotted on a trisected plane to visualize the specificity space. Each peptide is described by 3 vectors, each projecting the negative binding free energy for Mcl-1, Bfl-1, or Bcl-x_L, from the origin (0,0) toward one of three corners of an equilateral triangle. The vectors are summed to produce a coordinate in 2D space that quantifies the peptide binding preference for the three receptors. This projection removes the absolute quantification of affinity and emphasizes paralog binding selectivity.

Table 3.1. Summary statistics of datasets collected.

Reference	Receptor concentration (nM)	# unique sequences	# standards	Pearson R of Ā to standards	RMSE of energy mapped standards (kcal/mol)	Replicate overlap	Replicate RMSE (kcal/mol)	Replicate Pearson R
Bcl-xL_r1	1	2679	17	0.82	0.56			
Bcl-xL_r2	1	3457	18	0.85	0.50	1749	0.35	0.91
Bfl-1_r1	100	1292	16	0.88	0.33			
Bfl-1_r2	100	3489	16	0.84	0.39	975	0.21	0.95
Mcl-1_r1	1	3326	16	0.89	0.47			
Mcl-1_r2	1	3480	16	0.92	0.40	2315	0.21	0.98

SORTCERY measures affinity ($\bar{A}$) in arbitrary units related to what FACS gates each clone is distributed across. Theory predicts that $\bar{A}$ will be linearly correlated with binding free energies over a certain resolution range, under certain conditions[23]. To test this relationship and to map affinity measurements to kcal/mol, peptide standards spanning the SORTCERY dynamic range were individually titrated on the yeast cell surface with each of the three receptors to determine dissociation constants (Figures 3.2-3.4). Measured $\bar{A}$ values correlated with individually measured binding free energies with Pearson R = 0.81-0.92 (see Table 3.1). We used these measurements to map $\bar{A}$ to binding free energies in kcal/mol (see Methods). Linear fits for 16-18 standards per dataset gave RMSE of 0.34-0.56 kcal/mol over a range of dissociation constants from 0.07 nM to 290 nM (Figure 3.1A).

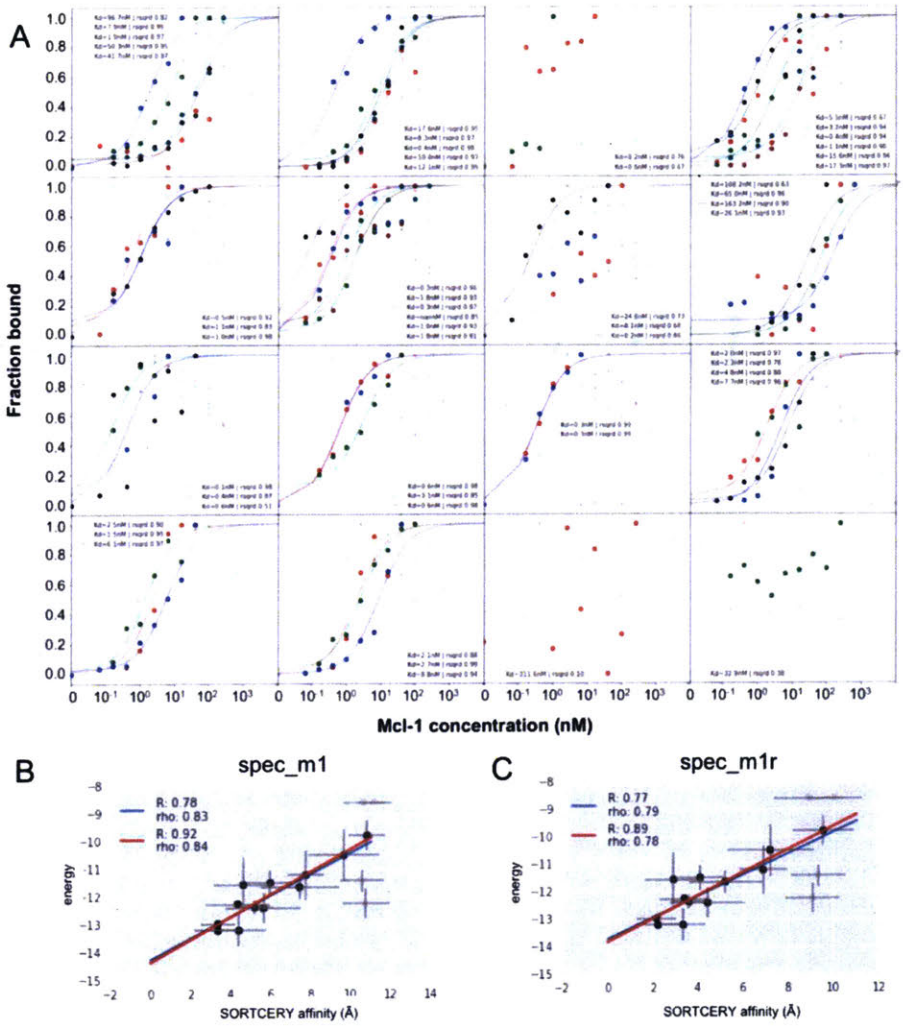

Figure 3.2. Mcl-1 titrations of peptide standards spanning the SORTCERY dynamic range. A) Individual titrations are shown, one standard per plot. Experimental replicates are represented as different colors. Fits to data are shown as solid lines. B-C) Correlation of the SORTCERY mean affinity coordinate (Å) to binding energy in kcal/mol is shown. Error bars for dissociation constants indicate standard deviations for the individual titrations shown in A. Error bars for the SORTCERY mean affinity coordinates indicate the standard deviation of the population across gates. The blue lines show the correlation for all of the data points. The red lines show the correlation excluding points that did not have a numerical K_D and points whose titration curves saturated at lower binding signal than SORTCERY theory expected.

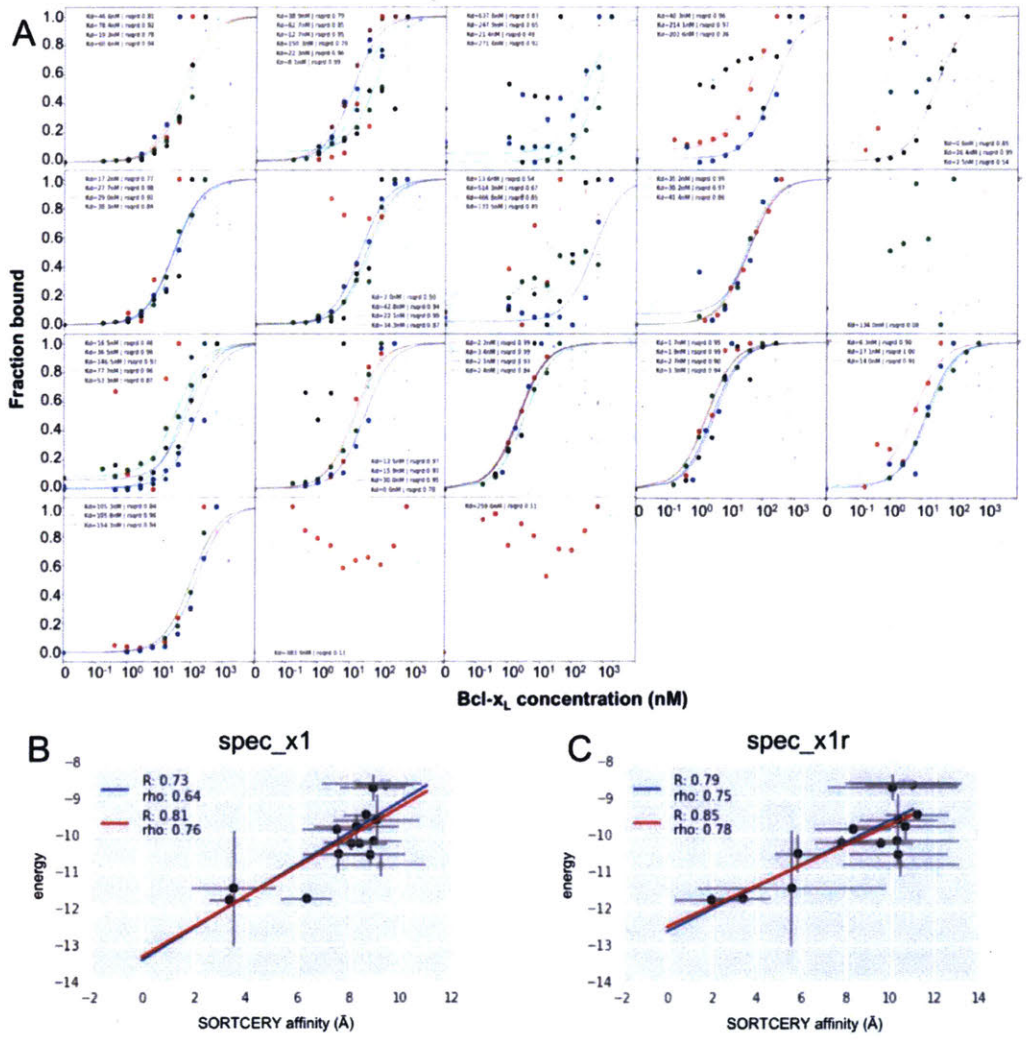

Figure 3.3. Bcl-x_L titrations of peptide standards spanning the SORTCERY dynamic range. A) Individual titrations are shown, one standard per plot. Experimental replicates are represented as different colors. Fits to data are shown as solid lines. B-C) Correlation of the SORTCERY mean affinity coordinate (Ā) to binding energy in kcal/mol is shown. Error bars for dissociation constants indicate standard deviations for the individual titrations shown in A. Error bars for the SORTCERY mean affinity coordinates indicate the standard deviation of the population across gates. The blue lines show the correlation for all of the data points. The red lines show the correlation excluding points that did not have a numerical K_D and points whose titration curves saturated at lower binding signal than SORTCERY theory expected.

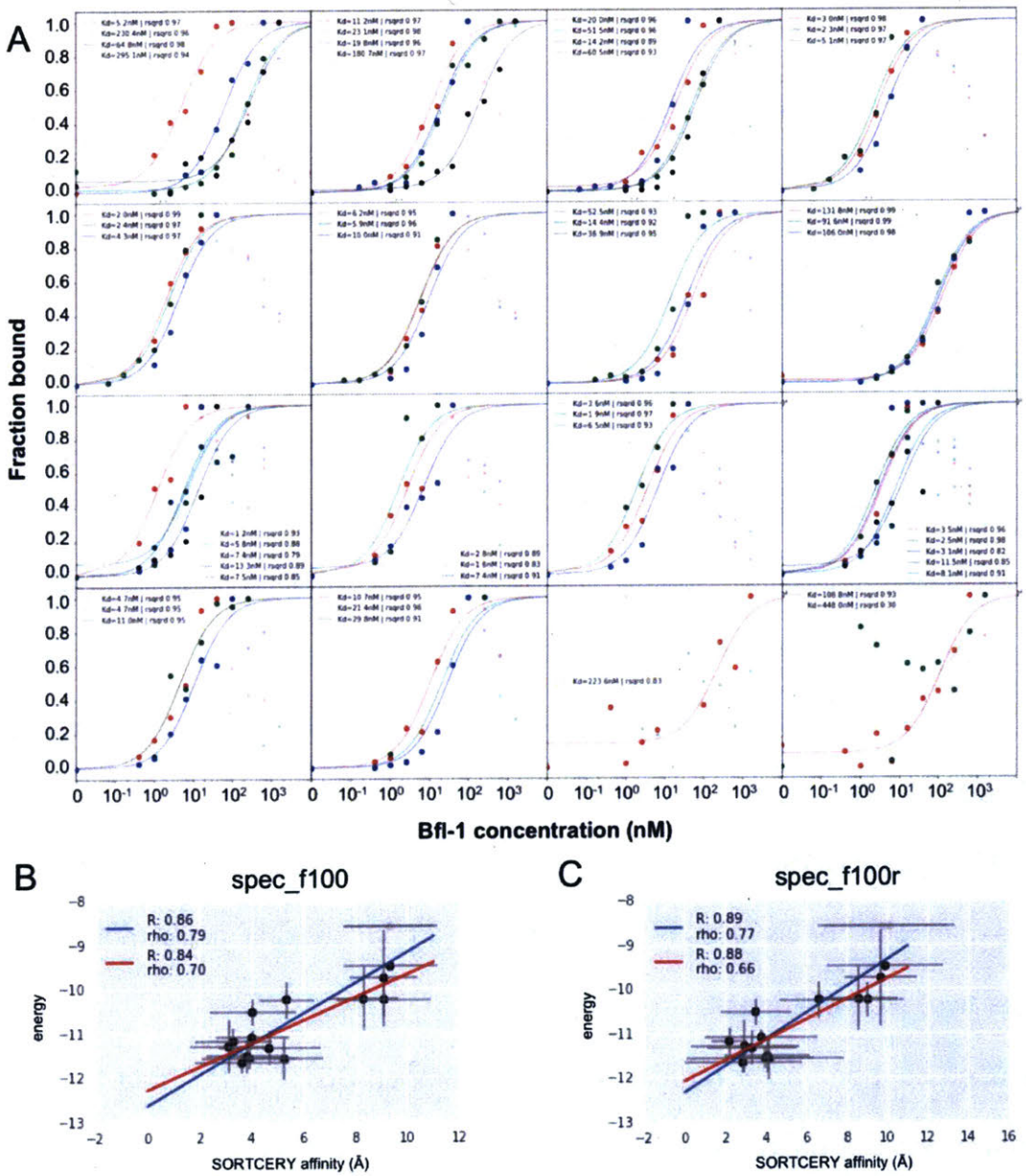

Figure 3.4. Bfl-1 titrations of peptide standards spanning the SORTCERY dynamic range. A) Individual titrations are shown, one standard per plot. Experimental replicates are represented as different colors. Fits to data are shown as solid lines. B-C) Correlation of the SORTCERY mean affinity coordinate (Ā) to binding energy in kcal/mol is shown. Error bars for dissociation constants indicate standard deviations for the individual titrations shown in A. Error bars for the SORTCERY mean affinity coordinates indicate the standard deviation of the population across gates. The blue lines show the correlation for all of the data points. The red lines show the correlation excluding points that did not have a numerical K_D and points whose titration curves saturated at lower binding signal than SORTCERY theory expected.

We quantified binding for 5769 unique peptide in this experiment. Binding energies computed in two replicates were highly reproducible, with Pearson R values of 0.91-0.98. For 420 peptides, we obtained affinities for all three proteins Mcl-1, Bfl-1, and

Bcl-x_L. Other peptides were either not observed in all three data sets or had affinity values outside the range we could quantify. To visualize the binding selectivity landscape of the 420 sequences, we plotted the affinity of each peptide for each protein in three dimensions (one dimension for each target protein) and projected this plot into two dimensions, giving a trisected plane representation (Figure 3.1B). Peptides with three measured binding energies included examples with 100-fold specificity for binding Mcl-1 over Bfl-1 or Bcl-x_L. In contrast, the most selective binders of Bfl-1 or Bcl-x_L had only a 10-fold preference for those proteins.

We reasoned that if we could use amped SORTCERY data to build a computational model to capture how sequence determines binding, we could predict binding free energies for peptides not measured in our experiments and generate a more complete binding landscape. We tested two different models. Peptide binding free energy was either expressed as a sum of independent contributions from individual residues (linear model), or as a sum of contributions from residue pairs (polynomial model of order two) (see Methods).

We used support vector regression against amped SORTCERY data to fit the residue contributions for each model[26]. We compared the performance of linear vs. polynomial models trained on each data set using nested cross-validation. The second-order polynomial models consistently outperformed linear models trained on the same data, when evaluated using a validation set of sequences that was non-overlapping with the training data (see Figure 3.5A).

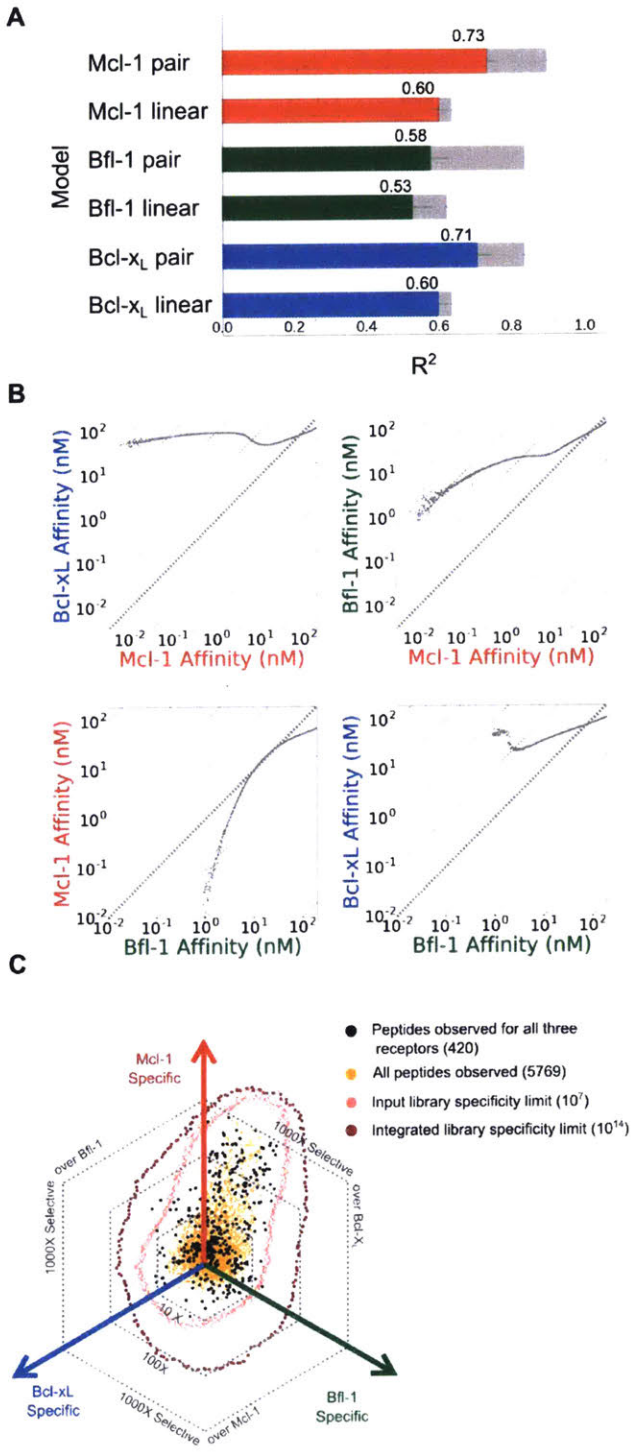

Figure 3.5. Computational models built on SORTCERY datasets. A) Nested cross-validation performance for linear and polynomial models trained on Mcl-1, Bcl-x_L and Bfl-1 datasets Bcl-x_L_r1, Bfl-1_r1 and Mcl-1_r2. Light grey bars correspond to the average R^2 of models trained and evaluated on the same data. Colored bars correspond the average R^2 of models evaluated on data held out from training in nested-cross validation. B) Specificity and affinity tradeoffs for BH3 peptides binding to Mcl-1 vs. Bfl-1. All 27,696,384 peptides in the designed library were computationally scored for binding to Mcl-1, Bfl-1, and Bcl-x_L. For a given target receptor (x axis), peptides were binned by the predicted target affinity. The median affinity of the off-target (y axis) is plotted for each bin. The shaded fill indicates the 25th and 75th percentiles. Lines parallel to the 1:1 line indicate increasing fold selectivity. C) Map of the Mcl-1, Bcl-x_L, Bfl-1 specificity landscape. Receptor-specific affinity models were used to explore specificity space. Black points plot the specificity coordinates of the 420 sequences with experimentally measured Mcl-1, Bfl-1, and Bcl-x_L binding energies. Orange points plot the specificity coordinates of all peptides observed to bind at least one receptor, using the model to predict the missing coordinate(s). Models can also define extremes in the specificity space for all theoretical library members, including those that were not observed experimentally (pink), A further extrapolation can map the predicted boundaries of specificity for an integrated library space that includes all substitutions that were sampled in any of the six original input libraries (brown). See methods for details.

We used the polynomial models to investigate whether high affinity for one protein is predicted to correlate with high affinity for others, as has been observed using

other predictors[25]. To investigate tradeoffs between selectivity and affinity, we compared predicted peptide binding affinities for pairs of receptors. The tradeoffs observed depended on which proteins were compared. For most pairs, there is a positive correlation of the binding affinities. For sequences in the input library, the peptides predicted to bind most tightly to Mcl-1 were predicted to bind >1000-fold weaker to Bcl-x_L and >100-fold weaker to Bfl-1, on average (Figure 3.5B). This suggests that identifying tight Mcl-1 binders that are specific for that target may not be difficult, and indeed several peptides with this property have been published[14]. In contrast, the peptides from these libraries that were predicted to bind tightest to Bfl-1 were predicted to bind more than 10 times more weakly to Bcl-x_L, but greater than 10 times more tightly to Mcl-1, on average (Figure 3.5B). This analysis suggests that it might be difficult to identify high-affinity binders of Bfl-1 that do not bind to Mcl-1, which is consistent with prior observations from library screening experiments[27].

Models that can be used to predict unmeasured affinity values made it possible to plot all 5769 peptides from our experiment in three-dimensional specificity space; these values are shown in orange in Figure 3.5C. We can extrapolate even further, to compute the predicted distribution of all 27,696,384 input library sequences, the vast majority of which of which were not tested experimentally for binding to any of the three proteins. The extremes of this distribution are shown in light pink in Figure 3.5C; the results predict that our input library was enriched in Mcl-1 specific sequences, relative to Bfl-1 or Bcl-x_L specific sequences. Finally, although our models were trained on sequences from the input library space, we can make predictions about sequences that lie outside this space. For example, we can consider the space of 10^{14} sequences that

includes all combinations of residues that were considered at any position in any library. This space, which we call the *integrated library space* (Table 3.2), includes many residue combinations that were never sampled experimentally, including sequences that mix and match residues from the BIM and PUMA backgrounds. Thus, the model is not necessarily expected to make accurate predictions in these regions of the sequence landscape. To visualize the integrated library space, we solved for the Pareto frontier of selectivity (Figure 3.5A), i.e. for sequences that are predicted to be optimally specific. Sequences at this boundary (dark pink in Figure 3.5A) demonstrate that predicted selectivity can be as much as tenfold greater in the integrated space than in the input library space. The models predicted a modest opportunity to increase Mcl-1 specificity beyond what we observed in the SORTCERY screen, but predicted that the integrated library contains members with much enhanced specificity for Bfl-1 or Bcl-x_L, relative to the input library.

Table 3.2. Summary of mutational spaces.

Position	BIM	PUMA	Bfl-1 Specific Library	Bcl-x_L Specific Library	Mcl-1 Specific Library	Integrated Library
1g	P	W			AGPRSTW	AGPRSTW
2a	E	A	AEIKLPQTV	DEGHIKLMNQRSV		ADEGHIKLMNPQRSTV
2b	I	R			ACDFGHLPRSVY	ACDFGHI LPRSVY
2c	W	E			DEHQ	DEHQW
2d	I	I			AITV	AITV
2e	A	G	ACDGSY		AGISTV	ACDGISVY
2f	Q	A				AQ
2g	E	Q	CDFGHILNRSVY			CDEFGHILNQRSVY
3a	L	L				L
3b	R	R		ADEGKNRST	AEGIKRTV	ADEGIKNRSTV
3c	R	R				R
3d	I	M	ACFGILPRSTV	ADFHILNPSTVY		ACDFGHILMNPRSTVY
3e	G	A		AG		AG
3f	D	D				D
3g	E	D	DEHIKLMNQV			DEHIKLMNQV
4a	F	L	ADFHILNPSTVY		ADFHILNPSTVY	ADFHILNPSTVY
4b	N	N		ADHILNPTV	DEHKNQ	ADEHIKLNPQTV
4c	A	A		ADEGKNRST		ADEGKNRST
4d	Y	Q				YQ
4e	Y	Y	AFILPSTV	ACDGHNPRSTY		ACDFGHILNPRSTVY
4f	A	E				AE
4g	R	R				R
5a	R	R				R

To evaluate the predictive power of our models at the boundaries of the integrated library space, and test the utility of the models for practical applications, we used them to design selective peptide binders of Bcl-2 family members. We designed three sets of peptides to bind selectively to just one of Mcl-1, Bfl-1, or Bcl-x_L, and three sets of bispecific peptides to bind selectively two out of three receptors: Mcl-1 and Bcl-x_L, Mcl-1 and Bfl-1, or Bcl-x_L and Bfl-1. In both cases we used constrained optimization to balance the dual objectives of tight binding to the target(s) and weak binding to the off-target(s)[28]. For the single-receptor specific peptides, we maximized predicted target-binding affinity, with a constraint on the affinity for off-target proteins that was implemented as a lower limit on the predicted binding free energy (Figure 3.6B).

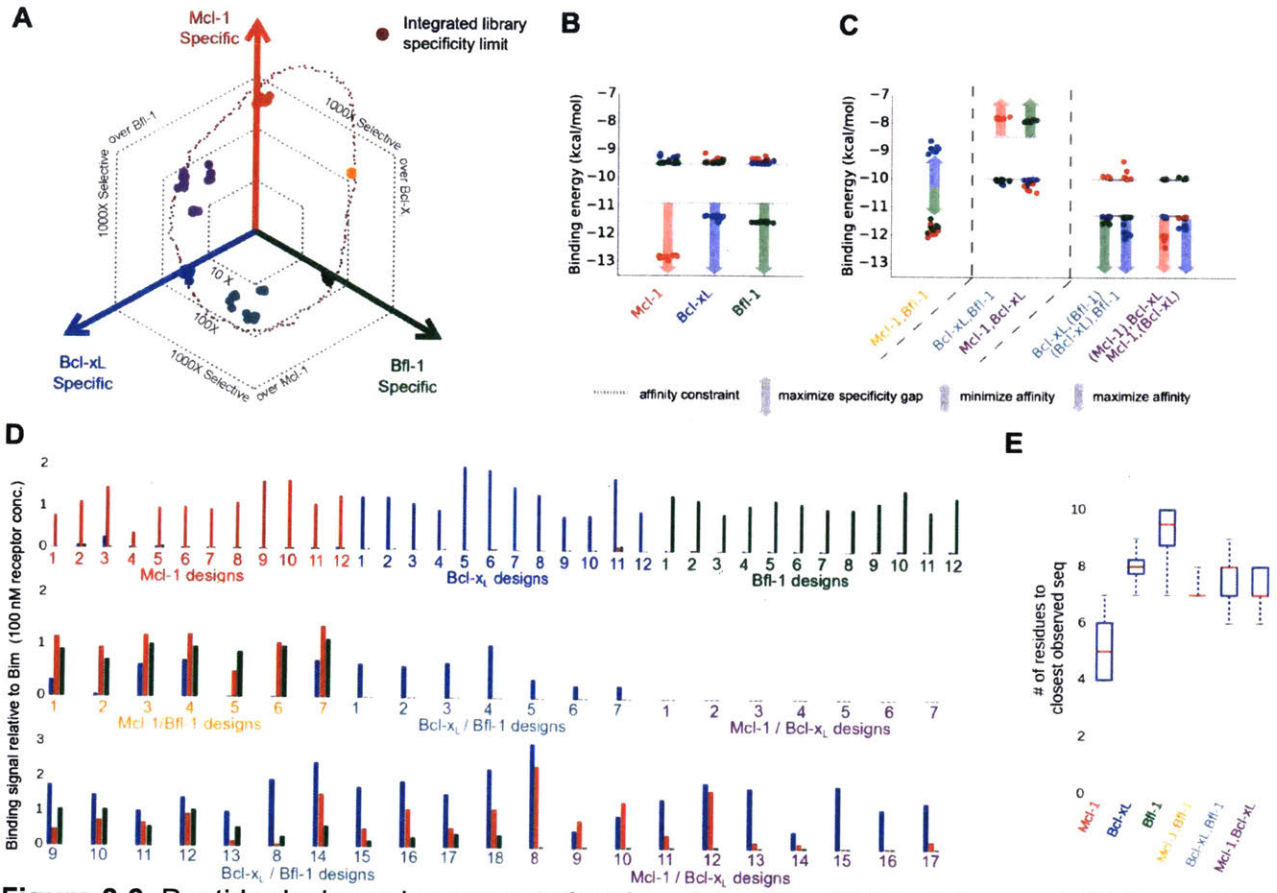

Figure 3.6. Peptide design using computational models of the Mcl-1, Bcl-x_L, and Bfl-1 specificity landscape. A) Designed peptides plotted in the the specificity landscape. Selective peptides were designed to bind to Mcl-1 (Red), Bfl-1 (Green), or Bcl-x_L (Blue), without cross-reacting with the other two receptors. Bispecific peptides were designed to interact with Mcl-1/Bfl-1 (orange), Bcl-x_L/Bfl-1 (teal), and Mcl-1/Bcl-x_L (purple), without binding tightly to the off-target receptor. B-C) Selective sequences were designed with constraint optimization. Monospecific peptides were designed to maximize the binding affinity to the target receptor and constrained to bind weakly to off-target receptors. Bispecific peptides were designed to maximize the specificity gap, minimize off-target affinity, or maximize target affinity. D) Ratio of experimentally measured design binding signal to Bim binding signal for Mcl-1 (red), Bcl-x_L (blue) or Bfl-1 (Green) receptors. The designs are color-coded for the objective targets. (Mcl-1 - red, Bcl-x_L - Blue, Bfl-1 Green, Mcl-1/Bfl-1 Orange, Bcl-x_L/Bfl-1 Teal, Mcl-1/Bcl-x_L - Purple). E) Boxplot of the maximum sequence similarity of the designed peptides to any previously observed sequence in the training dataset. Designed peptides were all at least 4 mutations from any previously observed peptide measured by SORTCERY, and some differed in 10 positions from the closest characterized library member.

To evaluate whether the peptides that were designed to bind to just one protein had the desired specificity traits, the peptides were expressed on the surface of *Saccharomyces cerevisiae* and evaluated for binding using fluorescence activated cell

sorting (see Methods, Tables 3.3-5). For each sequence, the median binding fluorescence signal at 100 nM was measured and normalized using the saturated binding signal of BIM, a native BH3 sequence with K_D < 1 nM on the surface of yeast (Figure 3.6D). All 36 of 36 monospecific peptides designed and tested demonstrated the desired selectivity for the target protein. The dissociation constants for the designs binding to their targets were all estimated to be lower than 100 nM, with 28 lower than 10 nM, and 5 lower than 1 nM. All of the off-target binding affinities for the designs were weak, with estimated K_Ds greater than 1000 nM. These values compare favorably with the reported affinities and specificities of previously reported selective Bcl-2 binders that were identified by screening targeted libraries of $>10^6$ sequences[13,14,25,27].

Table 3.3. Mcl-1 specific designs.

name	sequence
M1	GRSELEVVQELVRIGDIVVAYF
M2	GRSEYEYIQELVRIGDEVDAYF
M3	GRSLYEYIQELIRIGDEVTAYF
M4	GRSLLEYIQELIRIGDEVIAYF
M5	GRSELEYIQELVRIGDEVDAYF
M6	GRGQLEYIQELIRIGDIVDAYF
M7	GRSELEYIQELIRIGDNVDAYF
M8	GRSELEYIQELIRIGDIVDAYF
M9	GRSQYEVIQELIRIGDIVLAYF
M10	GRSEYEYIQELIRIGDNVDAYF
M11	GRSEYEYIQELIRIGDIVDAYF
M12	GRGQYEYIQELIRIGDIVDAYF

Table 3.4. Bcl-x_L specific designs.

name	sequence
X1	GQTLIWYGASLRRYADEFAKQR
X2	GQTLIWYGAQLRRYADEFAKQR
X3	GQPLIWFGASLRRGADEFAKQR
X4	GQTLIWYGAQLRRVADDFAKQR
X5	GQTAIWYGASLRRAADEFAKQR
X6	GQSLIWFGASLRRGADEFAAQR
X7	GQPLIWFGAQLRRGADEFAAQR
X8	GQSMIWYGASLRRAADEFAKQR
X9	GQTLIWYGAQLRRYADDFAKQR
X10	GQRLIWYGAQLRRYADDFAKQR
X11	GQTLIWFGASLRRGADEFAAQR
X12	GQGLIWYGAQLRRVADDFAKQR

Table 3.5. Bfl-1 specific designs.

name	sequence
F1	GRRVRHIAQGLRRAGDQLDAYG
F2	GQRVRHIAQGLRRTGDQLDAYG
F3	GRRVVHIAAGLRRTGDQLEAQG
F4	GQRVVHIAAGLRRTGDQLEAYG
F5	GQRVVHIAQGLRRTGDQLEAQG
F6	GQRVVQIAAGLRRTGDQLEKYG
F7	GQRVVQIAQGLRRTGDQLEKQG
F8	GRRVVQIAAGLRRTGDQLEKQG
F9	GRRVRHIAQGLRRAGDQLDKYG
F10	GRRVVQIAAGLRRAGDQLEKYG
F11	GQRVVQIAQGLRRAGDQLEKYG
F12	GRRVVQIAQGLRRAGDQLEKQG

To design bi-specific peptides, we first identified sequences that maximized the difference between the predicted affinities for targets Mcl-1 and Bfl-1 vs. off-target Bcl-x_L (see Methods, Table 3.6). All seven peptides that were designed this way bound to Bfl-1

and Mcl-1 with nanomolar affinity and bound to off-target Bcl-x_L with K_D greater than 1000 nM. This may be the easiest bi-specific design problem, because our analysis in Figure 3.5B predicted that affinities for Mcl-1 and Bfl-1 are more strongly correlated than are affinities for Mcl-1 and Bcl-xL or Bfl-1 and Bcl-xL. Peptide designs 1, 2, 5 and 6 all showed evidence of strong binding to Mcl-1 and Bfl-1 at 100 nM, with very low or undetectable binding to Bcl-x_L at the same concentration.

Table 3.6. Mcl-1 and Bfl-1 bi-specific designs.

name	sequence
MF01	GRRIDEIAQILRRIGDHIEKYI
MF02	GRWIDQIAQFLRRIGDHIEKYI
MF03	GRRVDEIAQILRRIGDNIEEYI
MF04	GRRVDEIAQILRRIGDNINEYI
MF05	GRRIDEIAQILRRIGDHVEKYI
MF06	GRRVDEIAQILRRIGDNVTTYI
MF07	GRRVDEIAQILRRIGDQIEEYI

For the other combinations of targets, we suspected that tight and specific binding might be harder to achieve, and we tested other approaches. The first was to minimize the affinity of peptides for the off-target while constraining the predicted energy of binding to the targets to be < -10 kcal/mol. From two attempts at bi-specific design using this protocol, targeting either Mcl-1 and Bcl-x_L or Bfl-1 and Bcl-x_L, neither gave peptide with the desired profiles. The designs either bound to Bcl-x_L but not Bfl-1, or did not bind to either target. This led us to try a third protocol that involved minimizing target binding energy, subject to a constraint that off-target binding energy be greater than -10 kcal/mol (Figure 3.6C). Because there are two targets for a bi-specific design, we ran

these target affinity-maximizing calculations twice. For the target that was not used for binding score optimization, we imposed an upper-limit on the binding energy of -11 kcal/mol. We used these two strategies to design binders of Mcl-1 and Bcl-x_L, and binders of Bcl-x_L and Bfl-1 (Tables 3.7,8). We obtained several dual-specific peptides that bound tightly to Mcl-1 and Bcl-x_L, with little or no binding to Bfl-1, as shown in Figure 3.6D. However, peptides designed to bind to Bcl-x_L and Bfl-1 often bound those proteins with good signal at 100 nM protein concentration, but also bound to Mcl-1 as well. Our best dual-specific Bcl-xL/Bfl-1 inhibitor was peptide XF13 which was ~10 fold selective over Mcl-1.

Table 3.7. Mcl-1 and Bcl-x_L bi-specific designs.

name	sequence
MX1	GRSQIWYVQELVRGGDVNHAYR
MX2	GRSQIWYDQELVRSGDVNAAYR
MX3	GRSQIWYDQELVRSGDENAAYR
MX4	GRSQIWYDQELVRYADVNAAYR
MX5	GRSQIWYDQELVRYGDVNAAYR
MX6	GRSQIWYVQELVRSGDVNHAYR
MX7	GRSEIWYDQELVRSGDVNAAYR
MX08	GQWLRWVIAELIRIADEFHAQY
MX09	GQWLYWVAAELVRIADDFLAQR
MX10	GQSLIWFIAELARIGDEFHEYY
MX11	GQWLIWYIAELIRIADEFHAQF
MX12	GQWLRDVVAELARIADEFHAQY
MX13	GQWLIWYIAELRRYADEFHAQI
MX14	GQWLIWVAAQLRRYADEFHAQR
MX15	GQWLIWYAAELARLADDFHAQR
MX16	GQWLIWYAAQLARIADEFHAQR
MX17	GQSLIWYIAELARIADEFAAQY

Table 3.8. Bcl-x_L and Bfl-1 bi-specific designs.

name	sequence
XF1	GRRVVWIGQGLKRLADEYHKYA
XF2	GRREVWLSQSLKRIADQFQKYL
XF3	GRREIWLSQYLKRIADLFQKYL
XF4	GRREIWLSQSLKRIADMFQKYL
XF5	GRREIWLSQSLKRIADLFQKYL
XF6	GQRVDDFGQGLKRVADEYHAQA
XF7	GRREVWLSQSLKRIADQFQTYL
XF08	GQRLIWIGAGLRRLADEFDKQA
XF09	GQRIIWIAAELRRAADELDKQI
XF10	GQRIIWIAAELRRAADQLDAQI
XF11	GQRIIWIGAELRRLADELDKQV
XF12	GQRIIWIAAELRRAADQLDKQY
XF13	GQRIIWIAAGLRRLADELDKQL
XF14	GQALIWIGAELRRLADEFNKQL
XF15	GQRLIWIGAELRRLADEFDKQL
XF16	GQPLIWIGAELRRLADEFNKQV
XF17	GQRLIWIGAELRRLADDFDKQY
XF18	GQRLIWIGAELRRLADEFNKQA

All of the peptides that were designed and tested were dissimilar from the sequences used to train the models. Each design was at least 4, and as many as 10 mutations away from any previously observed sequence (see Figure 3.6E). This establishes that the regression models were able to make accurate predictions about regions of the sequence landscape well outside of the region they were trained on. The sequences were on average ~4 mutations away from others in each design set.

Encouraged by our initial results, we picked six designs for further analysis. Two sequences from each set of monoselective designs were chosen based on the initial cell display data. We performed binding titrations from 0.66 to 1000 nM, measuring binding signal on the cell surface. The Mcl-1 designs (M1 and M9) bound Mcl-1 with K_d

< 0.66 nM and bound Bcl-x_L and Bfl-1 with K_d > 1000 nM (Figure 3.7). These are upper bounds on the dissociation constant because the binding signal for the Mcl-1 specific designs was at or near saturation at 0.66 nM Mcl-1, and near baseline in 1 μM Bfl-1 and Bcl-x_L. Concerns about ligand depletion limited the low end of our titrations, and non-specific binding limited the high end. Likewise, we found that the Bcl-x_L specific designs X1 and X7 bound their target tightly (Kd values of 1.56 nM and 0.088 nM, respectively) and had negligible binding to Bfl-1 and Mcl-1 up to at least 1000 nM. Bfl-1 specific designs F4 and F10 bound to Bfl-1 with K_D = 13.98 nM and 3.21 nM, respectively, and had negligible binding to Bcl-x_L and Mcl-1.

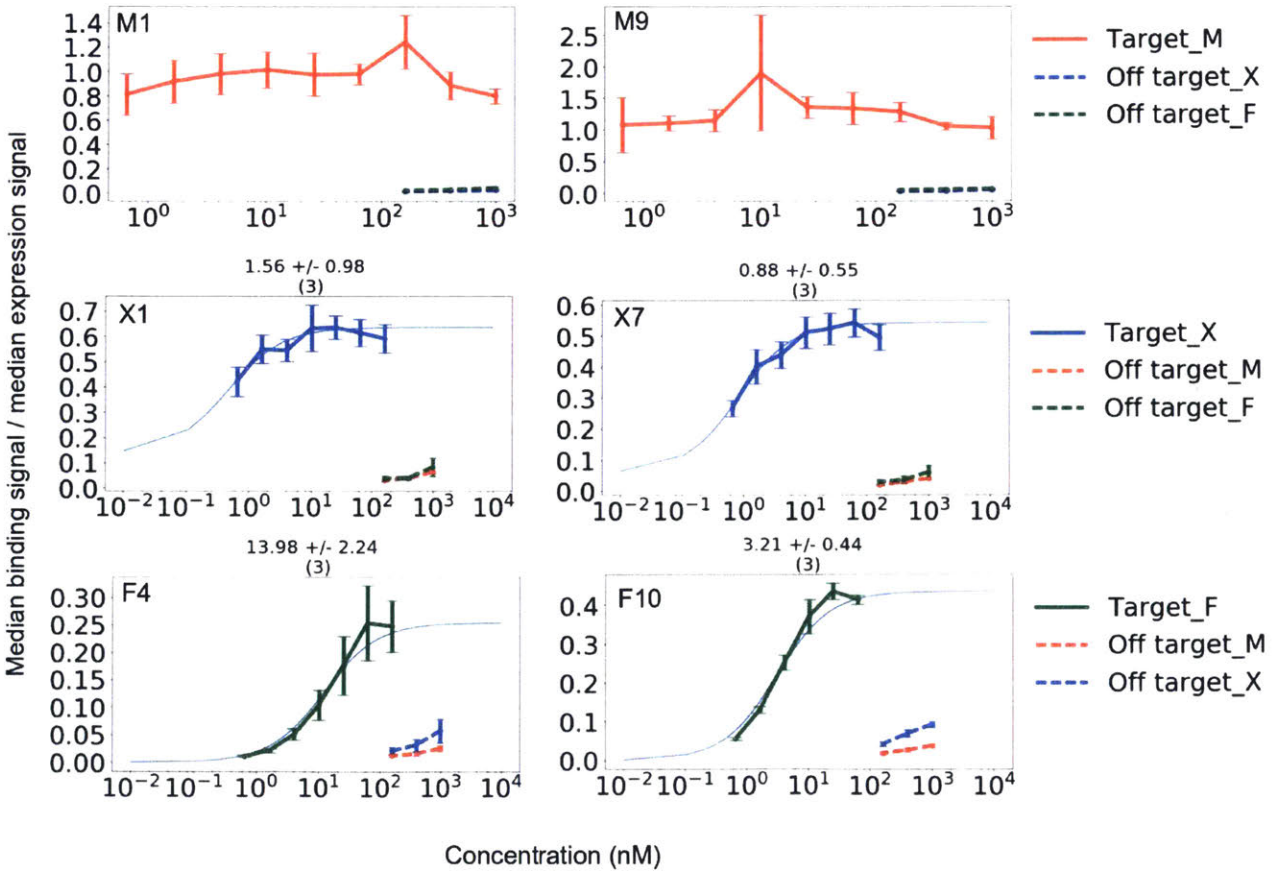

Figure 3.7. Yeast cell-surface binding curves for 6 receptor-specific peptide designs tested against Mcl-1 (red), Bfl-1 (green), and Bcl-xL (blue). The Mcl-1 designs bind tightly with K_D < 0.6 nM for Mcl-1 and >> 1 uM for Bcl-xL and Bfl-1. The Bcl-xL designs bind with K_D ~ 1 nM for Bcl-xL and >> 1 uM for Bfl-1 and Mcl-1. The Bfl-1 designs bind with K_D 3-14 nM for Bfl-1 and >> 1 uM for Bcl-xL and Mcl-1.

Given that the designed peptides have sequences very different from natural BH3 sequences, we tested whether they bind in the same site as known BH3 peptides. Protein binding to all 6 of the tested designs was abolished by the addition of BIM, in a dose-dependent manner, consistent with competitive binding at the same site. Moreover, we solved X-ray crystal structures of F4 and F10 bound to Bfl-1(Figures 3.8,9). Both complexes, Bfl-1:F4 and Bfl-1:F10, were resolved at high resolution (1.48 Å In both cases) and the structures show that the designed peptides bind to Bfl-1 in a geometry very similar to that of natural BH3s. Figure 3.9 shows a superposition of each structure with the structure of Bfl-1 bound to Bim, emphasizing the high similarity.

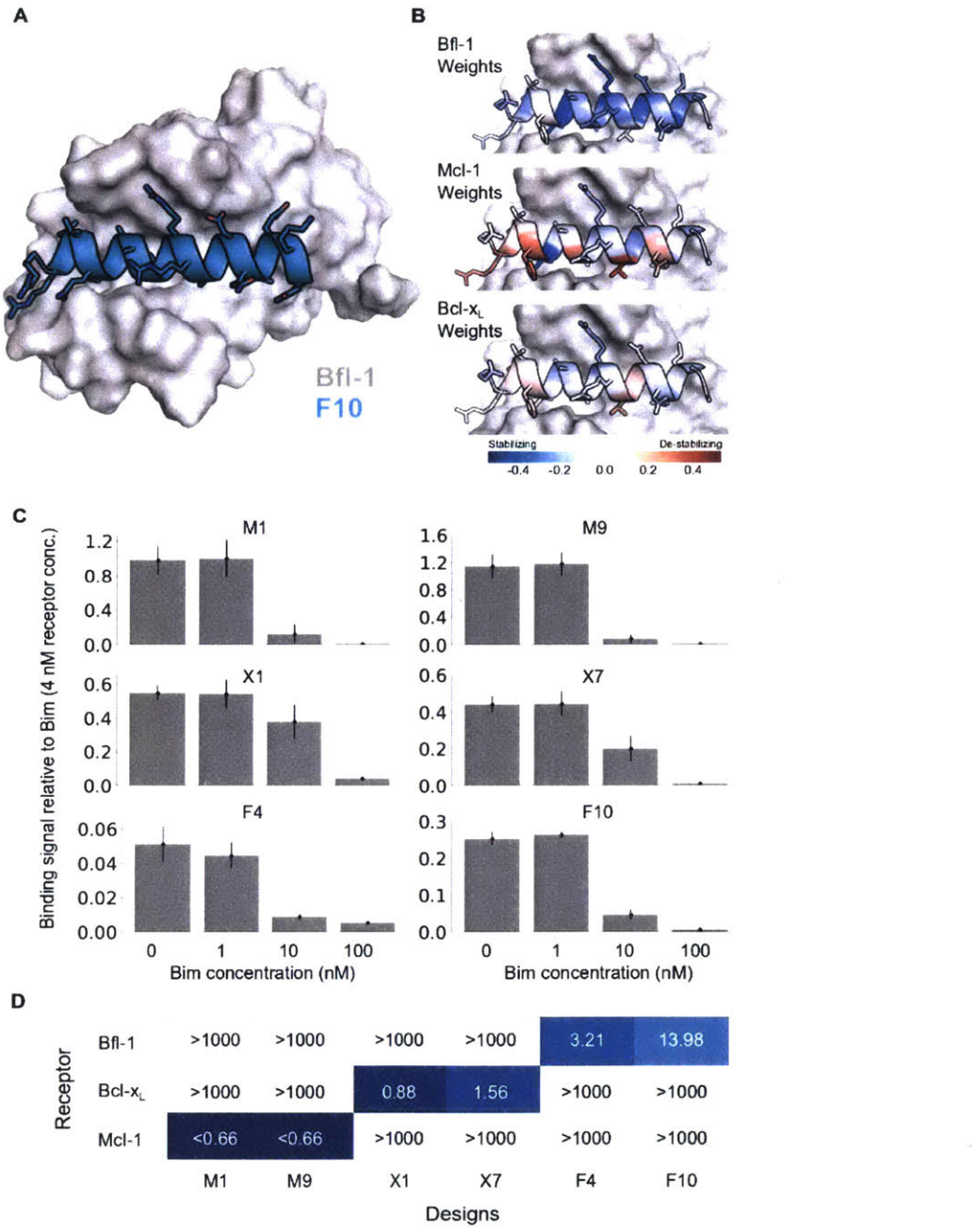

Figure 3.8. Designed peptides directly target the binding grooves of Bfl-1, Bcl-x_L, and Mcl-1. A) A high resolution (1.48 Å) X-ray crystal structure of Bfl-1 specific peptide F10 (cyan cartoon) with Bfl-1 (gray surface). B) Visualization of the polynomial model weights for each residue in F10. C) Competition with unlabeled Bim peptide for binding to 6 receptor-specific peptide designs. Binding was assayed using cell-surface displayed peptide. D) Yeast cell-surface binding K_Ds for 6 receptor-specific peptide designs tested against Mcl-1 (red), Bfl-1 (green), and Bcl-xL (blue).

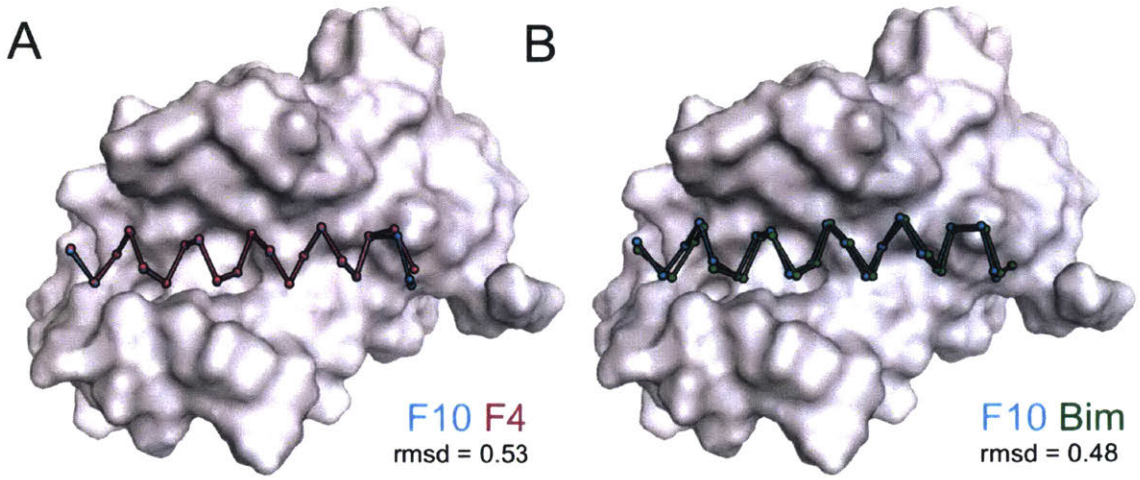

Figure 3.9. High resolution crystal structures of designed peptides show F4 and F10 bind similarly to each other and to Bim BH3. A) Structural aligments of F4 (magenta ribbon) and F10 (cyan ribbon) bound to Bfl-1 (gray surface). Structures were aligned on Bfl-1. B) Structural aligments of F4 (magenta ribbon) and Bim (green ribbon) bound to Bfl-1 (gray surface). Structures were aligned on Bfl-1.

Table 3.9. Summary of X-ray data collection and refinement statistics.

	Bfl-1:F4	**Bfl-1:F10**
Data Collection		
Space Group	P 1 21 1	P 1 21 1
Cell parameters		
a, b, c	43.22 42.947 46.762	43.266 42.907 47.029
α, β, γ	90 114.733 90	90 114.73 90
Rmeas	0.069 (0.411)	0.065 (0.366)
Rpim	0.030 (0.218)	0.026 (0.189)
Mean I/σ(I)	27.72 (2.22)	28.06 (2.58)
Completeness (%)	92.01 (61.95)	97.41 (85.60)
Redundancy	4.5 (2.7)	5.4 (2.9)
Refinement		
Resolution (Å)	37.76 - 1.481 (1.534 - 1.481)	42.72 - 1.482 (1.535 - 1.482)
Unique Reflections	23970 (1596)	25472 (2195)
Rwork/Rfree	0.1343/0.1658 (0.1776/0.2755)	0.1380/0.1712 (0.1540/0.2409)
Number of non-hydrogen atoms	1562	1608
Wilson B-factors	19.88	16.43
Rmsd		
Bond lengths (Å)	0.007	0.011
Bond angles (°)	0.76	1.28

Values in parentheses are for the highest-resolution shell.

A benefit of performing rational design using predictive models, such as the ones we used here, is that the models provide detailed hypotheses about why certain complexes are stable vs. unstable. Figure 3.8B shows the residue contribution weights from our three different models mapped onto the structure of F10 bound to Bfl-1 using a heatmap to indicate residues that are net stabilizing vs. destabilizing. The favorable contributions of most residues to Bfl-1 binding are reflected in a mostly blue colored peptide, at top. In contrast, our models for Bcl-x_L and Mcl-1 binding highlight, in red, residues that are predicted to destabilize binding and thereby contribute to specificity.

The model weights indicate that the specificity of the designs comes from contributions from many residues throughout the peptide, although some residues such as V3d are predicted to be particularly important for disfavoring interactions with off-target proteins.

Discussion

Deep sequencing combined with library display technologies now makes it possible to accurately describe and model larger parts of the protein interaction universe than ever before. Amped SORTCERY provides a method to quantitatively determine binding energies of thousands of diverse ligands in high throughput, and we used it to measure peptide binding to a family of 3 structurally, functionally, and evolutionarily related proteins: Bfl-1, Mcl-1, and Bcl-x_L, mapping the specificity landscape. We further expanded our description of the specificity landscape using models trained on the experimental data. We demonstrated that statistical models derived by regression could be used to design protein sequences up to ten mutations away from the training set, and experimental testing confirmed that all of the designed monospecific peptides and many of the dual-receptor specific had the desired binding profiles.

One interesting observation is that our designed peptides were more specific for their targets than was predicted by our models. The restricted dynamic range of the SORTCERY affinity assay might help explain this, because it limited our ability to accurately measured how destabilizing some mutations are. Models that underestimate destabilizing effects could lead to overestimates of how well the designs bind off-target proteins. Performing SORTCERY at higher concentrations could enable more accurate measurement of weaker affinities.

Many statistical models assume that the effects of multiple mutations are additive, even though epistasis can be pervasive and its effects significant[29–33]. Prior work suggests that epistasis can be important for determining the binding of BH3 peptides to Bcl-2 family proteins. For example, Jenson *et al.* demonstrated that there can be a context dependence to the effect of substitutions made in Bim vs. Puma BH3 peptides[25]. Specificity inducing mutations in the Puma BH3 context did not provide specificity in the Bim BH3 context[25]. Jenson *et al.* additionally observed energetic coupling between N-terminal and C-terminal residues in a designed Bfl-1 selective binder. DeBartolo *et al.* reported only a modest correlation between the mutational effects of point residue changes in Bim vs. Noxa BH3 peptides for Mcl-1 binding, and in Bim vs. Bad for Bcl-x_L binding[34]. A residue may influence another by interacting with it directly. Additionally, non-additivity can arise when mutations change the docking of the peptide in the binding groove, thereby altering contributions from any residues that are re-positioned by the structural change.

Coupling between residues poses a challenge for modeling because substantial amounts of data are required to accurately capture epistatic effects with a statistical model. Each mutation must be observed in sufficiently many sequence contexts to determine the relevant dependencies. By analyzing $\Delta\Delta G$ values from high-throughput SORTCERY experiments, we found evidence of non-additivity, indicating that our datasets do sample context-dependent events. Consistent with residue-residue coupling contributing to binding, we found that second-order polynomial models evaluated on the validation data consistently outperformed linear models trained on the same data. In other words, the linear models can't describe the data as accurately because they fail to

capture some replicable structure in the data that the polynomial models capture through the pair terms.

Strikingly, we were able to use data collected in multiple local sequence spaces to build models that had utility for navigating the binding landscape outside of those spaces. In our initial input libraries, the peptides were sourced from six individual libraries. Although each library covered a distinct set of sequences, we combined the observations to build a single model and demonstrated success identifying sequences within the larger, integrated library space, despite these sequences never having been experimentally sampled. Notably, the tests that we challenged our models with were design tasks. Design may be an easier task than prediction in regions of the landscape that are remote from the training data. This is because regression modeling captures the average contribution of a residue or residue pair in different contexts. If the training data are dominated by a single canonical peptide binding mode, then average residue contributions may be good estimates of the actual contributions of residues in this binding mode. A model with these features would be good at describing the canonical mode, and at designing sequences that bind well in that mode. Such a model would be less good at scoring peptides that bind with a different geometry. Consistent with this, X-ray crystallography revealed that designs F4 and F10 closely imitate the binding poses of Bim BH3 (Figure 3.9). Also consistent with this, our models underestimate the Bfl-1 specificity of previously described peptide FS2. FS2 binds to Bfl-1 in a shifted and rotated geometry relative to other known BH3 peptides, and the residue weights that are appropriate for those peptides do not provide accurate binding predictions for FS2 (although FS2 is still recognized as a tight and Bfl-1 selective binder).

An advantage design guided by this type of model is that once the model is built, searching sequence space is trivial, and it is simple to optimize for features that can be hard to screen for experimentally. Here, we took data from libraries that were carefully designed for mono-selectivity and used it to design bi-specific binders, which may not be present in the input libraries, and even if they are, would require a long series of affinity and specificity maturation cycles to identify. One could imagine adding additional constraints to design for features that would be even more difficult or impossible to screen for experimentally, such as charge, which can impact solubility and cell delivery, or minimal predicted immunogenicity. The formalism of the design optimization can readily accommodate diverse constraints on protein sequence.

The increasing ease with which it is possible to generate and screen peptide libraries suggests that mapping landscapes through model building, as we have done here, could become a useful and routine tool in the repertoire of protein design methods. An interesting question for the future is what sequence space should be sampled to support initial model building. Naive empirical models will be most accurate within or close to the sequence space on which they were trained, and one way to broaden this space would be to measure affinities for sequences that vary more sites and residues. However, there is a tradeoff between increasing library diversity and obtaining adequate coverage of combinations of residues. Sampling from broader sequence space additionally decreases the chances of observing binders. In this work, we biased the input sequences towards those deemed likely to bind by using prior modeling and experimental analysis of the Bcl-2 family; this focused our sampling.

Structure-based design, using experimental or predicted complex structures, may represent a promising way to achieve this for other protein families.

Methods

Yeast growth and sorting

Yeast cultures were diluted from glycerol stocks to an OD_{600} of 0.05 in SD+CAA (5 g/L casamino acids, 1.7 g/L yeast nitrogen base, 5.3 g/L ammonium sulfate, 10.2 g/L Na_2HPO_4-$7H_2O$ and 8.6 g/L NaH_2PO_4-H_2O, 2% glucose) and grown for 12 hr at 30 °C. Each culture was then diluted to an OD_{600} of 0.005-0.01 in SD+CAA and grown to an OD_{600} of 0.1–0.6 at 30 °C. To induce expression, 40 mL of each culture was diluted into 1L SG+CAA (5 g/L casamino acids, 1.7 g/L yeast nitrogen base, 5.0 g/L ammonium sulfate, 10.2 g/L Na_2HPO_4-$7H_2O$ and 8.6 g/L NaH_2PO_4-H_2O, 2% galactose) and grown for 20-24 hr at 30 °C. Cells were filtered with either a 0.45 µm bottle-top filter or a 96-well plate filter, washed twice with BSS (50 mM Tris, 100 mM NaCl, pH 8, 1 mg/ml BSA), and resuspended in BSS with least 10-fold molar excess target protein and incubated for 2 h at room temperature with gentle shaking. Cells were filtered, washed twice in chilled BSS, resuspended in a 1:100 dilution of mouse anti-HA (Roche, RRID:AB_514505) and rabbit anti-c-myc antibodies (Sigma, RRID:AB_439680) primary antibodies in a volume of 2 mL per 10^8 cells, and incubated for 15 min at 4 °C. Cells were filtered, washed twice in chilled BSS, resuspended in a 1:40 dilution of APC rat anti-mouse (BD, RRID:AB_398465) and 1:100 dilution of PE goat anti-rabbit (Sigma, RRID:AB_261257) secondary antibodies in a volume of 2 mL per 10^8 cells, and incubated in the dark for 15 min at 4 °C. Cells were filtered and washed 2x in chilled

BSS before resuspending the labeled cells in BSS and using BD FACSAria flow cytometer or a BD FACSCanto using FACSDiva software for cell sorting or analysis.

High-throughput affinity sorting and sequencing

To select a diverse pool of ~10,000 unique BH3 sequences for multi-receptor Sortcery, we grew the six yeast display libraries described in Jenson *et al.* and pooled the libraries prior to incubating with 100 nM Bfl-1, Mcl-1, or Bcl-x_L[25]. Cells were sorted into 12 gates set to separate binders of different affinities as described in Reich *et al.*[24] Sorted cells were grown overnight in SD+CAA. An equal number of cells from the Bfl-1, Mcl-1, and Bcl-x_L sorts were pooled together to make a final pool of ~10,000 cells. Of the ~3,333 cells from each sort, most were selected from the highest affinity gate (~540 cells) and the fewest were selected from the lowest affinity gate (~25 cells) with a linear sampling gradient in between. The mixed library was grown overnight and stored in glycerol stocks.

To experimentally determine affinities of yeast-displayed peptides for Bfl-1, Mcl-1, and Bcl-xL, we sorted the mixed library into 12 affinity gates and subsequently deep-sequenced DNA from cells collected in each gate following the Sortcery protocol described in detail by Reich *et al.*[24]

Designed clones were verified for their specificity preferences with titrations.. The median binding signal of the binding population was recorded for each clone and applied to estimate an approximate KD. Clones were assigned to the bin at which the estimated 1/2 max binding signal would occur. Sequences for which the signal was below 1/2 max signal of Bim at 1000 nM were assigned as >1000nM.

Crystallography

Crystals of Bfl-1 in complex with F4 and F10 were grown in hanging drops over a reservoir containing 1.8 M ammonium sulfate, 0.1 M MES pH 7.0 at room temperature. The protein was mixed with peptide at a 1:1 molar ratio and concentrated to 4 mg/ml in 20 mM Tris, 150 mM NaCl, 1% glycerol, 1 mM DTT, pH 8.0. The hanging drops contained 1.5 µL of complex mixed with 1.5 µL of reservoir solution. Crystals were cryo-protected (2.0 M lithium sulfate with 10% glycerol) and flash frozen. Diffraction data were collected at the Advanced Photon Source at the Argonne National Laboratory, NE-CAT beamline 24-ID-C. Both datasets were integrated and scaled to 1.48 Å using HKL2000 and phased using PHENIX ridged body refinement of chain A of structure 4ZEQ using PHENIX[35,36]. The peptide was built into the remaining difference density. Several iterations of refinement using PHENIX and COOT to improve the structural models[36,37].

Computational Processing of SORTCERY Data

Filtering sequences for high-fidelity reads

Deep-sequencing data were filtered for high quality reads with at least 99% base call accuracy and matching specified multiplex barcodes used to individually identify each experiment. Paired-end reads that did not overlap were discarded, and overlapping DNA segments were reassembled. Unique sequences that had at least 100 reads were processed for further analysis.

Generating clone profiles over gates and average affinity coordinates

Clonal cell counts per gate were estimated as a function of the deep sequencing read counts. Because different numbers of cells are collected in different gates, read

counts do not map directly to cell counts. To calculate the cell count for sequence *x* in a given gate *i* , $n_i(x)$, we first calculated the clone's relative frequency in that gate as the number of reads for sequence x in gate *i*, $r_i(x)$, divided by the sum of all reads for all sequences for gate *i*. The clone's relative frequency is then scaled by the observed number of cells recorded to hit gate *i* in a fixed amount of time, c_i.

$$n_i(x) = \left(\frac{r_i(x)}{\sum_j^{ALL} r_i(j)} \right) * c_i$$

Calculated cell counts were normalized to determine the probability distribution over gates for each sequence. The probability of finding clone *x* in gate *i* is given by:

$$p_i(x) = \frac{n_i(x)}{\sum_{k=1}^{12} n_k(x)}$$

To mitigate the effects of sequencing error on our analysis, DNA sequences were clustered by sequence similarity using USEARCH with a 3 percent identity cutoff. Within each DNA cluster, the sequence with the most reads was assigned as the parent of the cluster and all other sequences were assigned as daughters. Daughter probability distributions over gates were compared to parent profiles. A daughter sequence was split into its own cluster if its probability distribution over gates differed significantly from the parent probability distribution (chi-squared test with Bonferroni correction: alpha-value < 0.005/# clones). Otherwise, daughter sequences were combined with parent sequences and each cluster was assigned a new probability distribution profile over

gates. Sequences that only occurred in one gate were removed, because profiles for individual clones measured independently always span multiple gates. We also removed sequences with non-unimodal profiles using a custom python script.

The probability distribution of cells over gates for each sequence approximates the distribution of measured clones along an axis of affinity[23]. Profiles were used to compute an mean affinity coordinate, Ā, for each sequence using:

$$\text{Mean coordinate value} = \sum_{i=1}^{i=12} i \cdot p_i$$

DNA sequences were translated into protein sequences for all subsequent analyses, yielding a list of protein sequences and their associated Ā, values. Redundant protein-to-energy mappings originating from synonymous mutation were removed.

Sequences that may have originated from spurious mutation, PCR error, and cross-library contamination were removed from the dataset by filtering for only sequences that matched the designed library input using regular expression on the DNA level.

Sequences were classified into three categories of affinity (unresolvable tight, resolvable, and unresolvable weak). These sequences were separated based on the calculated shape of the probability distribution function of the peptide across FACS gates. If the maximum mode of the distribution occurred in gate 1 or 12, the binder was

classified as resolvable tight or weak. The remaining sequences were classified as resolvable.

Mapping mean affinity coordinate to ΔG

The average affinity coordinates for different clones reflect relative binding affinities, but absolute values are specific to a given experiment. To compare affinity values across experiments, we used standards to calibrate the affinity axis ito give binding free energy in kcal/mol. Standards were selected to span the SORTCERY affinity range of each experiment. For each standard, a binding curve was measured via yeast titration and fit to give the standard free energy of binding. We applied linear regression to map $\bar{A}$, values to energies. Although a linear fit is an approximation of the true relationship between $\bar{A}$, and $\Delta G_{binding}$, fitting the theoretical curve gave minimal differences in values.

Regression modeling to relate peptide sequence to $\Delta G_{binding}$

Support vector regression (SVR) models were trained to predict SORTCERY-measured affinity from protein sequence. SVR solves for a function that has at most epsilon$_i$ deviation from the observed value: $\hat{y}_i - y_i < \epsilon$ where $\hat{y}_i = w^T x_i + b$. As this constraint problem is not always feasible, slack variables zeta$_i$ are introduced for each data point and minimized. This results in the primal form of the SVR regression problem, which balances model complexity and performance as follows:

$$\min_{w,b,\zeta,\zeta^*} \frac{1}{2} w^T w + C \sum_{i=1}^{n} (\zeta_i + \zeta_i^*)$$

$$\text{subject to } y_i - w^T \phi(x_i) - b \leq \varepsilon + \zeta_i,$$
$$w^T \phi(x_i) + b - y_i \leq \varepsilon + \zeta_i^*,$$
$$\zeta_i, \zeta_i^* \geq 0, i = 1, ..., n$$

The epsilon parameter defines a range of insensitivity to noise and the *C* parameter defines the cost of adding slack to the model. *C* can be interpreted as a scalar that varies the complexity of the model. Smaller *C* allows the model to be simpler by permitting more slack on the model optimization. The epsilon parameter and *C* parameter for the final models are identified via nested cross-validation. SVR was used as implemented in sklearn[38].

Protein sequences were converted into numerical vectors via a binary amino acid encoding. This procedure encodes a protein sequence of length n into a n*20 length vector where each position/residue is represented as a one or zero, depending on whether the position/residue is present in the sequence. For a peptide of length 22, as for Bcl-2-peptide interactions, the resulting encoding is a binary vector of length 440, with 22 non-zero values.

A generalizability score was determined for each dataset via 10-fold nested cross-validation. An input dataset is split into 10, top-level subsets. Each top-level subset (1/10 of data) is a validation dataset *V* which will be each report the performance of models trained on the remaining 90% of data *Tr.*

The models trained on the dataset *Tr* retrieve their hyperparameter from a nested ten-fold cross-validation within the dataset *Tr.* Dataset *Tr* is partitioned in 10

parts , where now each part (*Te*) is used to test models trained on the remaining 90% of data (*S*) A grid of hyperparameters, were evaluated (epsilon and *C*) on each *Te* and the best performing hyperparameters inform the models trained on *Tr*. The grid of parameters explored 2^{-14} - 2^{6} for C and epsilon [0 - 1], in 0.05 intervals Performance of models trained on *Tr* and evaluated on *V* reports an estimate of generalizability. The best hyper-parameters for the final models were selected by args which performed the best on the *Te* datasets. (The *V* dataset is only used to report generalizability).

We tested a linear kernel $x^T z$ and a second order polynomial kernel $(x^T z)^2$ in our model building and comparisons. This primal optimization problem is solved in the dual form by construction of the Lagrangian objective function, which is beyond the scope of this paper[26].

Support vector regression models were used as implemented in Scikit-learn. Scikit-learn solves the support vector regression objective function in dual form and returns the dual weights as a solution to the fitting problem. To extract out the component, pairwise weights from the dual coefficients, the following function was applied.

$$w = \sum_{i=1}^{\ell} (\alpha_i - \alpha_i^*) x_i$$

x_i is the expanded polynomial vector of a given training input point and (α_i -α_i^*) is the dual coefficient. This equation tells us that the weight vector is a weighted sum of the expanded polynomial vectors. The dual coefficient can be interpreted as the weighted contribution of the data point to the weight vector[26].

Design with integer linear programming

Six design objectives were pursued with integer linear programming (ILP). Monospecific peptides were designed to bind to Bcl-x_L, Mcl-1, or Bfl-1. Bispecific peptides were designed to bind Bcl-x_L and Mcl-1, Bcl-x_L, and Bfl-1, or Mcl-1 and Bfl-1. These peptides were designed to bind selectively to their intended receptor by maximizing the target binding affinity, maximizing the specificity gap, or by minimizing the off-target binding affinity. For each set of designs, 200 sequences were iteratively solved with ILP, from which 7-12 sequences were selected to be evaluated. The models weights used for design were derived from functions trained from an earlier curated datasets which did not aggregate on DNA sequence similarity.

Designed sequences were restricted to select from residues in the input library space and excluded Cys residues. However, sequences could choose residues from either Bim or Puma scaffold sequences interchangeably which expanded the potential sequence space to the order of 10^{14}.

Constraints were included during optimization to prevent including residues with low confidence. The sequence space was restricted to allow only position/residue terms that were observed at least 25 times in all three training datasets. The models are prone to overfit rare examples, thus, adding constraints such that a given residue must be observed frequently helps to prevent designing in spaces with low confidence.

Designing sequences with ILP also required including formal constraints that describe properties of a peptide. For example, a peptide must only have one residue at each position. Also, if a residue is selected for design at a given position, the

corresponding squared term must also be included. Finally, pair terms for which the component terms have both been included must also be included.

The scoring function is the sum of the receptor-specific pairwise weights multiplied by the one-dimensional binary indicator vector Phi(x). For a sequence of length n, this is equivalent to the sum the product of pair weights and indicator variables x_i and x_j. The variables x_i and x_j identify whether an amino acid is present at a specific position. Receptor-specific energy functions were developed for Bcl-x_L, Mcl-1, and Bfl-1. These are referred to as X, M, and F below.

$$y = W^T \Phi(x) = \sum_{i=1}^{n \cdot 20} \sum_{j=1}^{n \cdot 20} W_{ij} x_i x_j$$

To design receptor-specific peptides, sequences maximized binding affinity to the target receptor were solved for (*i.e.* to minimize binding energy). Constraints were imposed to require that the designs bind the target with $\Delta G \leq -10.9$ kcal/mol (10 nM) and bind the two off targets with $\Delta G \geq -9.5$ kcal/mol (Kd greater than 107.9 nM). The off-target affinity boundary was selected to be the affinity at which the population of non-resolvable weak binders started to appear. An example of the Bcl-x_L receptor-specific designs is provided below.

$$
\begin{array}{ll}
\min & X(x) \\
\text{subject to} & F(x) > -9.5 \qquad \text{Bfl-1 off-target constraint} \\
& M(x) > -9.5 \qquad \text{Mcl-1 off-target constraint} \\
& X(x) < -10.9085 \qquad \text{Bcl-xL target constraint} \\
& N(x_i) > 25 \qquad \text{for } i = 1, \ldots, 22 \quad \text{Frequency constraint}
\end{array}
$$

The design routine generates 200 peptide sequences. To select the set of sequences to be experimentally tested, applied a consensus-based approach by rescoring all designs using six re-trained energy functions for each of the three receptors. The six SVR models were trained with linear or polynomial kernels on three different sets of experimental data, for each receptor and averaged. Models were trained on replicate 1, replicate 2, or a union of replicate 1 and replicate 2 datasets. Twelve sequences for each receptor were selected to be evaluated. These 12 sequences were selected for the largest mean specificity.

For the bispecific designs targeting Bcl-x_L and Bfl-1 (with specificity against Mcl-1) or the bispecific designs targeting Mcl-1 and Bcl-x_L (with specificity against Bfl-1), the sequences that minimized the off-target affinity were solved for. Constraints were added to require tight binding of the two targets, ΔG <= -10 kcal/mol, and weak binding to the off-target, ΔG >= -8.5 kcal/mol. The following shows the constraints for designing Bcl-x_L and Mcl-1 bispecific peptides:

$$
\begin{array}{ll}
\max & F(x) \\
\text{subject to} & F(x) > -8.5 \qquad \text{Bfl-1 off-target constraint} \\
& M(x) < -10 \qquad \text{Mcl-1 target constraint} \\
& X(x) < -10 \qquad \text{Bcl-xL target constraint} \\
& N(x_i) > 25 \qquad \text{for } i = 1, \ldots, 22 \quad \text{Frequency constraint}
\end{array}
$$

To select the set of sequences to be experimentally tested, all of the designs were rescored using 6 re-trained energy functions for each of the 3 receptors as described above. Seven bispecific sequences with the largest mean specificity were selected to be tested.

To design bispecific peptides that bind to Mcl-1 and Bfl-1, without binding tightly to Bcl-x_L, I solved for sequences that maximized the gap between Bfl-1 and Bcl-x_L binding energies. (This is equivalent to maximizing the set of weights derived from the difference of Bcl-x_L and Bfl-1 models). Constraints were added to require that the Mcl-1 and Bfl-1 binding energies that differ by at most 0.2 kcal/mol. No additional binding energy constraints were applied to the target or off-target binding energies.

$$
\begin{array}{lll}
\max & D_{x-f}(x) & \\
\text{subject to} & D_{f-m}(x) <= 0.2 & \text{Target similarity constraint} \\
 & D_{f-m}(x) >= -0.2 & \text{Target similarity constraint} \\
 & N(x_i) > 25 \quad \text{for } i = 1, \ldots, 22 & \text{Frequency constraint}
\end{array}
$$

To select the set of sequences to be experimentally tested, I re-scored all designs using 6 re-trained energy functions for each of the 3 receptors as described above. Seven bispecific sequences with the largest mean specificity were selected to be tested.

To redesign the bispecific peptides, we added additional residue constraints, optimized target binding as an objective function (rather than maximizing the specificity gap or minimizing the stability of the off-target), and added additional requirements, as described below, to select a more diverse set of sequences.

To prevent the potential inclusion of destabilizing residues in the designs, we limited the sequence space to include only those residues observed in tight binding peptides for the target (peptides with SORTCERY ΔG < -10.5 kcal/mol). We added constraints to require that the predicted binding energy for each of the two targets be less than -11.3 kcal/mol. This boundary was chosen because it was the minimal predicted binding affinity among the successful mono-receptor specific sequences. Furthermore, we chose to minimize the binding energy of the targets instead of maximizing the off-target energy. Given that ILP can only optimize one objective at a time, we solved two optimizations for each dual-specificity design problem, one optimizing the binding energy to the first target, and the second optimizing the binding energy to the second target. To enforce specificity we imposed a constraint on the off-target binding energy: ΔG >= -10 kcal/mol. The optimization problem was therefore:

$$
\begin{array}{lll}
\min & X(x) & \\
\text{subject to} & F(x) > -9.5 & \text{Bfl-1 off-target constraint} \\
& M(x) < -11.3 & \text{Mcl-1 target constraint} \\
& X(x) < -11.3 & \text{Bcl-xL target constraint} \\
& N(x_i) > 25 \quad \text{for } i = 1, \ldots, 22 & \text{Frequency constraint} \\
& x_i \in \mathit{binders} \quad \text{for } i = 1, \ldots, 22 & \text{Residue constraint}
\end{array}
$$

To select the ten best Bcl-x_L and Bfl-1 bispecific peptides and ten best Mcl-1 and Bcl-x_L bispecific sequences, we applied the consensus-based method to compute average scores for each design binding to each receptor. We selected the top 5 sequences, based on affinity for one of the targets, that had at least two mutations relative to higher ranking designs.

In the second round of design for Bcl-x_L and Bfl-1 bispecific peptides and Mcl-1 and Bcl-x_L bispecific sequences, we used FlexPepDock to score the population of sequences designed to confirm whether the changes in our optimization problem were consistent with structural models.

Solving for boundaries of peptide specificity

Input library

The boundary of specificity for the input library was identified by estimating a solution to the concave hull problem for the full set of 27,696,384 library members. After mapping each sequence to an x,y coordinate, we estimated the shape by plotting the minimum and maximum y values for each group of rounded x values (2 decimal places) and vice versa.

Integrated library

The boundary of specificity for the integrated library space was calculated via ILP. The angular and radial coordinate on the 2D plot is determined by the ratio of binding affinity of a given peptide for the three receptors. At any given coordinate, there are two target receptors and an off-target receptor. The radial position is determined by the energy gap between the tighter of the two target binders and the off-target binder. The angular coordinate is determined by the affinity ratio between the two target binders. For every pair of target receptors, Mcl-1/ Bcl-x_L, Mcl-1/Bfl-1, Bcl-x_L/Bfl-1, the energy gap between the two pairs is fixed as a constant between -6.8 and 6.8 kcal/mol, and the sequence with the lowest off-target affinity is identified via ILP. This optimization problem identifies a sequence that lands on the boundary of specificity. (This boundary is still constrained by the need to have 25 observations per receptor)

Plotting specificity vs. affinity tradeoffs

All 27,696,384 peptides in the designed library were computationally scored against Mcl-1, Bfl-1, and Bcl-x_L. For a given target receptor, all peptides were binned by the predicted target affinity. The median affinity of the off-target is plotted for each bin.

Acknowledgements

We thank the Koch Institute Flow Cytometry Core Facility for assistance with FACS sorting, Koch Institute Bioploymers and Proteomics Facility for peptide synthesis, and the MIT Structural Biology Core Facility for assistance with X-ray crystallography. We thank members of the Keating lab, especially L. Reich for help with experimental troubleshooting, V. Frappier for helping with structural analysis, and G. Foight for help with library design. Part of this work was conducted at the Northeastern Collaborative Access Team beamlines, which are funded by the National Institute of General Medical Sciences from the National Institutes of Health (P41 GM103403). The Pilatus 6M detector on 24-ID-C beam line is funded by a NIH-ORIP HEI grant (S10 RR029205). This research used resources of the Advanced Photon Source, a U.S. Department of Energy (DOE) Office of Science User Facility operated for the DOE Office of Science by Argonne National Laboratory under Contract No. DE-AC02-06CH11357. The content is solely the responsibility of the authors and does not necessarily represent the official views of the National Institutes of Health or the U.S. Department of Energy.

References

1. Tonikian R, Zhang Y, Sazinsky SL, et al. A Specificity Map for the PDZ Domain Family. Eddy SR, ed. *PLoS Biol.* 2008;6(9):e239. doi:10.1371/journal.pbio.0060239.
2. Opferman JT. Attacking cancer's Achilles heel: antagonism of anti-apoptotic BCL-2 family members. *FEBS J.* August 2015. doi:10.1111/febs.13472.
3. Foight GW, Keating AE. Locating Herpesvirus Bcl-2 Homologs in the Specificity Landscape of Anti-Apoptotic Bcl-2 Proteins. *J Mol Biol.* 2015;427(15):2468-2490. doi:10.1016/j.jmb.2015.05.015.
4. Souers AJ, Leverson JD, Boghaert ER, et al. ABT-199, a potent and selective BCL-2 inhibitor, achieves antitumor activity while sparing platelets. *Nat Med.* 2013;19(2):202-208. doi:10.1038/nm.3048.
5. Roberts AW, Seymour JF, Brown JR, et al. Substantial susceptibility of chronic lymphocytic leukemia to BCL2 inhibition: results of a phase I study of navitoclax in patients with relapsed or refractory disease. *J Clin Oncol.* 2012;30(5):488-496. doi:10.1200/JCO.2011.34.7898.
6. Roberts AW, Davids MS, Pagel JM, et al. Targeting BCL2 with Venetoclax in Relapsed Chronic Lymphocytic Leukemia. *N Engl J Med.* 2016;374(4):311-322. doi:10.1056/NEJMoa1513257.
7. Kotschy A, Szlavik Z, Murray J, et al. The MCL1 inhibitor S63845 is tolerable and effective in diverse cancer models. *Nature.* 2016;538(7626):477-482. doi:10.1038/nature19830.
8. Schoenwaelder SM, Jarman KE, Gardiner EE, et al. Bcl-xL–inhibitory BH3 mimetics can induce a transient thrombocytopathy that undermines the hemostatic function of platelets. *Blood.* 2011;118(6).
9. Rudin CM, Hann CL, Garon EB, et al. Phase II Study of Single-Agent Navitoclax (ABT-263) and Biomarker Correlates in Patients with Relapsed Small Cell Lung Cancer. *Clin Cancer Res.* 2012;18(11).
10. Montero J, Sarosiek KA, DeAngelo JD, et al. Drug-Induced Death Signaling Strategy Rapidly Predicts Cancer Response to Chemotherapy. *Cell.* 2015;160(5):977-989. doi:10.1016/j.cell.2015.01.042.
11. Ni Chonghaile T, Sarosiek KA, Vo T-T, et al. Pretreatment mitochondrial priming correlates with clinical response to cytotoxic chemotherapy. *Science.* 2011;334(6059):1129-1133. doi:10.1126/science.1206727.
12. Moldoveanu T, Follis AV, Kriwacki RW, Green DR. Many players in BCL-2 family affairs. *Trends Biochem Sci.* 2014;39(3):101-111. doi:10.1016/j.tibs.2013.12.006.
13. Dutta S, Ryan J, Chen TS, Kougentakis C, Letai A, Keating AE. Potent and specific peptide inhibitors of human pro-survival protein Bcl-xL. *J Mol Biol.* 2015;427(6 Pt B):1241-1253. doi:10.1016/j.jmb.2014.09.030.
14. Foight GW, Ryan JA, Gullá S V, Letai A, Keating AE. Designed BH3 Peptides with High Affinity and Specificity for Targeting Mcl-1 in Cells. *ACS Chem Biol.* 2014;9(9):1962-1968. doi:10.1021/cb500340w.
15. Dutta S, Chen TS, Keating AE. Peptide ligands for pro-survival protein Bfl-1 from computationally guided library screening. *ACS Chem Biol.* 2013;8(4):778-788. doi:10.1021/cb300679a.
16. Mandell DJ, Kortemme T. Computer-aided design of functional protein interactions. *Nat Chem Biol.* 2009;5(11):797-807. doi:10.1038/nchembio.251.
17. Berger S, Procko E, Margineantu D, et al. Computationally designed high specificity inhibitors delineate the roles of BCL2 family proteins in cancer. *Elife.* 2016;5:1422-1432. doi:10.7554/eLife.20352.
18. McLaughlin RN, Poelwijk FJ, Raman A, Gosal WS, Ranganathan R, Ranganathan R. The spatial architecture of protein function and adaptation. *Nature.* 2012;491(7422):138-142. doi:10.1038/nature11500.

19. Wiedemann U, Boisguerin P, Leben R, et al. Quantification of PDZ domain specificity, prediction of ligand affinity and rational design of super-binding peptides. *J Mol Biol.* 2004;343(3):703-718. doi:10.1016/j.jmb.2004.08.064.

20. Whitehead TA, Chevalier A, Song Y, et al. Optimization of affinity, specificity and function of designed influenza inhibitors using deep sequencing. *Nat Biotechnol.* 2012;30(6):543-548. doi:10.1038/nbt.2214.

21. Rocklin GJ, Chidyausiku TM, Goreshnik I, et al. Global analysis of protein folding using massively parallel design, synthesis, and testing. *Science.* 2017;357(6347):168-175. doi:10.1126/science.aan0693.

22. Bedbrook CN, Yang KK, Rice AJ, Gradinaru V, Arnold FH. Machine learning to design integral membrane channelrhodopsins for efficient eukaryotic expression and plasma membrane localization. Maranas CD, ed. *PLOS Comput Biol.* 2017;13(10):e1005786. doi:10.1371/journal.pcbi.1005786.

23. Reich LL, Dutta S, Keating AE. SORTCERY-A High-Throughput Method to Affinity Rank Peptide Ligands. *J Mol Biol.* 2015;427(11):2135-2150. doi:10.1016/j.jmb.2014.09.025.

24. Reich L "Luther," Dutta S, Keating AE. Generating High-Accuracy Peptide-Binding Data in High Throughput with Yeast Surface Display and SORTCERY. In: ; 2016:233-247. doi:10.1007/978-1-4939-3569-7_14.

25. Jenson JM, Ryan JA, Grant RA, Letai A, Keating AE. Epistatic mutations in PUMA BH3 drive an alternate binding mode to potently and selectively inhibit anti-apoptotic Bfl-1. *Elife.* 2017;6:e25541. doi:10.7554/eLife.25541.

26. Smola AJ, Schölkopf B. A tutorial on support vector regression. *Stat Comput.* 2004;14(3):199-222. doi:10.1023/B:STCO.0000035301.49549.88.

27. Dutta S, Chen TS, Keating AE. Peptide ligands for pro-survival protein Bfl-1 from computationally guided library screening. *ACS Chem Biol.* 2013;8(4):778-788. doi:10.1021/cb300679a.

28. Grigoryan G, Reinke AW, Keating AE. Design of protein-interaction specificity gives selective bZIP-binding peptides. *Nature.* 2009;458(7240):859-864. doi:10.1038/nature07885.

29. Podgornaia AI, Laub MT. Protein evolution. Pervasive degeneracy and epistasis in a protein-protein interface. *Science.* 2015;347(6222):673-677. doi:10.1126/science.1257360.

30. Carter P, Wells JA. Functional interaction among catalytic residues in subtilisin BPN'. *Proteins Struct Funct Genet.* 1990;7(4):335-342. doi:10.1002/prot.340070405.

31. Horovitz A. Non-additivity in protein-protein interactions. *J Mol Biol.* 1987;196(3):733-735. http://www.ncbi.nlm.nih.gov/pubmed/3681975. Accessed April 13, 2018.

32. Gregoret LM, Sauer RT. Additivity of mutant effects assessed by binomial mutagenesis. *Proc Natl Acad Sci U S A.* 1993;90(9):4246-4250. http://www.ncbi.nlm.nih.gov/pubmed/8483940. Accessed April 13, 2018.

33. Sarkisyan KS, Bolotin DA, Meer M V., et al. Local fitness landscape of the green fluorescent protein. *Nature.* 2016;533(7603):397-401. doi:10.1038/nature17995.

34. DeBartolo J, Dutta S, Reich L, Keating AE. Predictive Bcl-2 family binding models rooted in experiment or structure. *J Mol Biol.* 2012;422(1):124-144. doi:10.1016/j.jmb.2012.05.022.

35. Otwinowski Z, Minor W. [20] Processing of X-ray diffraction data collected in oscillation mode. *Methods Enzymol.* 1997;276:307-326. doi:10.1016/S0076-6879(97)76066-X.

36. Adams PD, Afonine P V, Bunkóczi G, et al. PHENIX: a comprehensive Python-based system for macromolecular structure solution. *Acta Crystallogr D Biol Crystallogr.* 2010;66(Pt 2):213-221. doi:10.1107/S0907444909052925.

37. Emsley P, Lohkamp B, Scott WG, Cowtan K. Features and development of Coot. *Acta Crystallogr D Biol Crystallogr.* 2010;66(Pt 4):486-501. doi:10.1107/S0907444910007493.

38. Pedregosa F, Varoquaux G, Gramfort A, et al. Scikit-learn: Machine Learning in Python. January

2012. http://arxiv.org/abs/1201.0490. Accessed April 14, 2018.

Chapter 4

Tertiary structural motif sequence statistics enable rapid discovery of novel ligands for anti-apoptotic Bfl-1 and Mcl-1

V. Frappier, J.M. Jenson, and A.E. Keating designed and wrote the study. V. Frappier, J. Zhou, and G. Grigoryan designed peptides with dTERMen, V. Frappier performed the benchmarking, and J.M. Jenson performed all of the experiments.

Abstract

Understanding the relationship between sequence and structure well enough to design novel sequences from a structural template has been a longstanding goal in protein design. To this end, the Protein Data Bank (PDB) has been a key resource for defining and developing the general design criteria for structural features like rotamer positions and dihedral angles. Here, we show that by decomposing protein structures from the PDB into sets of well-defined, non-contiguous structural motifs (TERMs) it is possible to rapidly and accurately predict the binding energies of peptide-protein interactions at least as well as existing state-of-the-art methods without computationally expensive structural relaxation and minimization or experimental screening. We demonstrate the potential of this approach by designing highly diversified peptides more than 14 mutations away from their naturally occurring counterparts to target the anti-apoptotic proteins Bfl-1 and Mcl-1. We found that 15 of 17 designs bound tightly to their intended target. Further, high-resolution structures of the designed peptides revealed at least one example where a mutation was accommodated by minor adjustments in backbone geometry that would not have been predicted if modeling was performed on a rigid scaffold. These observations suggest new approaches to design novel protein binders.

Introduction

Protein-protein interactions (PPIs) are central to nearly all biological processes[1], play a major role in cell homeostasis[2], and contribute to pathology in countless human diseases[3]. Reagents that can disrupt PPIs are highly sought after for basic research and therapeutic development. The primary reason that there are so few PPI inhibitors, relative to the 400,000 predicted biologically functional PPIs[4], is that the size and complexity of many protein interfaces make them difficult to target[5]. For example, large binding sites that have multiple, widely spaced hotspots are notoriously difficult to disrupt with small molecules, as are flat interfaces that lack pockets[6,7]. Antibodies and nanobodies can be used to block PPIs and have the advantage, relative to small molecules, of binding to larger protein interfaces. But the difficulty of delivering such large molecules into the cell, coupled with the low stability of some antibody-derived agents in the reducing environment of the cytoplasm, has largely limited their application to extracellular targets or chemically permeabilized cells *ex vivo*. Furthermore, there are many PPI interfaces that are difficult to target with antibodies.

Peptides provide a complementary and highly promising approach to targeting PPI interfaces[8–10]. Peptide-protein interactions are ubiquitous in nature, where there are many examples of short segments in a protein binding to large, structurally complex protein surfaces. The latest delivery technologies make targeting intracellular proteins with peptides increasingly possible. For example, peptides can be delivered into cells by chemically modifying them to increase hydrophobicity and hide hydrogen bonds[11,12], conjugating them to transduction domains (such as cell-penetrating peptides, CPPs)[13–15], or delivering them using cationic lipid carriers[16]. Nevertheless, there are well-known

obstacles to developing useful peptide inhibitors. Peptides derived from naturally occurring sequences have non-optimal pharmacological properties, because they weren't selected for function as reagents or therapeutics. Furthermore, native ligands often have a binding specificity profile different from what is desired for a given application. Significant sequence optimization is typically required to minimize off-target binding, increase protease sensitivity, reduce immunogenicity, and improve pharmacokinetics. Not all of these potential pitfalls are unique to peptides, but there can be many failure modes in the peptide development pipeline. Because we lack the ability to predict pharmacological potential *a priori*, an ability to rapidly generate numerous diverse peptide sequences that tightly bind/inhibit a target PPI would be transformative for the development of peptide therapeutics.

Current approaches for discovering diverse peptide PPI inhibitors for inclusion in drug development pipelines are sometimes effective but are inefficient. The state of the art of discovering novel proteins or peptides that modulate function relies heavily on experimental screening. However, experimental screening of peptide libraries requires that one choose a sequence/structure scaffold in advance, which is often a naturally occurring ligand, around which only a vanishingly small fraction of the sequence space can be queried. This approach, which selects for the "best" binders in a population, does not typically provide diverse leads. Rational design, *e.g.* using computational models to search sequence-structure space on a much larger scale, can effectively guide screens into spaces far beyond those represented in nature[17]. However, given the essentially infinite space to explore, and the difficulty of accurately predicting the best binders, the success rates of rational, structure-based methods have so far been low.

Successful design studies have used prior information about known binding sequences, or known binding hot-spot residues, to help define the design strategy and guide the search. This limits the diversity of solutions that can be discovered. Furthermore, even when such information about sequence/structure elements that promote binding is available and can be exploited, computational design often must be followed by extensive optimization using experimental screening to identify functional designs.

Recent methodological developments have shown that mining sequence-structure relationships from the Protein Data Bank (PDB) has the potential to improve the efficiency and efficacy of structure based modeling and design. It has long been recognized that protein structures are composed of recurring structural elements, and the large number of solved structures now makes it possible to compile a finite, yet near-complete, list of the recurring tertiary structural motifs (here called TERMs) that are needed to construct any protein structure[18]. Recent analyses have also demonstrated that TERMs have characteristic sequence preferences that can be detected by statistical analysis of solved structures. These observations provide the foundation for a formalism that can quantify the quality of fit of any sequence on any specified structural scaffold[19]. This is exactly what is needed to predict the influence of a sequence mutation, or to perform computational design as a sequence optimization problem for a given structure.

TERM-based computational analyses have already demonstrated utility for challenging modeling tasks. For example, a statistical analysis of TERM sequences is remarkably effective at discriminating between good and poor structure prediction models, on par with or exceeding leading model quality assessment metrics[19]. Zheng *et*

al. also showed that TERM sequence statistics capture aspects of protein thermodynamics and can be used to predict stability changes upon mutation as well as, or better than, state-of-the-art physics-based or statistical methods. Finally, TERM-based sequence-structural relationships can be applied to protein design. We call design using TERM sequence statistics *dTERMen* (design with TERM energies), and Mackenzie *et al.* have shown that this approach to identifying the best sequence for a given structure recapitulates native-like sequences given either NMR or X-ray native backbones and can be used to rationalize observed evolutionary variation[18]. As a method for protein design, dTERMen is distinct from many other existing methods because it does not at any stage perform explicit modeling of the designed structure. This leads to substantial time savings, but could potentially lead to problems including steric clashes or other structural frustration.

In this work, we applied dTERMen to a new application: analyzing and re-designing peptide binders of biomedically important proteins. As targets, we chose the anti-apoptotic proteins Bfl-1 and Mcl-1. These proteins are members of the Bcl-2 protein family, along with paralogs Bcl-2, Bcl-x_L, and Bcl-w. Bfl-1 and Mcl-1 promote cellular survival by binding to and sequestering pro-apoptotic BH3 domains and have well-established roles supporting cancer cell survival and the development of chemoresistance[20,21]. However, there are no clinically approved inhibitors targeting Bfl-1 or Mcl-1, despite considerable interest and investment. Small molecules, peptides, and mini-proteins have been described as potential inhibitor leads[10,22–25], but given the high attrition rates of inhibitor leads during development, success is not yet assured. Therefore, we tested the ability of dTERMen to generate additional peptide sequences

that can be included as scaffolds for ongoing drug-development pipelines. Our success validates dTERMen as a promising and novel approach for rapid early stage discovery.

Results

Benchmarking dTERMen performance

To evaluate the potential of dTERMen for designing peptide ligands for Bfl-1 and Mcl-1, we tested its performance on a variety of PPI prediction tasks using binding data for Bcl-2 family proteins. dTERMen has not previously been used to predict binding affinities, and in fact the method is parameterized using sequence preferences from only single-chain structural motifs. Nevertheless, the binding of peptides to Bcl-2 proteins is a coupled binding-and-folding reaction that resembles single-chain protein folding in some respects, and the resulting complexes share characteristics of folded structures, including a globular arrangement of packed helices and a hydrophobic core at the interface. Furthermore, there is precedent for extrapolating single-chain statistics to model PPIs[26].

To evaluate binding prediction performance, we used a dataset consisting of 4386, 4491 and 3805 measurements of peptides binding to Bcl-x_L, Mcl-1 and Bfl-1, respectively. Affinity values were obtained using SORTCERY[27,28], a high-throughput method for quantifying dissociation constants of peptides displayed on the surface of *Saccharomyces cerevisiae*. The peptides that were tested contained between 1 and 8 mutations made in the background of the BH3 sequences of human BIM or PUMA, and had SORTCERY-determined dissociation constants of 0.1 to 320 nM (binding energies of -13.8 to -8.9 kcal/mol), with some peptides classified simply as binding tighter or more weakly than the extremes of this range.

We defined several prediction tasks using the Bcl-2 family interaction data. The easiest task was to discriminate the 20% tightest binders of a particular protein from sequences that were observed in the 20% weakest binding affinity, at the concentration tested (1 nM for Mcl-1 and Bcl-x_L, 100 nM for Bfl-1). We also defined an enrichment task, which involved identifying the top 10% highest affinity binders and, finally, the extremely difficult test of predicting quantitative affinities within a 5 kcal/mol range in binding energies. In addition, we tested the ability of dTERMen and other methods to predict the binding preferences of peptides for one Bcl-2 family protein vs. another. Here, too, we defined easier and more challenging tasks, first asking if we could correctly predict the binding behavior of peptides that interact tightly with one protein but not detectably with another, and second testing the ability of different methods to predict differences in measured binding energies. As input into the calculations, we used a subset of solved structures of Bcl-2 protein-peptide complexes that were selected to span observed binding geometries. We compared the performance of dTERMen with that of commonly used methods Rosetta[29] and FoldX[30].

Table 4.1. Predicted performance of dTERMen compared to Rosetta and FoldX.

	mean_AUC	mean_cor	mean_spec	mean_Enrich
FoldX_mean	0.752035	0.311641	0.184434	21.377008
FoldX_min	0.856194	0.471359	0.385888	29.141456
Rosetta_mean	0.752452	0.335921	0.268465	24.443816
Rosetta_min	0.783532	0.373168	0.288744	26.037904
dTERMen_mean	0.772331	0.368573	0.292424	30.848460
dTERMen_min	0.804637	0.408427	0.364274	35.606232

mean_AUC= Predicted ability to discriminate between the tightest 20% and weakest 20% of binders, averaged across Bcl-xL, Mcl-1, and Bfl-1 SORTCERY datasets.
mean_corr= Observed correlation with measured affinities, averaged across Bcl-xL, Mcl-1, and Bfl-1 SORTCERY datasets.
mean_spec= Ability to predict differences in measured binding energies between proteins, averaged across Bcl-xL, Mcl-1, and Bfl-1 SORTCERY datasets.
mean_Enrich= enrichment of top 10% of binders, averaged across Bcl-xL, Mcl-1, and Bfl-1 SORTCERY datasets.
FoldX, Rosetta, and dTERMen_mean= average performance over all structural models
FoldX, Rosetta, and dTERMen_min= best performing structural model in tested set.

We first tested whether different modeling approaches could discriminate high affinity binders from peptides that were not observed to bind or bind weakly at the concentrations tested. We ran a binary classification test and report the results in Table 4.1 as the area under the receiver operating characteristic (ROC) curve (AUC). An AUC value of 1 corresponds to a perfect discrimination of peptides labeled as tight binders vs. non-binders, and an AUC value of 0.5 represents the performance of random guessing. We found that that predictive power varies significantly as a function of the template using for modeling. One striking example comes from the FoldX predictions made on the Bcl-x_L dataset, where the AUC values range from 0.39 *(worse than random)* to 0.82 based on the template used for modeling. In one case, multiple complexes found in one crystal structure (5C6H) gave AUC values ranging from 0.65 to 0.82. Unfortunately, there is no reliable way to know, *a priori*, which template will give the best results. We chose to report in Table 4.1 the average performance of each method over all templates. Performance averaged for all protein targets shows that dTERMen (AUC_{avg} = 0.77) has similar predictive power to the other scoring methods, Rosetta (AUC_{avg} = 0.75) and FoldX (R_{avg} = 0.75). However, this small difference is driven by better performance on the Bcl-x_L dataset, for which dTERMen (AUC_{avg} = 0.75) is better than Rosetta (AUC_{avg} = 0.69) or FoldX (AUC_{avg} = 0.69). As expected, the Pearson correlation values between the binding energies and prediction values for each template follow an almost identical trend than the AUC values. Performance averaged for all protein targets shows that dTERMen (R_{avg} = 0.37) is marginally better than the other scoring methods, Rosetta (R_{avg} = 0.34) and FoldX (R_{avg} = 0.31). Moreover, some methods perform significantly better on some templates than others, and no single

method is consistently better than the others (table 4.1). This analysis shows that dTERMen has predictive performance on par with some of the most commonly used structure-based prediction tools, and thus has potential for application in protein design.

Many applications seek the tightest binding sequences, given that these may have the greatest potential as reagents or therapeutics. But discriminating tight binders from weaker binders is more difficult than recognizing the difference between tight binders and non-binders. We used an enrichment test to evaluate method performance on this task. Specifically, we used each method to rank all of the 4386, 4491 or 3805 sequences that had measured affinity values for Bcl-x_L, Mcl-1 or Bfl-1. We then examined the top 10% of ranked sequences to determine what proportion of the top 10% of experimental binders were captured. For a perfect method, the answer would be 100%. Results for dTERMen, FoldX and Rosetta are reported in Table 4.1. Overall, dTERMen ($Binder_{avg}$ = 31%) has better enrichment value than Rosetta ($Binder_{avg}$ = 24%) and FoldX ($Binder_{avg}$ = 21%). In contrast to the other benchmark metrics, dTERMen tends to be consistently better than the other methods, for which it scores better for 69% of the templates. In the other tasks, however, this value is around 38%, which is close to random.

It is not surprising that binding affinity predictions depend on the input template structures, particularly for dTERMen and FoldX, which do not perform template structure backbone relaxation (dTERMen does not perform any structural modeling at all). We were struck, however, by the strong dependence of the predicted binding affinities on the choice of template structure and thought this might be an area where dTERMen could provide an advantage. The robustness of prediction performance to

very small differences in input structures was evaluated using 294 pairs of closely related templates with binding site and peptide backbone atom RMSD < 1 Å. For each pair, we computed the correlation of predicted binding energies for all peptides with measured dissociation constants. On average, dTERMen (Ravg = 0.77) is much less sensitive to small differences in input template than FoldX (Ravg = 0.55). When run with default options, the Rosetta (Ravg = 0.60) "relax" protocol is similar to FoldX, although further structural sampling could, at least in theory, lead to a convergence of the Rosetta predictions made on different templates, albeit at a higher cost in computing time.

For all methods, prediction performance could potentially be increased by using a more aggressive conformational search, such as peptide re-docking or MD simulation, although this would be computationally expensive for benchmarks of this size (around 140,000 complexes). A more computationally tractable approach to structural sampling is to evaluate each sequence on a finite number of input structures, and take the lowest predicted binding energy (corresponding to the most stable complex) as the predicted energy. This variation in scoring protocol was tested for all 3 benchmarks: tight binder/non-binder discrimination, tight binder enrichment, and affinity correlation. A summary of the performance is reported in Table 4.1. Without exception, performance improved for all methods when more templates were used. Compared to Rosetta and dTERMen, FoldX benefited the most from the additional sampling: where expected performance increased from 0.31 to 0.47 for Pearson correlation to binding affinity values, 0.75 to 0.85 for AUC values, and from 21% to 29% for enrichment of top binder.

dTERMen designs

Because dTERMen performed at least as well as established scoring functions in benchmarking, we reasoned that it might be useful for designing peptide binders. The only input that must be specified for dTERMen is the design template structure. We chose 5 structures as design templates: two structures of Bfl-1 complexes and three structures of Mcl-1 complexes. Templates were chosen to sample structural diversity, because distinct templates could potentially provide access to distinct sequence spaces.

For Bfl-1 targeted designs, we selected the structure of Bfl-1 bound to the natural ligand PUMA (PDB ID 5UUL) and of Bfl-1 bound to a Bfl-1 selective peptide (FS2) that was identified in a previously reported screen (PDB ID 5UUK)[23]. Because the backbones of PUMA and FS2 are shifted 1.2 Å and rotated 17° relative to one another in the Bfl-1 binding pocket[23], we expected to see differences in the optimal sequences identified by dTERMen for these two templates. For the Mcl-1 targeted designs, we used structures of Mcl-1 bound to the natural ligand BIM (PDB ID 2PQK[31]) and to a stapled variant of the natural ligand BID (PDB ID 5C3F[32]); these two structures have similar binding modes (peptide RMSD < 1), but the Mcl-1 protein has differences in the binding pocket. We also used a structure of peptide FS2 bound to Mcl-1. FS2 has low affinity for Mcl-1 (K_d > 3 uM) but engages the protein in a unique binding pose (PDB ID 5UUM)[23].

Four sequences were designed on each template, using slightly different versions of dTERMen and imposing constraints on the identities of some residues. Specifically, the residue at position 4b of many native BH3 peptides serves as an N-terminal helix cap for helix 5 of Mcl-1 or Bfl-1. This residue is often asparagine,

aspartate or histidine. dTERMen chose threonine at this position, and a careful investigation into why revealed that the database of single-chain structures used to extract TERM statistics did not contain any examples of a corresponding TERM with asparagine, which is apparently a motif found only in inter-chain arrangements. We chose to fix position 4b as asparagine to mitigate the risk of using inappropriate statistics for this inter-chain TERM. BH3 residue 3b also makes a helix-capping interaction in some solved structures, so in half of the designs (F01-F04, M01-M04) we retained the wild-type residue from PUMA (arginine) or BIM (alanine) at this site.

Figure 4.1 shows sequence logos built from the top 100 sequences that were designed on each template. As anticipated, the peptide sequences designed on different templates were highly distinct. Particularly notable is the variability at the highly conserved positions 3a and 3f. In the natural BH3 sequences position 3a is highly conserved as a leucine. Although dTERMen overwhelmingly chose leucine at this position for designs templated on 5UUL and 5C3F, there was unanticipated sequence diversity predicted for the other design templates. Most notably, designs from the 5UUK and 5UUM templates preferred isoleucine and methionine over leucine. Position 3f is conserved an aspartate in the natural sequences, but dTERMen chose a variety of residues across all the templates. Furthermore, the designed sequences were very different from any previously known BH3 sequences. Figure 4.1B shows the minimum number of mutations between 18 designed peptides and the natural BH3s.

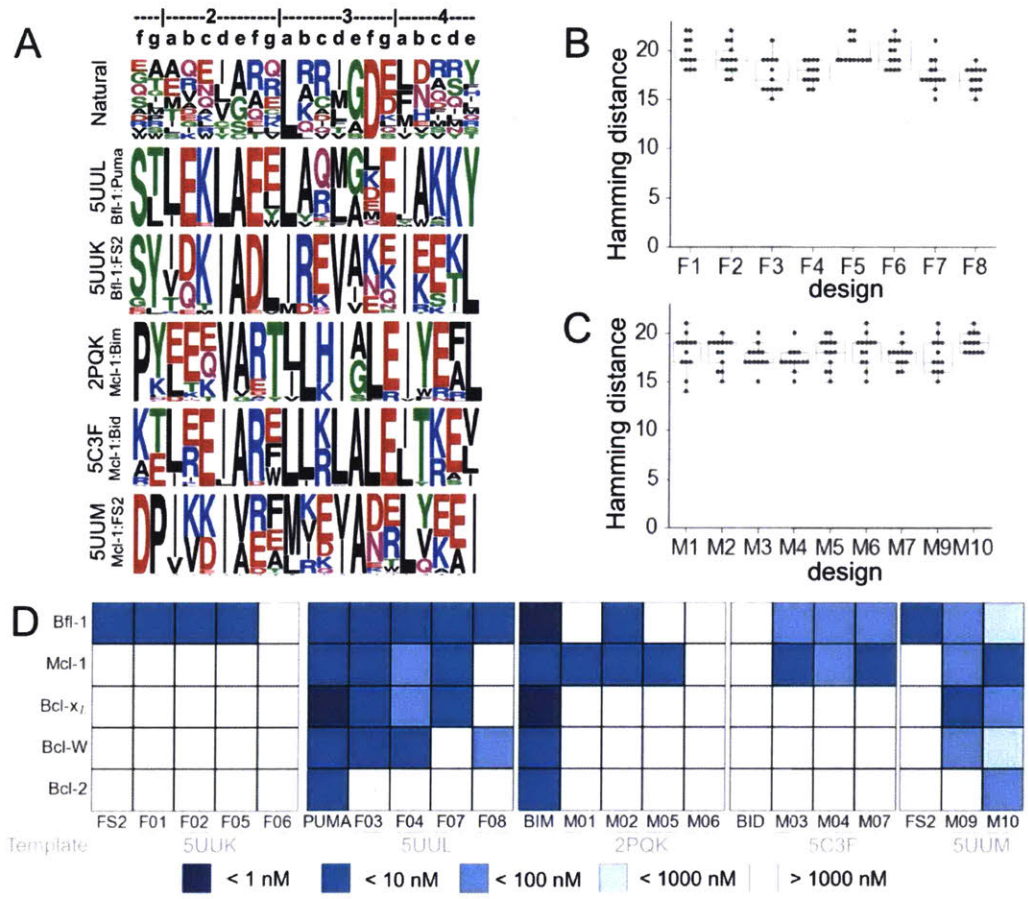

Figure 4.1. dTERMen as a predictive tool. A) Sequence logos generated by the dTERMen scoring function for each of the design templates (5UUL, 5UUK, 5C3F, 2VM6, and 5UUM). Heptad notation for the peptide sequences is shown above the logos. A list of the natural BH3s is in Table 4.2. B-C) The top-scoring sequences from A were selected for experimental testing. The sequences of the top Bfl-1 designs (B) and the top Mcl-1 designs (C) were compared to known natural ligands. A list of the top sequences is shown in supplementary table 2. D) The designed sequences were cloned into yeast for cell surface display and the binding affinities of the designs were approximated using a sparse titration. This enabled qualitative comparison of the design binding affinities to the templates. All measurements were performed at least twice.

To evaluate the predictions made by dTERMen, 17 designed peptides were selected for experimental testing. An additional sequence designed on template 5C3F was not tested because it was very similar to design M07. Peptide sequences are listed in Table 4.3. Protein binding was assayed by yeast-surface display. Binding data from yeast-surface display assays have been shown to correlate well with solution affinity measurements, and numerous BH3 peptides shown to be tight binders on the yeast cell

surface have been validated as having high affinity in solution. When the dTERMen designs were assayed for target binding, 7 out of 8 of the peptides designed to bind Bfl-1 gave strong binding signal at 100 nM Bfl-1 and 8 of 9 sequences designed to bind Mcl-1 gave similarly strong signal at 100 nM Mcl-1 (Figure 4.1D). Measurements at 4 concentrations allowed us to put bounds on the cell surface dissociation constants, as reported in Figure 4.1D. The results show that a constraint on the helix-capping residue at position 3b was not necessary for these sequences to bind their targets tightly; peptides with and without this residue fixed bound tightly to their targets. Peptides designed based on the 5UUM template, a complex that includes Mcl-1 bound to low-affinity ligand FS2, bound approximately 100 fold more tightly than did FS2 itself.

Table 4.2. List of Natural BH3 sequences composing the sequence logo in Figure 4.1A

Name	Sequence	AA Position
PUMA	EQWAREIGAQLRRMADDLNAQYERRR	131
BIM	MRPEIWIAQELRRIGDEFNAYYARRV	142
NOXA	AELEVECATQLRRFGDKLNFRQKLLN	19
BAD	LWAAQRYGRELRRMSDEFVDSFKKGL	104
BAK	SSTMGQVGRQLAIIGDDINRRYDSEF	68
BAX	DASTKKLSECLKRIGDELDSNMELQR	53
HRK	SSAAQLTAARLKALGDELHQRTMWRR	27
BMF	HQAEVQIARKLQCIADQFHRLHVQQH	127
BIK	MEGSDALALRLACIGDEMDVSLRAPR	51
BID	EDIIRNIARHLAQVGDSMDRSIPPGL	80
MULE	GVMTQEVGQLLQDMGDDVYQQYRSLT	1970
BECLIN	GGTMENLSRRLKVTGDLFDIMSGQTD	106
BOK	PGRLAEVCAVLLRLGDELEMIRPSVY	60

Table 4.3. Alignment of BH3 sequences from template structures (bold) and dTERMen designed sequences.

Name	Sequence ----2------3-----4--- efgabcdefgabcdefgabcdefg	PDB ID
FS2	**-QWVREIAAGLRRAADDVNAQVE-**	**5UUK**
F1	-SYVDKIADVMREVAEKINSDLT-	
F2	-SYIDKIADLIRKVAEEINSKLE-	
F5	-SYVDKIADLMKKVAEKINSDLT-	
F6	-SYIDKIADLIDKVVEEINSKLE-	
PUMA	**-QWAREIGAQLRRMADDLNAQYER**	**5UUL**
F3	-SLLEKLAEELRQLADELNKKFEK	
F4	-SLLEKLAEYLRQMADEINKKYVK	
F7	-SLLEKLAEELAQLADELNKKFEK	
F8	-SLLEKLAEYLAQMGDEINKKYVK	
BIM	**GRPEIWIAQELRRIGDEFNAYYA-**	**2PQK**
M1	APKEKEVAETLRKIGEEINEALK-	
M2	APYLEQVARTLRKIGEEINEALR-	
M5	APKEKEVARTLIKIGEEINEALK-	
M6	APYLEQVARTLLHIGMEINEALR-	
BID	**EDIIRNIARHLABVGDBBDRSI--**	**5C3F**
M3	DKTLEEIARELAKLAEEIDKEI--	
M4	DKTLEEIARWLARLALEIDKEI--	
M7	DKTLEEIARELLKLALEIDKEI--	
FS2	**-QWVREIAAGLRRAADDVNAQVER**	**5UUM**
M9	-DIEQEIAEALKEVADELSKAIED	
M10	-DVVLSVAETLRELADRLYEEINT	

B= Norleucine

The two designed peptides that did not bind their targets with high affinity were F6 and M6. F6 is the only peptide we designed with a residue larger than alanine or glycine at position 3e. Position 3e is uniformly conserved as small in all native BH3 motifs and in previous designed binders of Bfl-1 and Mcl-1. Modeling F6 on template 5UUK with Rosetta highlights clashes due to the close proximity of the Ca position of F6 position 3e and the backbone of Arg 88 in helix 5 of Bfl-1 (Figure 4.2G). It seems likely that valine is too large to be accommodated at this site. For design M6, it seems likely that the substitution of arginine and aspartate at positions 3b and 3f of BIM with leucine and methionine, and concomitant disruption of a charged network between the peptide and the protein may have been destabilizing. These features are consistent with F6 and M6 not binding to any of the Bcl-2 family members we tested.

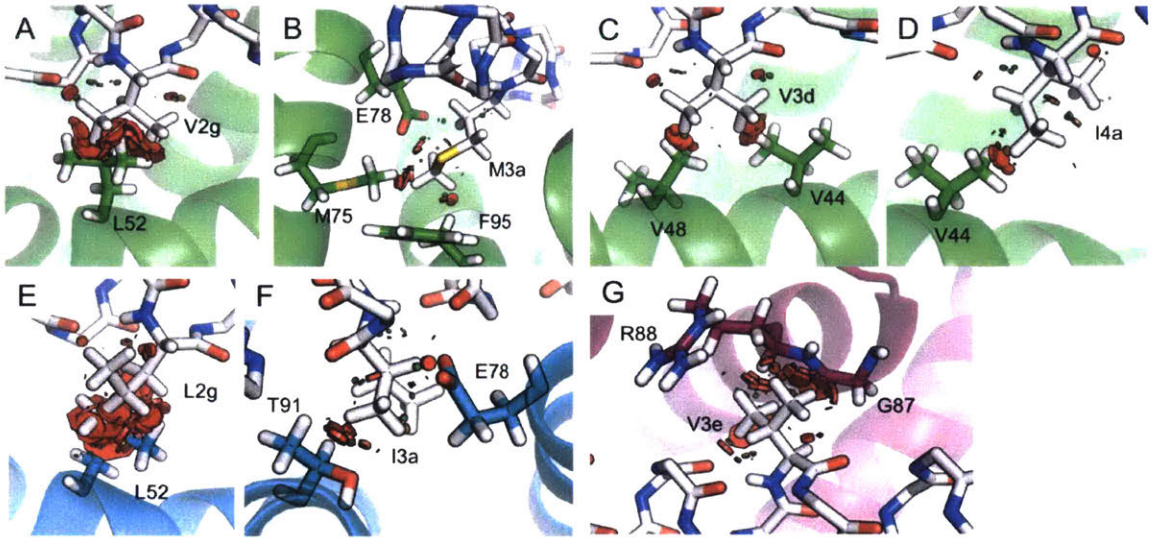

Figure 4.2. Side chain clashes for dTERMen designs on 5UUK (FS2:Bfl-1) template. A representative sample of residues from the dTERMen designs were predicted to clash for all rotamers in model structures, even with side chain repacking in Rosetta. The backbone dependent rotamers with the least predicted clashing are shown. (A) Valine at position 2g of F1 (gray) is predicted to clash (red disks) with L52 of Bfl-1 (green). (B) Methionine at position 3a of F1 (gray) and F5 is predicted to have minor clashes with M75, E78, and F95 of Bfl-1 (green). (C) Valine at position 3d of F1 (gray), F2, F5 and F6 is predicted to clash with V44 and V48 of Bfl-1 (green). (D) Isoleucine at position 3e of F1 (gray), F2, F5 and F6 is predicted to clash with V44 of Bfl-1 (green). (E) Leucine at position 2g of F2 (gray), F5, and F6 is predicted to clash with L52 of Bfl-1 (blue). (E) Isoleucine at position 3a of F2 (gray) and F6 is predicted to have minor clashes with E78 and T91 of Bfl-1 (blue).

There is substantial interest in developing Bcl-2 family paralog selective inhibitors. To determine whether our designs cross-react with other anti-apoptotic family members, we tested binding of each peptide to Bcl-x_L, Bcl-2, Bcl-w, Mcl-1 and Bfl-1. Interestingly, the Bfl-1 binders that were designed on the structure of PUMA bound to Bfl-1 bound tightly to most if not all five proteins, like the parent PUMA peptide. In contrast, peptides designed on 5UUK, the structure of FS2 bound to Bfl-1, were > 100-fold selective for Bfl-1, like FS2 itself. The data were less clear for Mcl-1 binders, some of which were selective (M1, M5) and some of which were not (M2, M3, M4, M6, M7) (Figure 4.1D).

To determine whether the designed peptides maintained the binding mode of peptides in the templates they were designed on, we solved crystal structures for four of

the peptides that bound tightest to their targets: F1 and F4 in complex with Bfl-1, and M1 and M7 in complex with Mcl-1 (Figure 4.3). Statistics for data collection and refinement are reported in Table 4.4.

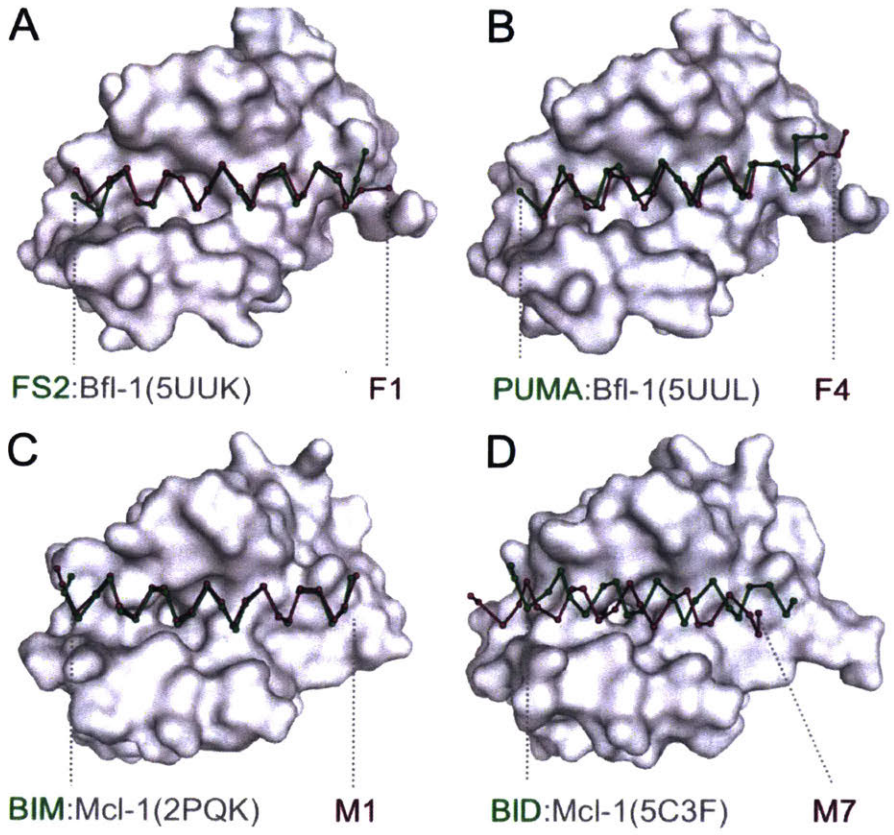

Figure 4.3. Structural comparison of designs and their templates. X-ray crystal structures of F1 bound to Bfl-1 (A), F4 bound to Bfl-1 (B), M1 bound to Mcl-1 (C), and M7 bound to Mcl-1 (D) are compared to their design templates (green ribbon and gray surface). The designed peptides are shown in purple.

Table 4.4. Summary of X-ray data collection and refinement statistics.

	Bfl-1:F1	Bfl-1:F4	Mcl-1:M1	Mcl-1:M7
Data Collection				
Space Group	P 1 21 1	P 1 21 1	P 21 21 21	P 32 2 1
Cell parameters				
a, b, c	43.223 42.92 47.718	43.466 42.905 46.666	64.792 69.733 84.853	80.758 80.758 57.95
α, β, γ	90 115.957 90	90 114.206 90	90 90 90	90 90 120
Rmeas	0.078 (0.399)	0.078 (0.43)	0.137 (0.981)	0.122 (.0698)
Rpim	0.029 (0.169)	0.036 (0.259)	0.047 (0.398)	0.045 (0.338)
Mean I/σ(I)	30.92 (2.9)	22.4 (2.0)	15.6 (0.655)	18.32 (1.49)
Completeness (%)	91.49 (77.84)	94.60 (74.42)	95.81 (67.33)	97.31 (78.96)
Redundancy	6.5 (4.3)	4.1 (1.9)	7.7 (3.9)	6.7 (3.4)
Refinement				
Resolution (Å)	38.86 - 1.587 (1.644 - 1.587)	42.56 - 1.752 (1.815 - 1.752)	24.3 - 1.945 (2.015 - 1.945)	26.77 - 2.247 (2.327 - 2.247)
Unique Reflections	19602 (1654)	15074 (1193)	27713 (1926)	10410 (831)
Rwork/Rfree	0.1706/0.1952 (0.2372/0.2628)	0.1826/0.2074 (0.2626/0.3506)	0.1993/0.2340 (0.3105/0.3380)	0.1771/0.2122 (0.2314/0.2456)
Number of non-hydrogen atoms	1623	1528	3055	1481
Average B-factors	21.08	26.3	29.58	39.34
Rmsd				
Bond lengths (Å)	0.006	0.003	0.005	0.011
Bond angles (°)	0.77	0.54	0.93	1.38

Values in parentheses are for the highest-resolution shell.

The structure of F1 in complex with Bfl-1, resolved to 1.58 Å, shows that this peptide binds very similarly to FS2 in template 5UUK (Figure 4.3A). It is striking how similar the pocket-facing positions of the designed peptide F1 and template peptide FS2 are, even though the sequence identity of these two peptides is low (27%) and no information about the FS2 sequence was used in the design process. Modeling F1 onto the FS2 backbone in structure 5UUK indicates a minor clashes are anticipated between M3a with residues in the P2 pocket (M75, F95, and E78), I4a with V44 in helix 2 of Bfl-1, and V3d with V48 and V44 of helix 2 of Bfl-1 (Figure 4.2). Substantial clashes are anticipated between V2g and L52 of helix 2 of Bfl-1, but the solved structure shows how backbone adjustments can accommodated this residue. The small clash appears to be the reason the C-terminus departs from its path in 5UUK. There are also deviations between the N-terminus of FS2 in 5UUK and F1 in our new structure, which appear to arise from changing tryptophan at position 2 to tyrosine, as well as from a change in N-

terminal capping. FS2 is capped at the N terminus by the acetyl group, whereas for F1 this is a networked interaction involving S1f and D2b.

We solved the structure of F4 bound to Bfl-1 to 1.75 Å and found that the C-terminal end of the peptide rearranges (Figure 4.3B). In the original template (5UUL), the helix begins to unwind around position 4d, but in the redesigned structure it the last three or four residues are in an extended conformation. This could be due to mutation of position 22 from glutamate to valine, as it ends up being flipped down and in an extended conformation. We also found that dTERMen had poor statistics for structural elements at the C-terminus of 5UUL, which might have contributed to the helical unwinding. At the N-terminus, the sequence of F4 is very different from that of PUMA; there is only 1 conserved position in the last 10 residues. A very important change is glycine to alanine at position 2e. In 5UUL this is a very tightly packed helix-helix position, where only glycine can sterically fit, but TERM statistics indicated that alanine is common in very similar geometries. The solved structure shows how the F4 helix shifted slightly to accommodate alanine and other sequence changes.

We solved the structure of M1 bound to Mcl-1 to 1.95 Å and found that that it binds very similarly its template 2PQK (Figure 4.3C). However, the structure of M7 bound to Mcl-1 at 2.25 Å resolution revealed a substantial change in the binding mode of the peptide relative to the positioning of stapled BID in the design template (Figure 4.3D). The helix is shifted in the groove by 2.56 Å, and canonical BH3 interactions including aspartate at 3f and leucine at 3a are completely rearranged, as are the hydrophobic contacts (Figure 4.4B, C). In Mcl-1 alpha helix 4 is rearranged (Figure 4.4A). Interestingly, when evaluated using dTERMen, the M7 sequence scored worse

on the solved structure than it did on the template model. One complication in evaluating this structure is that there are close contacts between two copies of the Mcl-1:M7 complex near the C-terminal end of the binding groove and with alpha helix 4 of Mcl-1 (Figure 4.5). It is possible that these influenced the binding mode; we can't rule out at this time the possibility that crystal packing forces favored population of a minor structural species.

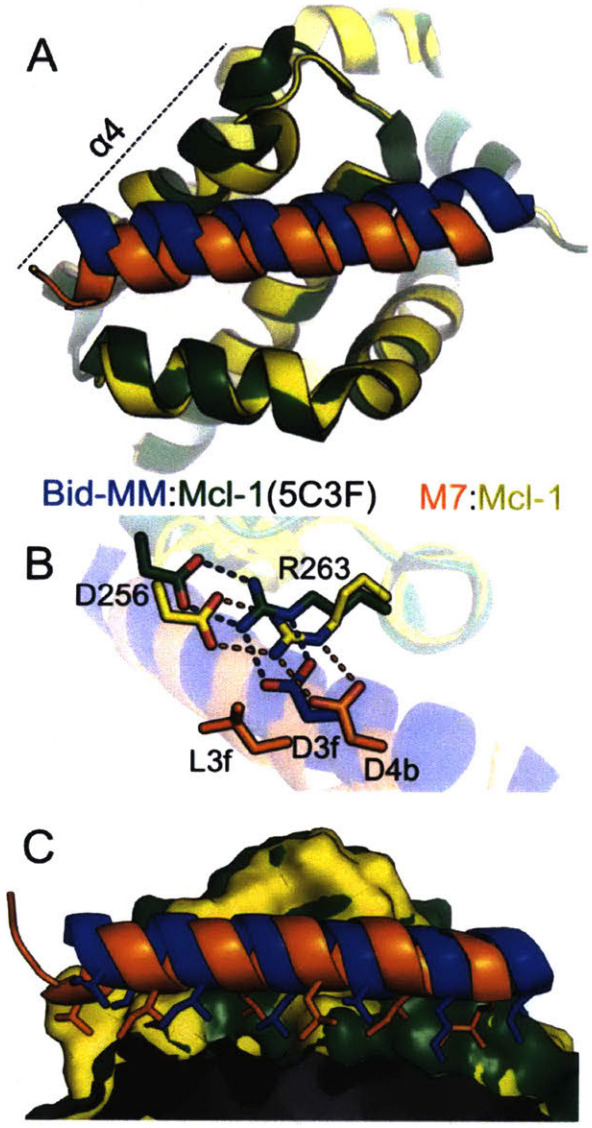

Figure 4.4. Comparison between the crystal structure of M7 (orange) in complex with Mcl-1 (yellow) and its design template 5C3F (Bid-MM in blue and Mcl-1 in green). A) Structural alignment reveals a rearrangement of alpha-helix 4 of Mcl-1. B) In 5C3F, as in most Mcl-1:BH3 structures, an aspartate in peptide position 3f forms a salt-bridge network with R263 and D256 of Bfl-1 (hydrogen bonds show as blue dashes). A similar salt-bridge network is observed in the M7:Mcl-1 complex, but with an aspartate one helical turn away in peptide position 4b (hydrogen bonds show as orange dashes). C) The shifted binding mode of M7 re-arranges hydrophobic contacts with Mcl-1 relative to those observed in the 5C3F structure.

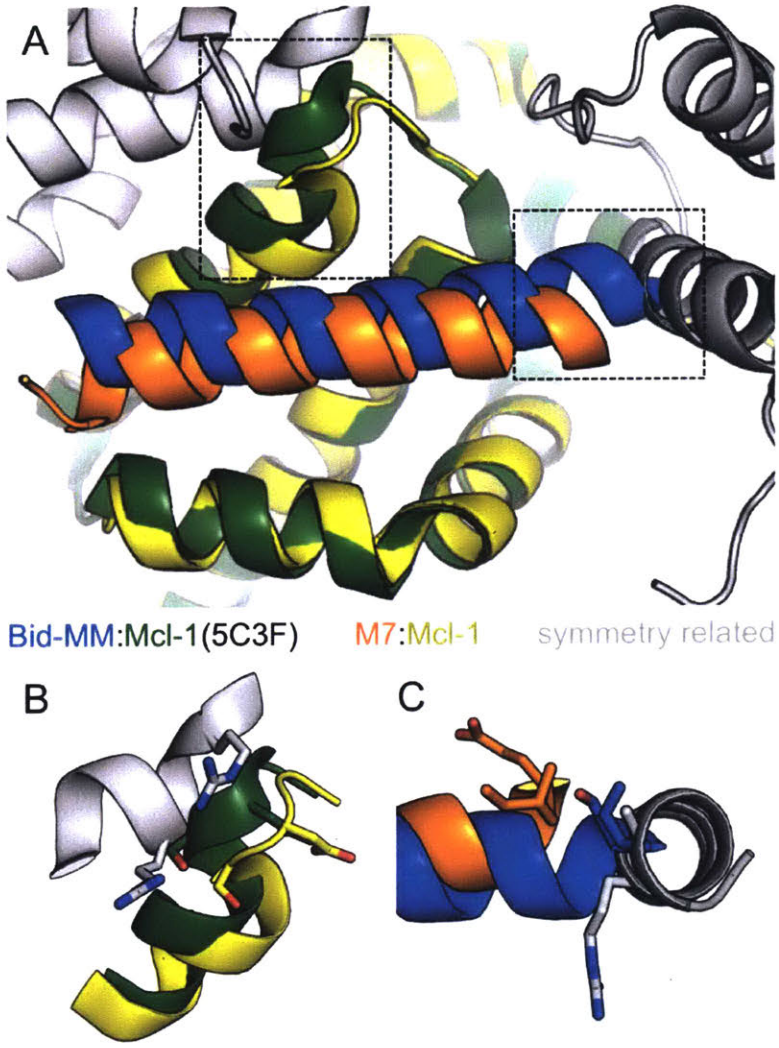

Figure 4.5. Crystal packing in the M7:Mcl-1 crystal structure. A) Symmetry related molecules (gray) in M7:Mcl-1 crystal would be expected to clash with the Mcl-1 conformation (B) and peptide conformation (C) observed in 5C3F.

There are a few features of design M7 that may account for this shift. First, alanine at position 10 is over packed when modeled on the 5C3F backbone. Nevertheless, we tested this design because wanted to assess whether the backbone would adjust to accommodate the mutation, as was observed in the structure of F4 bound to Bfl-1. Interestingly, 5C3F and 2PQK backbones are very similar around this position and dTERMen design calculations on both templates predicted that alanine and glycine were both favorable. Alanine was chosen as optimal in the 5C3F-based design,

whereas glycine was preferred for the 2PQK-based template. It may be that the Mcl-1-peptide complex could not relax sufficiently to accommodate the addition of a methyl group. Another element that may have contributed to the re-positioning of the peptide in the groove may be the choice of residues at positions 3f and 4b, which form an interface with the protein on one side of the helix. BID, and all other native BH3 peptides, have aspartate at position 3f, but in design M7 this residue is leucine, and position 4b is aspartate. In the crystal structure, peptide M7 is shifted such that Asp 4b can play a similar role to that of Asp 3f in 5C3F, by interacting with Arg 263 in Mcl-1 (Figure 4.4B).

In summary, x-ray crystallography revealed that backbone positioning of two of the crystalized designs were sub-angstrom matches of their design templates, one bound in a geometry that shared high similarly with its template, and the remaining design bound in an unexpected, dramatically shifted orientation.

DISCUSSION

Using dTERMen, we were able to rapidly design in entirely new regions of sequence space without the need for explicit modeling of complex structures or expensive experimental library screening. Previous work has shown that this is not a trivial task. Even in carefully designed libraries only < 8 mutations away from natural BH3 domains, most sequences fail to bind Bfl-1 and Mcl-1[22,23,33]. In contrast, with dTERMen, 15/17 of the designs bound with native-like affinity, even though the sequences were 14-22 mutations away from known BH3 binders (Figure 4.1B, C).

Our design protocol provided access to novel sequences. Some of the tight binders we discovered using dTERMen lack the highly conserved leucine and aspartate residues common to all known, native BH3 sequences (Figure 4.1A). This pair of

residues has been used in the past to define the BH3 motif. Not only do our results suggest that these residues are not necessary for binding, but they show that dTERMen is a useful tool for discovering binders that can't be predicted or even recognized based on conserved sequence features.

By using different design templates, we were able to find solutions in distinct regions of sequence space, as illustrated in Figure 4.1A. This may seem to be at odds with our finding that dTERMen is robust to small differences in input structure, but the templates used for design were deliberately chosen to sample different backbone geometries. We expected these templates to match with different TERMs from the PDB, and thus to generate different sequence predictions. Templates 5UUL and 2PQK included peptides with native sequences that have evolved for tight binding. Other templates we tested, 5C3F and 5UUM, featured peptides that bound their targets more than 3 orders of magnitude more weakly. It is interesting that both structures of high-affinity and low-affinity peptide complexes led to novel, high-affinity peptide binders when used as input to the design calculations. Design on other solved structures could potentially provide access to even greater diversity. Going beyond solved structures, it may be possible to perform dTERMen design on predicted structures with binding modes that are not represented in the PDB.

Designs that are diverse in sequence are potentially valuable because they provide opportunities to optimize pharmacological properties not related to binding. These properties could influence whether these peptides are disruptive to membranes and how readily they can be delivered to cells. Several studies have shown that the cell permeability of stapled helical peptides depends on peptide properties including charge

and hydrophobicity[34]. The charge of a peptide can also affect how efficiently it is loaded into nanoparticles. Different sequences will also have different cross-reactivity, immunogenicity, and protease sensitivity, so having many option to choose from increases the chances of developing useful reagents and lead therapeutics. Interestingly, design using dTERMen is compatible with imposing constraints on peptide properties such as net charge, so if the desired physical characteristics of a peptide inhibitor are known, they can be used to direct the search into promising sequence spaces.

The dTERMen scoring potential is based on sequence statistics for structural elements observed repeatedly in nature. There is no formal relationship between these statistics and protein stability or affinity, so the scoring may reflect any number of evolutionary pressures including stability, specificity, folding kinetics, solubility, or other factors. We interpret the success of dTERMen in design as evidence that whatever evolutionary forces may be contributing to the statistics, there must be a substantial contribution from the free energy of the sequence adopting the evaluated structure. The fact that we designed helix-helix interactions in this project, which are common in the PDB, may be part of the reason our dTERMen designs performed so well. This method is not expected to perform as well on structural motifs that are sparsely sampled in the PDB. However, more structures are deposited in the PDB every day, so the range of accessible design targets is expected to improve over time[19].

One attractive feature of dTERMen is that it doesn't require structural modeling or minimization; the design optimization is performed in sequence space. Although the PDB structure-mining that is needed to build the scoring function can be somewhat time

consuming, once such a function is derived, it is possible to perform design, or to evaluate thousands of sequences, in seconds. Another advantage of dTERMen is that there is a structural "fuzziness" built in, because the sequence statistics used for modeling are derived from close, but not exact, matches of TERMs. This makes the method more robust than FoldX to small variations in input structure, as shown in our benchmark testing, and also accounts for some amount of backbone relaxation. In this work, we saw one example where a mutation was accommodated (in peptide F4) that would not have been predicted if modeling was performed on a rigid scaffold. On the other hand, dTERMen design failures may result from over-packing the protein-peptide interface beyond what can be accommodated by small structural rearrangements. This may be what happened in designs F6 and M6, which did not bind tightly to their targets. Future design studies will help calibrate the methods so that diverse sequences can be obtained with high success rates. Combining dTERMen with a post-analysis procedure that includes all-atom modeling, e.g. using Rosetta, could be one way to recognize mutations that can vs. cannot be accommodated. Although this would increase the computational costs, such a secondary evaluation could readily be performed for a modest number (hundreds or thousands) of promising candidates designs.

One unexpected result from this work is that the specificity profiles of the designs were observed to be template dependent (Figure 4.1D). This is particularly striking in the case of the FS2 template. Although no off targets were considered during design, the peptides designed from the FS2 structure were highly Bf-1 selective and in fact provide outstanding leads for development as Bfl-1 targeting agents. This specificity of peptides F1, F2 and F5 may be a result of the unique way FS2 engages Bfl-1. FS2

adopts a non-canonical binding mode that has not been observed for natural BH3 ligands. It may be that the interactions that support the FS2 binding mode are under less evolutionary pressure to mirror those required for BH3 binding in the other family members and are thus more likely to be unique (Figure 4.6). This is consistent with the idea that a peptide that makes contacts outside of the conserved binding cleft can use these contacts to achieve intra-family specificity[24].

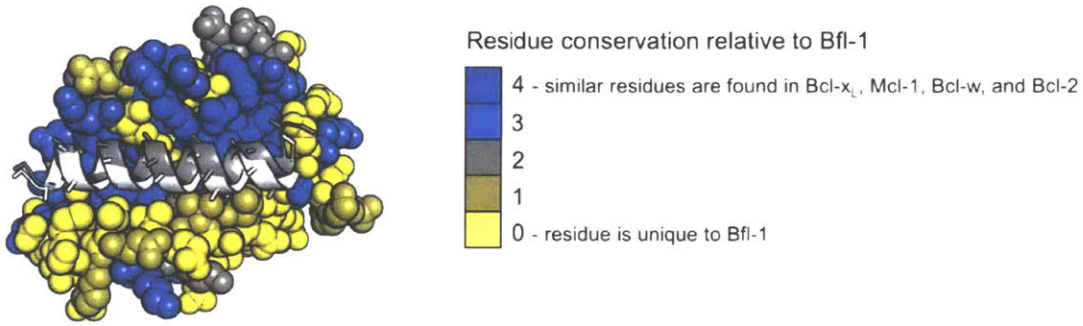

Figure 4.6. FS2 (white, cartoon) binding mode might have more potential than Puma (dark gray, cartoon) binding mode to interact with residues that are unique to Bfl-1 (colored spheres). Similarity based on Blosum62 matrix.

This proof-of-principle study makes us enormously enthusiastic about the potential of dTERMen for designing peptide binders and inhibitors. The ease of use, fast run times, and very high success rates on a difficult problem provide compelling evidence of the promise of this approach. There are ample opportunities to improve dTERMen further, for example by deriving TERM statistics from a database that includes protein-protein and protein-peptide interfaces, and/or combining this sequence-based design approach with all-atom modeling to better assess what mutations can be accommodated by structural relaxation. We look forward to tackling increasingly difficult

problems and moving the use of TERM statistics into the mainstream of modern protein design.

Methods

Yeast clones

EBY100 yeast cells were transformed using the Frozen-EZ Yeast Transformation II Kit (Zymo Research) according to the manufacturer's protocol. For a plasmid backbone, we used the Puma PCT plasmid[23] and digested it with xhoI (NEB) and nheI-HF (NEB) according to the manufacturer's protocol. The inserts were constructed with PCR using primers that encoded the peptide sequence flanked with at least 40 bp of the plasmid sequence on either side of the insertion site to facilitate homologous recombination. The inserts and plasmid backbones were mixed at a 5 to 1 ratio for transformation. The transformation mixture was spread onto SD + CAA plates (5 g/L casamino acids, 1.7 g/L yeast nitrogen base, 5 g/L ammonium sulfate, 10.2 g/L Na2HPO4-7H2O and 8.6 g/L NaH2PO4-H2O, 2% glucose, 15-18 g/L agar, 182 g/L sorbitol) and grown at 30 °C for 2 to 3 days. To confirm each strain, colony PCR followed by sequencing was performed on single colonies. Sequence verified colonies were grown overnight in SD+CAA (5 g/L casamino acids, 1.7 g/L yeast nitrogen base, 5 g/L ammonium sulfate, 10.2 g/L Na2HPO4-7H2O and 8.6 g/L NaH2PO4-H2O, 2% glucose). The saturated overnight cultures were diluted with to a final concentration of 15% glycerol and stored at -80 °C.

Yeast growth and FACS analysis

A small amount of frozen culture was scrapped from the top of frozen culture stocks to inoculate SD+CAA. After passaging overnight at 30 °C, cultures were diluted

to an OD_{600} of 0.005-0.01 in SD+CAA and grown to an OD_{600} of 0.1–0.6. Cells cultures were then diluted 25-fold with SG+CAA (5 g/L casamino acids, 1.7 g/L yeast nitrogen base, 5.0 g/L ammonium sulfate, 10.2 g/L Na2HPO4-7H2O and 8.6 g/L NaH2PO4-H2O, 2% galactose) to induce peptide expression and grown for 20-24 hr at 30 °C. To measure binding to surface-displayed peptides, cells were filtered with a 96-well plate filter (10^5-10^6 cells/well), washed twice with 150 µL BSS (50 mM Tris pH 8, 100 mM NaCl, 1 mg/ml BSA), and resuspended in BSS with least 10-fold molar excess target protein and incubated in the filter plate for 2 h at room temperature with gentle shaking for equilibration. To detect cell surface expression and binding of target protein, cell suspensions were filtered, washed twice in chilled BSS, resuspended in a 35 µL of 1:100 dilution of primary antibodies (mouse anti-HA, Roche, RRID:AB_514505 and rabbit anti-c-myc antibodies, Sigma, RRID:AB_439680) in BSS and with gentle shaking for 15 min at 4 °C. Cells were then filtered, washed twice in 150 µL chilled BSS, resuspended in 35 µL of a solution of secondary antibodies in BSS (1:40 dilution of APC rat anti-mouse, BD, RRID:AB_398465 and 1:100 dilution of PE goat anti-rabbit, Sigma, RRID:AB_261257) and incubated with gentle shaking in the dark for 15 min at 4 °C. Cells were filtered and washed twice more in 150 µL chilled BSS to remove unbound antibodies. Labeled cells were resuspended in BSS and analyzed using a BD FACSCanto with FACSDiva software.

Protein and peptide purification

Sequences for the myc-tagged Mcl-1, Bfl-1, Bcl-2, Bcl-w, and Bcl-x_L proteins used for binding assays can be found in (ref). Sequences for the untagged Bfl-1 and Mcl-1 proteins used for crystallography purified as previously described[23] and frozen at -

80 °C. The peptides used for crystallography were synthesized at the MIT biopolymers facility with N-terminal acetylation and C-terminal amidation and were purified by HPLC on a C-18 column with a linear gradient of acetonitrile and water. Purified peptides were lyophilized and resuspended in DMSO. Peptide masses were confirmed by mass spectrometry.

Crystallography

Crystals of Bfl-1 in complex with the designed peptides were grown in hanging drops. To set the drops, untagged Bfl-1 (8 mg/mL in 20 mM Tris, 150 mM NaCl, 1% glycerol, 1 mM DTT, pH 8.0) was mixed in equal molar ratio with the designed peptides. 1.5 µL of the Bfl-1/peptide mixture was pipetted onto a glass coverslip and mixed with with 1.5 µL of well solution (1.8 - 2.0 M NH_4SO_4, 50 mM MES pH 6.5). To cryoprotect the crystals, they were transferred into a solution of 2.0 M LiSO4 with 10% glycerol. Crystals were flash frozen in liquid nitrogen. Diffraction data were collected at the Advanced Photon Source at the Argonne National Laboratory, NE-CAT beamline 24-ID-C. The datasets were refined to 1.59 Å and 1.75 Å and scaled using HKL2000[35]. Phenix was used to phase with the Bfl-1 chain from PDB id 5UUK. The peptides were modeled into the difference densities using Coot. Iterative rounds of refinement and model building were performed using Phenix and Coot[36,37].

Crystals of Mc1-1 in complex with the designed peptides were grown in hanging drops. To set the drops, TCEP (100 mM) and $ZnSO_4$ (50 mM) was added at 10% volume to untagged Mcl-1 (8.5 mg/mL in 20 mM Tris, 150 mM NaCl, 1% glycerol, 1 mM DTT, pH 8.0) before adding equal molar amounts of the designed peptides. To grow crystals of Mcl-1 in complex with F1, 1.5 µL of the peptide protein mixture was mixed

with 1.5 µL of well solution (peg 3350, 50 mM bis-tris pH 8.5, 50 mM NH4CH3CO2). Crystals were cryoprotected by adding 3 µL of a solution of 37.5% glucose in peg 3350, 50 mM bis-tris pH 8.5, 50 mM $NH_4CH_3CO_2$ directly to the drop 0.5 µL at a time. To grow crystals of Mcl-1 in complex with F7, 2.5 µL of the peptide protein mixture was mixed with 0.5 uL of well solution (1.4 M sodium citrate pH 6.5, 0.1 M HEPES pH 7.5). To cryoprotect, crystals were transferred to 1.6 M sodium citrate pH 6.5, 0.1 M HEPES pH 7.5. Crystals were flash frozen in liquid nitrogen. Diffraction data were collected at the MIT X-ray core facility. The datasets were refined to 1.95 Å and 2.25 Å and scaled using HKL2000[35]. Phenix was used to phase with the Mcl-1 chain from PDB id 3PK1. The peptides were modeled into the difference densities using Coot[36]. Iterative rounds of refinement and model building were performed using Phenix and Coot[36,37].

Benchmarking

Automatic download and annotation of Bcl-2 protein-peptide complex structures Uniprot sequences for Bcl-x_L, Bfl-1 and Mcl-1 were retrieved from Uniprot and blasted against the PDB database (7 Nov 2017). Matched structures were downloaded and standardized by removing hydrogens and heteroatoms and transforming selenomethionine to methionine. Sequences were aligned and renumbered on their corresponding Uniprot template sequence using Needle. Regions that weren't matched or that were poorly aligned with the Uniprot sequence were removed from the structure. Chains of length [20,39] with residues that have more than 30% of their Voronoi surface in contact with the receptor were identified as interacting peptide. Unless specified, peptides containing non-natural amino acids were removed from the dataset. Only the first model of NMR ensembles was retained. If a structure included multiple complexes

in the asymmetric unit, these were split into new files and analyzed separately. Finally, chains were re-labelled so that the Bcl-2 protein is always chain A and the peptide is always chain B.

Alignment on binding site and method for comparing peptide binding geometry. For every complex, residues within 8 Å of any peptide atom were considered part of the binding site and all complexes were structurally aligned using only their protein binding-site atoms, using 3DCOMB. To define a common reference point for all bound peptides, each peptide carbon alpha was represented as a node and a edge was created if the distance between 2 nodes was below a threshold. The distance threshold was initially set at 2 Å and gradually increased by 0.1 Å until largest clique in the graph included all complexes . This clique represented a set of carbon alpha that are all within the distance threshold and represent the "anchor" used for setting the registry. This position was arbitrarily set to residue number 100. RMSDs between peptides in different complexes were calculated using this alignment using only overlapping nodes.

Structural scoring functions dTERMen[19], FoldX4.0[30], and Rosetta[29] were tested for their ability to predict peptide-protein binding affinity and specificity using binding data obtained using the SORTCERY protocol[27,28]. Scoring was based on 20-residue peptides. The scored segment was chosen by structural inspection to include those positions that make extensive contacts with the protein and that are unlikely to be influenced by crystal contacts in the templates used for modeling.

Each structure was used as a template for dTERMen, generating a scoring function for that template, i.e. a function that can score any peptide binding to the

template-structure protein. FoldX4.0 was used to predict binding affinity by first using FoldX4.0's "repair" function. Then, for each peptide in SORTCERY dataset, the repaired template was transformed using the "mutate" function to generate the sequence of peptide query and scored using the "complex" function. For Rosetta scoring, complex structures generated by FoldX were relaxed with Rosetta using Talaris2014 or BetaNov force fields. Relaxed structures were run through the surface analyzer "mover". Values from cross and separated ΔG were kept as predicted binding energy.

The predictive power of the different structural scoring functions and protocols was assessed by calculating the correlation between the binding energy determined by SORTCERY, in kcal/mol, and each method's predicted binding energy (in arbitrary units). Method's ability to identified top 10% binder vs. the rest was evaluated using AUC of ROC curve. Finally, some sequences are found in more than one dataset and their difference in binding energy represent their specificity. Using sequence that bind tightly at least of the 2 receptors, ability of methods to predict specificity was assessed by obtaining the correlation between experimental ΔΔG and predicted ΔΔG. Multiple templates were tested for each protein receptor, and the predictive power was evaluated for each template individually for binding affinity or all possible combinations for specificity. Average performance on all templates was reported and represents the expected value if a random template is chosen. We also report prediction performance using the template that gave the lowest energy for each sequence.

Acknowledgements

We thank the Koch Institute Flow Cytometry Core Facility for assistance with FACS analysis, Koch Institute Bioploymers and Proteomics Facility for peptide synthesis, and the MIT Structural Biology Core Facility for assistance with X-ray crystallography. Part of this work was conducted at the Northeastern Collaborative Access Team beamlines, which are funded by the National Institute of General Medical Sciences from the National Institutes of Health (P41 GM103403). The Pilatus 6M detector on 24-ID-C beam line is funded by a NIH-ORIP HEI grant (S10 RR029205). This research used resources of the Advanced Photon Source, a U.S. Department of Energy (DOE) Office of Science User Facility operated for the DOE Office of Science by Argonne National Laboratory under Contract No. DE-AC02-06CH11357. The content is solely the responsibility of the authors and does not necessarily represent the official views of the National Institutes of Health or the U.S. Department of Energy.

References

1. Rual J-F, Venkatesan K, Hao T, et al. Towards a proteome-scale map of the human protein–protein interaction network. *Nature*. 2005;437(7062):1173-1178. doi:10.1038/nature04209.
2. Morimoto RI, Cuervo AM. Protein homeostasis and aging: taking care of proteins from the cradle to the grave. *J Gerontol A Biol Sci Med Sci*. 2009;64(2):167-170. doi:10.1093/gerona/gln071.
3. Ryan DP, Matthews JM. Protein–protein interactions in human disease. *Curr Opin Struct Biol*. 2005;15(4):441-446. doi:10.1016/J.SBI.2005.06.001.
4. Chen TS, Petrey D, Garzon JI, Honig B. Predicting peptide-mediated interactions on a genome-wide scale. *PLoS Comput Biol*. 2015;11(5):e1004248. doi:10.1371/journal.pcbi.1004248.
5. Bakail M, Ochsenbein F. Targeting protein–protein interactions, a wide open field for drug design. *Comptes Rendus Chim*. 2016;19(1-2):19-27. doi:10.1016/J.CRCI.2015.12.004.
6. Wells JA, McClendon CL. Reaching for high-hanging fruit in drug discovery at protein–protein interfaces. *Nature*. 2007;450(7172):1001-1009. doi:10.1038/nature06526.
7. Arkin MR, Tang Y, Wells JA. Small-molecule inhibitors of protein-protein interactions: progressing toward the reality. *Chem Biol*. 2014;21(9):1102-1114. doi:10.1016/j.chembiol.2014.09.001.
8. Azzarito V, Long K, Murphy NS, Wilson AJ. Inhibition of α-helix-mediated protein–protein interactions using designed molecules. *Nat Chem*. 2013;5(3):161-173. doi:10.1038/nchem.1568.
9. Chang YS, Graves B, Guerlavais V, et al. Stapled α-helical peptide drug development: a potent dual inhibitor of MDM2 and MDMX for p53-dependent cancer therapy. *Proc Natl Acad Sci U S A*. 2013;110(36):E3445-54. doi:10.1073/pnas.1303002110.
10. Rezaei Araghi R, Bird GH, Ryan JA, et al. Iterative optimization yields Mcl-1-targeting stapled peptides with selective cytotoxicity to Mcl-1-dependent cancer cells. *Proc Natl Acad Sci U S A*. 2018;115(5):E886-E895. doi:10.1073/pnas.1712952115.
11. McGrath NA, Andersen KA, Davis AKF, Lomax JE, Raines RT. Diazo compounds for the bioreversible esterification of proteins. *Chem Sci*. 2015;6(1):752-755. doi:10.1039/C4SC01768D.
12. Mix KA, Lomax JE, Raines RT. Cytosolic Delivery of Proteins by Bioreversible Esterification. doi:10.1021/jacs.7b06597.
13. Schwarze SR, Ho A, Vocero-Akbani A, Dowdy SF. In vivo protein transduction: delivery of a biologically active protein into the mouse. *Science*. 1999;285(5433):1569-1572. http://www.ncbi.nlm.nih.gov/pubmed/10477521. Accessed April 16, 2018.
14. Fuchs SM, Raines RT. Polyarginine as a multifunctional fusion tag. *Protein Sci*. 2005;14(6):1538-1544. doi:10.1110/ps.051393805.
15. Stanzl EG, Trantow BM, Vargas JR, Wender PA. Fifteen years of cell-penetrating, guanidinium-rich molecular transporters: basic science, research tools, and clinical applications. *Acc Chem Res*. 2013;46(12):2944-2954. doi:10.1021/ar4000554.
16. Zuris JA, Thompson DB, Shu Y, et al. Cationic lipid-mediated delivery of proteins enables efficient protein-based genome editing in vitro and in vivo. *Nat Biotechnol*. 2015;33(1):73-80. doi:10.1038/nbt.3081.
17. Chevalier A, Silva D-A, Rocklin GJ, et al. Massively parallel de novo protein design for targeted therapeutics. *Nature*. 2017;550(7674):74-79. doi:10.1038/nature23912.
18. Mackenzie CO, Zhou J, Grigoryan G. Tertiary alphabet for the observable protein structural universe. *Proc Natl Acad Sci U S A*. 2016;113(47):E7438-E7447. doi:10.1073/pnas.1607178113.
19. Zheng F, Grigoryan G. Sequence statistics of tertiary structural motifs reflect protein stability. Srinivasan N, ed. *PLoS One*. 2017;12(5):e0178272. doi:10.1371/journal.pone.0178272.
20. Moldoveanu T, Follis AV, Kriwacki RW, Green DR. Many players in BCL-2 family affairs. *Trends Biochem Sci*. 2014;39(3):101-111. doi:10.1016/j.tibs.2013.12.006.

21. Opferman JT. Attacking cancer's Achilles heel: antagonism of anti-apoptotic BCL-2 family members. *FEBS J.* August 2015. doi:10.1111/febs.13472.

22. Foight GW, Ryan JA, Gullá S V, Letai A, Keating AE. Designed BH3 Peptides with High Affinity and Specificity for Targeting Mcl-1 in Cells. *ACS Chem Biol.* 2014;9(9):1962-1968. doi:10.1021/cb500340w.

23. Jenson JM, Ryan JA, Grant RA, Letai A, Keating AE. Epistatic mutations in PUMA BH3 drive an alternate binding mode to potently and selectively inhibit anti-apoptotic Bfl-1. *Elife.* 2017;6:e25541. doi:10.7554/eLife.25541.

24. Berger S, Procko E, Margineantu D, et al. Computationally designed high specificity inhibitors delineate the roles of BCL2 family proteins in cancer. *Elife.* 2016;5:1422-1432. doi:10.7554/eLife.20352.

25. Kotschy A, Szlavik Z, Murray J, et al. The MCL1 inhibitor S63845 is tolerable and effective in diverse cancer models. *Nature.* 2016;538(7626):477-482. doi:10.1038/nature19830.

26. DeBartolo J, Dutta S, Reich L, Keating AE. Predictive Bcl-2 family binding models rooted in experiment or structure. *J Mol Biol.* 2012;422(1):124-144. doi:10.1016/j.jmb.2012.05.022.

27. Reich LL, Dutta S, Keating AE. SORTCERY-A High-Throughput Method to Affinity Rank Peptide Ligands. *J Mol Biol.* 2015;427(11):2135-2150. doi:10.1016/j.jmb.2014.09.025.

28. Reich L "Luther," Dutta S, Keating AE. Generating High-Accuracy Peptide-Binding Data in High Throughput with Yeast Surface Display and SORTCERY. In: ; 2016:233-247. doi:10.1007/978-1-4939-3569-7_14.

29. Alford RF, Leaver-Fay A, Jeliazkov JR, et al. The Rosetta All-Atom Energy Function for Macromolecular Modeling and Design. *J Chem Theory Comput.* 2017;13(6):3031-3048. doi:10.1021/acs.jctc.7b00125.

30. Schymkowitz J, Borg J, Stricher F, Nys R, Rousseau F, Serrano L. The FoldX web server: an online force field. *Nucleic Acids Res.* 2005;33(Web Server):W382-W388. doi:10.1093/nar/gki387.

31. Fire E, Gullá S V, Grant RA, Keating AE. Mcl-1-Bim complexes accommodate surprising point mutations via minor structural changes. *Protein Sci.* 2010;19(3):507-519. doi:10.1002/pro.329.

32. Miles JA, Yeo DJ, Rowell P, et al. Hydrocarbon constrained peptides – understanding preorganisation and binding affinity. *Chem Sci.* 2016;7(6):3694-3702. doi:10.1039/C5SC04048E.

33. Dutta S, Chen TS, Keating AE. Peptide ligands for pro-survival protein Bfl-1 from computationally guided library screening. *ACS Chem Biol.* 2013;8(4):778-788. doi:10.1021/cb300679a.

34. Bird GH, Mazzola E, Opoku-Nsiah K, et al. Biophysical determinants for cellular uptake of hydrocarbon-stapled peptide helices. *Nat Chem Biol.* 2016;12(10):845-852. doi:10.1038/nchembio.2153.

35. Otwinowski Z, Minor W. [20] Processing of X-ray diffraction data collected in oscillation mode. *Methods Enzymol.* 1997;276:307-326. doi:10.1016/S0076-6879(97)76066-X.

36. Emsley P, Lohkamp B, Scott WG, Cowtan K. Features and development of Coot. *Acta Crystallogr D Biol Crystallogr.* 2010;66(Pt 4):486-501. doi:10.1107/S0907444910007493.

37. Adams PD, Afonine P V, Bunkóczi G, et al. PHENIX: a comprehensive Python-based system for macromolecular structure solution. *Acta Crystallogr D Biol Crystallogr.* 2010;66(Pt 2):213-221. doi:10.1107/S0907444909052925.

Chapter 5

Conclusions and future directions

There are many possible ways design peptides with desirable interaction profiles. My thesis work describes three distinct approaches to design tight and selective peptide inhibitors of anti-apoptotic proteins, with an emphasis on Bfl-1. In one approach, I used models built on small-scale mutational datasets and structure-based models to design peptide libraries of BH3 variants. These libraries were screened to identify tight and selective peptide inhibitors of Bfl-1. In another approach, I contributed to constructing a computational model of the specificity landscape of Bfl-1, Bcl-x_L, and Mcl-1 that was built on high-throughput affinity measurements of thousands of mutant BH3s. This data-driven model provided valuable insight in to the binding preferences of these related proteins and enabled us to design in a mutational space that is far larger than what is experimentally tractable. In a complementary approach, I described the use of a structure-based computational model built from sequence statistics extracted from the PDB to design BH3 mimetics with sufficient accuracy to forgo experimental screening.

This thesis describes the design of and experimental validation of more than 22 novel Bfl-1 inhibitors, 20 novel Mcl-1 inhibitors, and 12 novel Bcl-x_L inhibitors. The models used to design these peptides predict many hundreds of additional sequences with similarly promising interaction profiles. Although the peptides described in this thesis are far from orally available therapeutic drugs, these peptides do have immediate value as research tools. For example, peptides from this thesis are already being used by other research labs to study Bfl-1 function and to diagnose Bfl-1 dependence. Further, lessons from my work can inform future efforts develop the next generation of BH3 mimetics, as discussed below.

The data-driven approach described in chapter 3 of this thesis to design interaction specificity can be applied to other design tasks, including peptide delivery into cells. Factors such as positive charge, α-helicity, charge distribution, peptide sequence, and hydrophobicity have been proposed to contribute to cell uptake propensity[1]. However, much of what is currently known is about cellular delivery is inferred from (and biased by) the few sequences that have worked before. Given sufficient data, it should be possible to build a computational model to design peptides with improved cellular uptake. One of the major roadblocks to doing this is collecting a sufficiently large and diverse dataset to build a useful model. Some cell delivery platforms might be adaptable to high-throughput screening. One potential example is bioreversible esterification[2,3]. By esterifying carboxylate-containing side chains (aspartate and glutamate), the negative charge of the peptide is masked and the peptide is rendered more hydrophobic, facilitating translocation directly through the plasma membrane. Once inside the cell, endogenous esterases unmask the peptide's negatively charged side chains and it is thought that Coulombic repulsion with the anionic head groups of the plasma membrane prevents peptide escape. Because bioreversible esterification enables one-way trafficking directly across the membrane, there may be an opportunity to screen membrane translocation in esterase-containing liposomes, which can be readily adapted for high throughput screening. Alternatively, it might be possible to measure cell delivery in plate-based screens using a variety of reporters including functional readouts (like mitochondrial depolarization in the case of Bfl-1 inhibiting peptides), dye labeled peptides, or radiolabeled peptides.

The results in this thesis can potentially be applied to the development of small molecules targeting Bfl-1. For example, previous screens for small molecule inhibitors of Bfl-1 identified electrophilic small molecules as hits[4]. Presumably, this is because electrophilic small molecules have the potential to form covalent adducts with C55 of Bfl-1, which resides on the edge of the BH3 binding groove. The crystal structure of an electrophilic variant of a Bfl-1 selective peptide presented in Figure 2.20 could provide a valuable guide for rational design of small molecules to covalently react with C55 and make additional contacts in the BH3 binding groove. My thesis work also demonstrated that Bfl-1 is amenable to crystallization, opening the possibility that crystal soaking experiments with small molecule fragments might be a fruitful approach to designing small molecules to inhibit the Bfl-1 binding groove.

The results of my work also suggest peptide modifications that might improve the margin of specificity for Bfl-1, which could broaden the therapeutic window for future generations of potential therapeutic peptides. For example, one structural feature that is unique to Bfl-1 and might be leveraged in future work to augment Bfl-1 selectivity is glutamate at position 78 of Bfl-1. All anti-apoptotic Bcl-2 proteins including Bfl-1 have a deep, highly conserved hydrophobic pocket (P2 pocket) into which a highly conserved leucine (L3a) docks upon BH3 binding. But the P2 pocket of Bfl-1 is unusual in that it is formed with a gluatmate (at position 78) instead of all hydrophobic residues. Interactions with this unusual structural feature could potentially be leveraged to enhance Bfl-1 selectivity beyond what is reported in this thesis. Unlike natural BH3 motifs, which all have a leucine at position 3a, the designed peptide F1 described in chapter 4 of this thesis has a methionine at position 3a that docks into the P2 pocket. The X-ray structure

of F1 bound to Bfl-1 reveals that the terminal methyl of M3a is only 3.3 Å from the carboxyl group of E78. This structure could be used as a template to design peptides with unnatural amino acids that can make hydrogen bonds with E78 to enhance Bfl-1 selectivity.

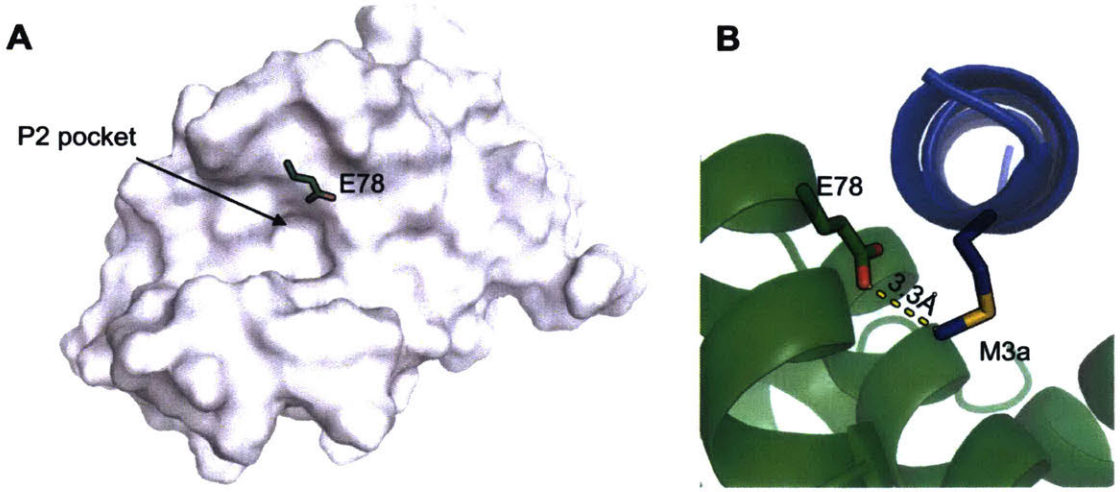

Figure 5.1. Structural positioning of glutamate at position 78 of Bfl-1. A) E78 of Bfl-1 forms one face of the otherwise hydrophobic P2 pocket of Bfl-1 (gray surface). B) The X-ray crystal structure of the designed Bfl-1 selective peptide F1 described in chapter 4 of this thesis (purple) bound to Bfl-1 (green). The close proximity between M3a of F1 and E78 of Bfl-1 is highlighted with a dotted yellow line.

The results in chapter 4 of this thesis show that dTERMen is an efficient approach to design novel BH3 peptides. Because the dTERMen scoring function is built upon common structural tertiary motifs found in many evolutionary distinct proteins, it may be possible to use dTERMen to predict non-obvious binding sites or to identify novel binding modes. An example of a relatively simple binding mode of interest might be a helix that binds the BH3 binding groove of Bfl-1 (or other anti-apoptotic protein) in a flipped conformation relative to canonical BH3 peptide binders. Binding in a reversed orientation might have the advantage of providing new, unexplored sequence spaces with new opportunities for selective binding.

In recent years, there has been significant progress in targeting Bcl-2 family proteins with BH3-mimetics. One outstanding example was the development of a small molecule (ABT-199) that selectively inhibits Bcl-2, which has been approved by the FDA for clinical use[5]. This required years of work, guided by intensive NMR studies of fragment binding[5–7]. Since then, small molecules selectively targeting Mcl-1 have also been developed[7]. This thesis, I describe the design of BH3 mimetic peptides with a high degree of specificity for Bfl-1. The design processes and peptide reagents developed in this work represent progress toward the larger goal of creating therapeutic peptides or small molecules selectively targeting Bfl-1 to treat human disease.

References

1. Bird GH, Mazzola E, Opoku-Nsiah K, et al. Biophysical determinants for cellular uptake of hydrocarbon-stapled peptide helices. *Nat Chem Biol.* 2016;12(10):845-852. doi:10.1038/nchembio.2153.
2. Mix KA, Lomax JE, Raines RT. Cytosolic Delivery of Proteins by Bioreversible Esterification. doi:10.1021/jacs.7b06597.
3. McGrath NA, Andersen KA, Davis AKF, Lomax JE, Raines RT. Diazo compounds for the bioreversible esterification of proteins. *Chem Sci.* 2015;6(1):752-755. doi:10.1039/C4SC01768D.
4. Mathieu A-L, Sperandio O, Pottiez V, et al. Identification of Small Inhibitory Molecules Targeting the Bfl-1 Anti-Apoptotic Protein That Alleviates Resistance to ABT-737. *J Biomol Screen.* 2014;19(7):1035-1046. doi:10.1177/1087057114534070.
5. Souers AJ, Leverson JD, Boghaert ER, et al. ABT-199, a potent and selective BCL-2 inhibitor, achieves antitumor activity while sparing platelets. *Nat Med.* 2013;19(2):202-208. doi:10.1038/nm.3048.
6. Oltersdorf T, Elmore SW, Shoemaker AR, et al. An inhibitor of Bcl-2 family proteins induces regression of solid tumours. *Nature.* 2005;435(7042):677-681. doi:10.1038/nature03579.
7. Kotschy A, Szlavik Z, Murray J, et al. The MCL1 inhibitor S63845 is tolerable and effective in diverse cancer models. *Nature.* 2016;538(7626):477-482. doi:10.1038/nature19830.